

Copyright Warning & Restrictions

The copyright law of the United States (Title 17, United States Code) governs the making of photocopies or other reproductions of copyrighted material.

Under certain conditions specified in the law, libraries and archives are authorized to furnish a photocopy or other reproduction. One of these specified conditions is that the photocopy or reproduction is not to be “used for any purpose other than private study, scholarship, or research.” If a user makes a request for, or later uses, a photocopy or reproduction for purposes in excess of “fair use” that user may be liable for copyright infringement,

This institution reserves the right to refuse to accept a copying order if, in its judgment, fulfillment of the order would involve violation of copyright law.

Please Note: The author retains the copyright while the New Jersey Institute of Technology reserves the right to distribute this thesis or dissertation

Printing note: If you do not wish to print this page, then select “Pages from: first page # to: last page #” on the print dialog screen

The Van Houten library has removed some of the personal information and all signatures from the approval page and biographical sketches of theses and dissertations in order to protect the identity of NJIT graduates and faculty.

INFORMATION TO USERS

While the most advanced technology has been used to photograph and reproduce this manuscript, the quality of the reproduction is heavily dependent upon the quality of the material submitted. For example:

- Manuscript pages may have indistinct print. In such cases, the best available copy has been filmed.
- Manuscripts may not always be complete. In such cases, a note will indicate that it is not possible to obtain missing pages.
- Copyrighted material may have been removed from the manuscript. In such cases, a note will indicate the deletion.

Oversize materials (e.g., maps, drawings, and charts) are photographed by sectioning the original, beginning at the upper left-hand corner and continuing from left to right in equal sections with small overlaps. Each oversize page is also filmed as one exposure and is available, for an additional charge, as a standard 35mm slide or as a 17"x 23" black and white photographic print.

Most photographs reproduce acceptably on positive microfilm or microfiche but lack the clarity on xerographic copies made from the microfilm. For an additional charge, 35mm slides of 6"x 9" black and white photographic prints are available for any photographs or illustrations that cannot be reproduced satisfactorily by xerography.

8701907

Marom, Shlomo Asher

COMPUTER AIDED STRESS ANALYSIS OF LONG BONES UTILIZING
COMPUTED TOMOGRAPHY

New Jersey Institute of Technology

D.Eng. Sci. 1986

University

Microfilms

International 300 N. Zeeb Road, Ann Arbor, MI 48106

PLEASE NOTE:

In all cases this material has been filmed in the best possible way from the available copy. Problems encountered with this document have been identified here with a check mark .

1. Glossy photographs or pages _____
2. Colored illustrations, paper or print _____
3. Photographs with dark background _____
4. Illustrations are poor copy _____
5. Pages with black marks, not original copy _____
6. Print shows through as there is text on both sides of page _____
7. Indistinct, broken or small print on several pages
8. Print exceeds margin requirements _____
9. Tightly bound copy with print lost in spine _____
10. Computer printout pages with indistinct print _____
11. Page(s) _____ lacking when material received, and not available from school or author.
12. Page(s) _____ seem to be missing in numbering only as text follows.
13. Two pages numbered _____. Text follows.
14. Curling and wrinkled pages _____
15. Dissertation contains pages with print at a slant, filmed as received
16. Other _____

University
Microfilms
International

COMPUTER AIDED STRESS ANALYSIS
OF LONG BONES
UTILIZING COMPUTED TOMOGRAPHY

by

Shlomo Asher Marom

Dissertation submitted to the Faculty
of the Graduate School of New Jersey Institute of Technology
in partial fulfillment of the requirements for the degree of
Doctor of Engineering Science
1986

APPROVAL SHEET

Title of
Dissertation: Computer Aided Stress Analysis of
Long Bones Utilizing Computed Tomography

Name of
Candidate: Shlomo A. Marom
Doctor of Engineering Science, 1986

Thesis and
Abstract Approved:

Dr. Martin J. Lindèn	_____	Date
Professor		
Department of Mechanical		
Engineering, New Jersey Institute		
of Technology		

_____	_____
_____	_____
_____	_____
_____	_____
_____	_____

© 1987

SHLOMO ASHER MAROM

All Rights Reserved

VITA

Name: Shlomo A. Marom

Degree: Doctor of Engineering Science, 1986

Secondary Education:

<u>Institute Attended</u>	<u>Dates</u>	<u>Degree</u>	<u>Date of Degree</u>
Technion, Israel Institute of Technology	1974-78	B.S.M.E.	1978
New Jersey Institute of Technology	1981-82	M.S.M.E.	1982
New Jersey Institute of Technology	1983-86	D.Eng.Sc.	1986

Major: Mechanical Engineering

Publications:

Master's Thesis, "Hyperthermia System with Mini-Computer Control: Design and Test", New Jersey Institute of Technology, Department of Mechanical Engineers, 1982.

Marom, S.A., Linden, M.J., Hussein, R., "Finite Element Stress Analysis of a Long Bone Utilizing Computed Tomography", Advances in Biomechanical Engineering, The American Society of Mechanical Engineering, November, 1985, pp. 667-668.

Linden, M.J., Marom, S.A., "Computer Stress Study of Bone with Computed Tomography", Annual Conference on Engineering in Medicine and Biology Proceedings, 1986.

Positions Held:

1978 - 1981 Mechanical Engineer. The Armament Research and Development Authority, Haifa, Israel.

1981 - 1986 Research Assistant. New Jersey Institute of Technology, The Department of Mechanical Engineering, Newark, New Jersey.

ABSTRACT

Title of Thesis: Computer Aided Stress Analysis of
Long Bones Utilizing Computed
Tomography

Shlomo A. Marom, Doctor of Engineering Science, 1986

Dissertation Director: Dr. Martin J. Linden

A computer aided analysis method, utilizing computed tomography (CT) has been developed, which together with a finite element program determines the stress-displacement pattern in a long bone section. The CT data file provides the geometry, the density and the material properties for the generated finite element model.

A three-dimensional finite element model of a tibial shaft is automatically generated from the CT file by a pre-processing procedure for a finite element program. The developed pre-processor includes an edge detection algorithm which determines the boundaries of the reconstructed cross-sectional images of the scanned bone. A mesh generation procedure then automatically generates a three-dimensional mesh of a user-selected refinement. The elastic properties needed for the stress analysis are individually determined for each model element using the radiographic density (CT number) of each pixel within the element borders. The elastic modulus is determined from the CT radiographic density by using an empirical relationship from the

literature. The generated finite element model, together with applied loads, determined from existing gait analysis and initial displacements, comprise a formatted input for the SAP IV finite element program. The output of this program, stresses and displacements at the model elements and nodes, are sorted and displayed by a developed post-processor to provide maximum and minimum values at selected locations in the model.

The model generation method is verified by applying the model generation procedures to an object of simple geometry and material properties, and comparing the computer aided analysis results with the analytical solution of the same model with the same boundary conditions. A convergence test was conducted to check the convergence of nodal displacements to asymptotic results as a function of refinements, and to determine an optimal number of selected elements for the three-dimensional mesh. A sample problem was modeled and analyzed to demonstrate the capabilities of the pre- and post-processors, using the scanned tibia section for the model. The analysis results were sorted, printed and displayed by the designated post-processor, and compared with tibia stress analysis results from the literature obtained by other methods.

This computer aided analysis method provides an automatic, versatile, noninvasive procedure for long bone modeling for finite element stress analysis.

For Esty

ACKNOWLEDGEMENTS

I wish to express my appreciation and gratitude to Professor Martin J. Linden whose advice and encouragement were my main support throughout the course of this study. In addition to his invaluable guidance, I have also benefited from his unlimited patience and excellent instruction.

I would also like to thank Dr. Rafaat Hussein for his generous advice and support throughout this work.

I would like also to acknowledge Dr. Clarence Mayott for his invaluable and knowledgeable remarks.

I would like to express my gratitude to the University of Medicine and Dentistry of New Jersey Orthopedic Research Laboratory members and the University Hospital CT operators for their cooperation and assistance.

TABLE OF CONTENTS

Chapter	Page
1. INTRODUCTION.....	1
1.1 Long Bone Morphology	2
1.2 Long Bone Mechanical Properties	8
1.3 Finite Element Method in Orthopedic Research	22
1.4 Computed Tomography in Bone Assessment	36
1.5 Objectives	45
2. METHODS.....	49
2.1 The Design of Auxiliary Software for a Finite Element Program.....	49
2.2 Scanning a Long Bone	54
2.2.1 Preparation for Scanning	54
2.2.2 Scanning Procedures	55
2.3 Designing a Pre-Processor for the Finite Element Program	61
2.4 Reconstruction and Display of the Scanned Cross Sectional Images	63
2.5 The Edge Detector.....	74
2.6 The Mesh Generation Strategy	81
2.6.1 Cylindrical Mesh	83
2.6.2 Cartesian Mesh	85
2.6.3 The Mesh Generator Structure...	86
2.7 The Node Selection Routine	88
2.8 The Node Display Routine	99
2.9 The Element Definition Routine.....	101

2.10	Elastic Properties Definition Routine	104
2.10.1	Radiographic - Apparent Densities Relationship	105
2.10.2	Elastic Modulus - Apparent Density Relationship	108
2.10.3	Average Properties of Model Elements	113
2.11	Generating the Finite Element Input File	119
2.12	Display of the Generated Model	120
2.13	Developing a Post-Processor	128
2.14	Verification of Model Generation Method	131
2.15	Convergence Tests	136
2.16	Demonstration Problem Analysis	141
2.16.1	Model and Boundary Conditions	142
2.16.2	Analysis Results and Interpretation	146
3.	SUMMARY AND DISCUSSION.....	156
3.1	The Computer Aided Analysis Method ..	156
3.2	Future Work	163
	APPENDIX A:TAPE ORGANIZATION.....	166
	APPENDIX B:TAPE AND FILE DIRECTORIES	167
	APPENDIX C:MAP ARRAY OF THE CT FILE	169
	APPENDIX D:RADIOGRAPHIC - APPARENT DENSITIES RELATIONSHIP.....	170
	APPENDIX E:CTPRO OUTPUT OF MODEL INFORMATION ...	171
	APPENDIX F:POST OUTPUT OF VERIFYING MODEL ANALYSIS.....	172

APPENDIX G:POST OUTPUT OF DEMONSTRATION PROBLEM ANALYSIS.....	175
APPENDIX H:POST OUTPUT FOR COMPARISON ANALYSIS.....	178
APPENDIX I:SAP IV OUTPUT INFORMATION OF DEMONSTRATING PROBLEM.....	179
BIBLIOGRAPHY.....	180

LIST OF FIGURES

<u>Figure</u>	<u>Page</u>
1. A General Block Diagram of the Designated Auxiliary Software for the FE Program.....	53
2. The Container Assembled with the Steel Wire Indications and the Tibia.....	56
3. The Assembled Container with the Tibia and the Standard on the CT Scanner.....	56
4. A Typical Scanned Cross Sectional Image of the Tibia, Container and Standard as Obtained by the CT/T 8800 Scanner.....	57
5. The Control Terminal of the CT/T 8800 Scanner during the Tibia Scanning.....	57
6. A Block Diagram of the Designated Pre-Processor CTPRO.....	62
7. The CT Reconstructed Image Using the MAP Array.....	66
8. Orientation of Reconstructed and Displayed Area of the Scanned Cross Sectional Image.....	71
9. Outline of Image Reconstruction and Display Routine.....	72
10. A Character Code Cross Sectional Image Displayed by VAX Line Printer.....	73
11. The Cross Section Borders set by the Edge Detector.....	75
12. The Cross Section Borders as Defined in the Edge Detector.....	79
13. The Borders of a Typical Long Bone Cross Section as Determined by the CTPRO Edge Detector.....	80
14. The Mesh Generator: General Block Diagram.....	87

15.	The Global Cartesian Coordinate System of the Finite Element Three-Dimensional Model.....	90
16.	Definition of Border Lines in the Model Cross Sectional Images.....	91
17.	Demonstration of the Node Numbering Method.....	98
18.	Display of Selected Nodes in Three Different X-Y Grids of Cross Section No. 8.....	100
19.	The Coordinate System of Eight Node Elements in SAP IV Finite Element Program..	101
20.	The Radiographic-Apparent Density Curve as Calculated by Least Square Method.....	109
21.	The Effect of the Apparent Density of Specimens on the Compressive Elastic Modulus (Carter and Hayes, 1977).....	112
22.	The Eight-Node Three-Dimensional Element Consists of Pixels in two Adjacent Cross Sectional Images.....	116
23.	The Element Consists of two Parallel Pixel Planes.....	117
24.	Determination of the Actual Element Borders by Geometrical Considerations.....	118
25.	The First Slice of the Three-Dimensional Finite Element Tibia Section Model.....	122
26.	Slices 1 to 3.....	123
27.	Slices 4 to 6.....	124
28.	Slices 7 to 9.....	125
29.	The Three-Dimensional Model: A View from -Y and +Y Directions.....	126
30.	The Three-Dimensional Model: A View from -X and +X Directions.....	127

31.	The Geometry and Boundary Conditions of the Verifying Model.....	132
32.	The Stress Pattern of σ_{zz} Bending Stress in the Verifying Model zz as Obtained by POST Post-Processor.....	133
33.	The Finest and the Most Coarse Mesh Sizes in the Convergence Test.....	139
34.	Convergence Test of Node Displacements in Mesh Refinements.....	140
35.	Forces and Moments Acting at the Knee Joint in Normal Gait (Harrington,1976).....	143
36.	The Loading and Boundary Conditions of the Demonstrating Problem Analysis.....	144
37.	Slice of Maximum Stress σ_{xx} (Element 13) and Maximum Resultant Displacement (Node 36).....	150
38.	Slice of Maximum σ_{yy} (Element 141).....	151
39.	Slice of Maximum σ_{zz} (Element 434).....	152
40.	Slice of Maximum τ_{xy} (Element 40).....	153
41.	Slice of Maximum σ_{max} (Element 41).....	154
42.	Slice of Minimum σ_{min} (Element 40).....	155

1. INTRODUCTION

The computer aided analysis procedure which is an objective of this study, together with a finite element program, determines the stress-displacement pattern in long bone sections, utilizing the computed tomography (CT) method. The CT data file of the scanned bone provides the geometry for the generated finite element model, while the CT radiographic densities provide the elastic properties for the model.

The next sections in this chapter include a literature survey in the areas of bone morphology and mechanical properties, the finite element method and the CT method. This review of the above subjects provides the background for this study, organized as follows: Sections 1.1 and 1.2 describe the long bone morphology and mechanical properties and the correlation between the apparent density and the mechanical properties in long bones, which allows using the CT information to determine the bone elastic properties. Section 1.3 describes the finite element method in orthopedic research and various modeling methods (including modeling by CT). Section 1.4 describes the CT method in bone assessment and the capabilities of this method in three-dimensional finite element modeling of long bones. Section 1.5 states the objectives of this study and the suggested course of work for their accomplishment. The second chapter describes the methods used to implement and perform the stated objectives.

1.1 Long Bone Morphology

Bone is a composite, viscoelastic, anisotropic material primarily composed of organic fibers (mainly collagen), inorganic crystals (hydroxyapatite), cement substance and water. The bones in the human body comprise the skeleton which gives the body mechanical stability, protects delicate organs, and serves as an anchorage for the muscles; thus making body movements possible through lever action. The bones also serve as a reservoir for calcium and phosphorus, and contain the bone marrow, the most important bloodforming organ.

Human bones may be described as belonging to one of five general categories: Long bones, such as the tibia, the femur and other leg and arm bones; Short bones, such as found in the wrist and ankle; Flat bones, such as the skull, and Irregular bones. In order to understand the properties and behavior of bone, it is necessary to consider other levels of structure in addition to the macroscopic size and shape. It is important to examine bone structure on many levels since all these levels interact in providing the bone with its characteristic properties. A description found quite reasonable in illustrating the hierarchial aspects of

the organization of bone, especially the long bones of the body, includes four levels of structure (Katz, 1980).

On the molecular level, bone is unique within the body in that it contains a mineral-like component in addition to the organic components. The major organic component of bone, as of all the connective tissues of the body, is collagen. Additional organic components (protein, polysaccharides, lipids, etc.), while only present in small amounts, play important roles in stabilizing the structural organization. This organic structure by itself would behave as a compliant material with good energy-absorbing characteristics (toughness), and other properties, generally with characteristics of polymers. The major inorganic phase of bone is hydroxyapatite (calcium), present in the form of small crystallites about $5 \times 20 \times 40$ nm (Woodward, 1962). This material by itself is quite rigid and stiff compared to collagen and its stiffness is approximately two-third that of steel. However, it is also quite brittle with poor impact resistance. The tiny crystallites are in intimate juxtaposition known as epitaxy in a highly organized geometrical arrangement with the collagen fibrils.

It is this admixture of organic and inorganic constituents which then comprises the second level of complex hierarchial structure, one which is heterogeneous and anisotropic (different properties in different

directions). This superposition of two quite diverse materials with significantly different properties results in what is known as a composite material, i.e., a material whose properties differ significantly from those of the original components.

In mature cortical (compact) bone, the collagen-hydroxyapatite composite is formed into densely packed concentric lamellar structures, the "Haversian system" or "Osteon." This is in contrast with another form of lamellar but not concentric bone, called "plexiform", which is often found in immature mammals. The osteon is essentially a cylindrical structure whose long axis courses somewhat irregularly along the long axis of the bone. It interfaces either with other osteons or with non-concentric lamellar groups, the interstitial lamellae. These highly organized lamellar groupings represent still another level of structural organization, denoted here as microstructural. The osteon represents a hierarchical composite material system as well. The concentric lamellar structures strongly bonded to one another and to the interstitial lamellae through the ground substance (cement line) may be viewed to form a composite material, or fiber reinforced composite. It appears that this microstructural organization is in part responsible for both, the elastic and the viscoelastic (or time-dependent deformational) behavior of macroscopic

bone (Katz, 1980).

The final level of structure is, of course, the macroscopic. On this level, the size and shape of the whole bone are considered. While each type of bone is of interest biomechanically, the long bones of the lower body, like the femur and the tibia, are of significant interest because of their role as the structural supports of the body, i.e., they are weight-bearing.

A human skeletal bone may be belonging to one of two types: compact (cortical) or cancellous (trabecular). The compact bone which has a shape of a relatively high density solid material comprises the cortex of long bone, while the cancellous bone in the human skeleton consists of a scaffolding of bony material arranged to form a sponge-like porous structure. The porous structures are quite variable in both size and shape, and can be described as a combined meshwork of bony trabeculae (rod like structures) and lamellae (thin plates). This structure of cancellous bone has been confirmed by several studies on cancellous bone structure. Whitehouse and Dyson (1974) used a scanning electron microscope to investigate the trabecular bone architecture in the proximal end of the human tibia and reported on a large variety of cancellous bone types. Singh (1978) studied the cancellous bone architecture using a stereoscopic microscope and classified a number of

distinct types of cancellous bone depending on the rods and plates proportion, thickness and direction in the bone.

In load bearing bones, such as the long bones of the leg, the function of the trabecular bone is to support and direct the operational loads through the ends of the long bones to the cortical bone of the diaphyses (the shafts). Evidence for the central role of the trabeculae in this function can be found in photoelastic studies which show that they are aligned in the directions of the normal stress trajectories to provide maximum strength with minimum weight. As an example, in the human knee, the femoral condyles rest on the tibial plateaus and serve to transmit the body weight to the lower leg. The condyles are roughly cylindrical structures and consist of a thick layer of cartilage, a thin layer of cortical bone, referred to as the subchondral plate, and the region of trabecular bone immediately underneath the plate. A mathematical model for the elastic properties of condylar structures developed by Burstein and co-workers (1970) has shown that at least under static conditions, the trabecular bone in the condyle is important in load carrying in that up to 80 percent of the surface loading is transmitted through the trabecular region.

The general structure of cancellous bone may be approximated as an open-cell two-phase composite (Mc Elhaney et al., 1970). One phase is bone while the other

phase consists of blood, red and yellow marrow, nerve tissue, and miscellaneous cell tissue and fluid. Because of its calcified nature, bone can grow only by apposition. That is, bone can increase in size only by adding material to one of its surfaces through a process known as bone remodelling. New bone added to the sides of trabeculae is usually deposited in the form of fairly even lamellae. As new lamellae are added to the sides of a trabeculae in a cancellous network, the spaces are correspondingly narrowed and filled. Accordingly, the continued deposition of fresh bone lamellae on trabeculae that enclose spaces soon affects the character of the bone in that it changes from a structure consisting of large spaces with little bone (cancellous bone) to one of narrow spaces with much bone (compact bone). All bone is porous, therefore, and the important structural feature that distinguishes so-called compact bone from cancellous bone is the quantity, size, shape and distribution of the cavities (McElhany et al., 1970; Carter and Hayes, 1976). The difference between these bone structures may be indicated by their apparent densities, i.e., their mass divided by their bulk volume. The most obvious difference between these two types of bone is their relative densities, or volume fractions of solids. Bone with a volume fraction of solids less than 70 percent is classified as cancellous; that over 70 percent, compact (Gibson, 1985).

1.2 Long Bone Mechanical Properties

The elastic and ultimate characteristics of bone are a description of the response of the tissue, in a mechanical sense, to stress, incurred as it performs its biological structural function. Those loading cycles that do not cause permanent irreversible change occur within the region of elastic tissue behavior. The response of the tissue in this region to external loads, that is, the relation between deformations and applied stresses, is characterized by the elastic constants of the bone tissue. This relation is known as the generalized Hook's Law and may be presented in a cartesian coordinate system by matrix notation:

$$\begin{bmatrix} \sigma_{xx} \\ \sigma_{yy} \\ \sigma_{zz} \\ \tau_{xy} \\ \tau_{yz} \\ \tau_{zx} \end{bmatrix} = \begin{bmatrix} C_{11} & C_{12} & C_{13} & C_{14} & C_{15} & C_{16} \\ C_{21} & C_{22} & C_{23} & C_{24} & C_{25} & C_{26} \\ C_{31} & C_{32} & C_{33} & C_{34} & C_{35} & C_{36} \\ C_{41} & C_{42} & C_{43} & C_{44} & C_{45} & C_{46} \\ C_{51} & C_{52} & C_{53} & C_{54} & C_{55} & C_{56} \\ C_{61} & C_{62} & C_{63} & C_{64} & C_{65} & C_{66} \end{bmatrix} \times \begin{bmatrix} \epsilon_{xx} \\ \epsilon_{yy} \\ \epsilon_{zz} \\ \gamma_{xy} \\ \gamma_{yz} \\ \gamma_{zx} \end{bmatrix}$$

where the coefficients $C_{11}, C_{22} \dots$ are the elastic constants of the material. The same equations in tensor notation:

$$\sigma_{ij} = C_{ijkl} \cdot \epsilon_{kl} \quad \text{where: } i, j, k, l = 1, 2, 3$$

The elastic properties of any given material may differ according to the direction in which testing is performed. If the properties are different in every direction, the material is said to be "anisotropic" and has thirty-six elastic constants in the elasticity tensor. If the material is isotropic in two out of the three directions, then it is "orthotropic" and has nine independent elastic constants. If, however, there is one plane in which the elastic properties are the same in every direction on the plane, the material is said to be "transversely isotropic" and has five elastic constants. Finally, if there is no directional independence of the elastic properties, the material is called "isotropic" and has only two elastic constants which are referred to as the Modulus of Elasticity and Poisson Ratio. Physically, the elastic modulus (stiffness) is the ratio between stress and strain, and Poisson ratio is defined as the negative of the ratio of transverse strain to longitudinal strain in the direction of uniaxial loading.

The values of trabecular and cortical bone mechanical properties have been calculated by many investigators who used various mechanical testing methods and ultrasonic measurements. The obtained values vary in a wide range depending on the type of applied test, the assumed degree of anisotropy and the specific bone specimens.

Mechanical values such as the moduli of elasticity in various directions, Poisson ratios, ultimate strength and more, were examined by many authors who tried to correlate them to the specimen density, microscopic structure and the topographic location in the bone structure. The results of such studies were reviewed by Evans (1973), Reilly and Burstein (1974), Katz (1980), Van Buskirk and Ashman (1981), Gibson (1985) and others.

Most of the studies aimed at the properties of the bone materials which comprise the long bone structures. In these studies, pieces taken from bones were tested by mechanical methods or ultrasonic measurements to determine their elastic properties. Most studies of long bone mechanical properties referred to one of the two types of bone tissue: cortical (compact) bone or trabecular (cancellous) bone. The function of trabecular bone in the human synovial joints, such as the knee joint, is to distribute the large contact stresses applied at the articular surfaces to the compact bone of the cortical shafts (Hayes et al., 1978). It is generally accepted that this function directly influences the structure and strength of the metaphyseal bone, a relationship known as Wolff's law. Hayes and Snyder (1981) and Cowin (1986), in recent investigations of Wolff's law, have provided strong support for the trajectorial theory of bone architecture. This theory states that the trabeculae are organized along the lines

of principal stress and, therefore, provide high strength with relatively low weight. Under static conditions, the trabecular bone relative contribution is 45 to 80 percent in bearing the surface condylar loading in the tibia (Burstein and Frankel, 1968; Rockoff et al., 1969; Burstein et al., 1970).

The anisotropy of the elastic and strength properties of bone has been demonstrated in uniaxial testing by a number of experimenters, some reviewed by Evans (1973). Most authors agree that human bone is both anisotropic and heterogeneous, and several studies use experimental methods to characterize the degree of anisotropy and to determine the elastic properties of bone as a function of anatomical position. The main difficulty in such experiments is that the traditional engineering methods for material properties determination are difficult to apply to bone tissue. Ultrasonic techniques offer some advantage in that they allow the use of smaller specimens of less complicated geometries than do mechanical testing methods.

Lang (1970), Van Buskirk and Ashman (1981), Ashman and co-workers (1984) and others used the ultrasonic technique of some variations to determine the five elastic constants of cortical bone assuming a transversely isotropic material. Lang (1970) and Reilley and Burstein (1974) showed that cortical bone is an orthotropic material that is approximately transversely isotropic.

These findings seem consistent with the observation that bone histologically displays the symmetry of a transversely isotropic material. Katz (1980) concluded that certain microstructural features suggest that cortical haversian bone is transversely isotropic in its symmetry while the plexiform nature of cortical lamellar bone makes it orthotropic. Ashman and his associates (1984) consider any cortical bone to be orthotropic because it is a combination of the two bone types so the lesser symmetry of orthotropy must be assumed.

The choice of material symmetry for an elastic model of compact bone depends to a large extent on the intended application of the elastic model by the investigator. For example, Huiskes (1982) indicates that the stress analysis of a human long bone is adequately served with an isotropic model. The data on the measured elastic constants of bone reported by Van Buskirk and Ashman (1981) show that the percentage difference between the orthotropic elastic constant values and the transversely isotropic elastic constant values are quite small, and unlikely to have a significant effect on the stress analysis of bone.

Data on mechanical properties of the cancellous (trabecular) bone at the proximal tibial epiphysis were reported in several studies. Behrens and co-workers (1974) used compressive tests of machined specimens of tibial cancellous bone to correlate the bone compressive

strength to its density. Lindhal (1976) used compression tests of cancellous bone to calculate the bone modulus of elasticity and the ultimate compression strength in various directions. Hvid and his associates (1983) studied the topographic variation of proximal tibial cancellous bone strength and elastic modulus in twelve knees from routine autopsies. They found that mechanical properties varied considerably from knee to knee, but the topographic patterns were remarkably constant. Goldstein and co-workers (1983) experimentally determined the elastic modulus and ultimate strength of human tibial trabecular bone as a function of metaphyseal (the tibia neck) location.

The trabecular bone tissue is considered by most authors as a nonhomogeneous, anisotropic, nonlinearly viscoelastic substance, and as such, its detailed properties are difficult to measure. However, the ratios of vertical to lateral stiffness ranges up to a factor of ten in the proximal tibia trabecular bone (Williams and Lewis, 1982). Thus, the anisotropy in stiffness can be considerable. The source of the anisotropy is obviously the details of the trabecular morphology with the existence of a preferred direction of structure leading to the anisotropy. As a consequence, long bones are much less stiff in the lateral direction than along the long axis, not only because there is less material to resist the load but because the lateral deformation occurs more

by bending of the resisting structures rather than by direct compression as appears to occur in the stiffest direction.

The mechanical behavior of bone, as the result of the application of a force, is influenced by the fact that bone is viscoelastic material (Galante et al., 1970; Whitehouse and Dyson, 1979; Townsend et al, 1975; Ducheyne et al., 1977). If the characteristic constants of a material are affected by the rate of deformation, then the material is said to be viscoelastic. Serious consideration has been given in recent years to examining the time dependent (viscoelastic) properties of bones. McElhaney and co-workers (1970) studied wet bovine cortical bone in compressional constant strain-rate experiments at six different strain rates. Since the leading portion of each of the stress-strain curves was linear, elastic moduli could be obtained. A threefold increase in the elastic modulus was observed with increasing strain rate. Wright and Hayes (1976) observed a more than doubling in elastic modulus with increasing strain rate on wet bovine femoral specimens in tension. They proposed a linear relationship between elastic modulus and the logarithmic function of the strain rate. In addition to these strain rate studies focusing on specimens of compact bone, there have been several investigations of the strain-rate sensitivity of the whole bone

(Mather, 1967; Burstein and Frankel, 1968; Carter, 1981). Recent work has focused attention on the viscoelastic properties of human trabecular bone (Pugh, Rose and Radin, 1973; Carter and Hayes, 1977; Goldstein et al., 1983). The obtained data of Pugh, Rose and Radin (1973) tend to justify the assumption that the general viscoelastic response of trabecular bone is essentially that of compact bone at strain rates lower than 2 percent. The effect of hydraulic strengthening, i.e., the effect of fluid in the open spaces between trabeculae, was noticeable only in higher strain rates. Compression tests of human and bovine trabecular bone specimens with and without marrow were conducted by Carter and Hayes (1977) at strain rates of 0.001 to 10.0 per second. The presence of marrow increased the strength, modulus and energy absorption of specimens only at the highest strain rate of 10.0 per second. This enhancement of material properties at the highest strain rate was due to the restricted viscous flow of marrow and the flow through the pores of the trabecular bone. Both strength and modulus of elasticity were approximately proportional to the strain rate raised to the 0.06 power.

Density is expressed in terms of weight per unit volume; thus, "Apparent density" is defined as the weight divided by the total volume of the sample, and "real density" is the weight divided by the volume

of the bone matrix, excluding the marrow vascular spaces, i.e., the density of the mineralized bone alone.

Many investigators have documented significant positive associations between apparent density and the strength and stiffness of cancellous bone (Galante et al., 1970; McElhaney et al., 1970; Carter and Hayes, 1976, 1977; Carter and Schwab, 1979; Harrigan et al., 1981; Saha et al., 1981). There is no question that other factors, such as orientation of trabeculae and microstructure, also influence the mechanical properties of cancellous bone (Pugh et al., 1973; Ducheyne et al., 1977; Carter and Hayes, 1977). However, this does not in any way negate the strong effects of apparent density differences on mechanical properties of bone. Even in studies in which trabecular arrangement was found to be an important structural variable, significant positive correlations between bone apparent density and strength or stiffness were also found. Reported statistical correlations between cancellous bone density and strength or stiffness range between 0.7 to 0.9 (Galante et al., 1970; McElhaney et al., 1970; Lindahl, 1976; Saha and Gorman, 1981). Thus, there is wide support in the literature for a strong positive association between apparent density and mechanical properties of cancellous bone.

Extending this relationship further, Carter and Hayes (1976,1977) have suggested that compact and cancellous bone can be viewed as a single material, with

mechanical property differences principally a function of variation in apparent density. This conclusion is supported by the fact that the compositions and the real densities of normal trabecular and compact bone tissue are similar (Gong et al., 1964; Galante et al., 1970). In addition, recent work has suggested that the microscopic material properties of trabecular bone are similar to those of compact bone (Martin, 1972; Pugh et al., 1973; Townsend et al., 1975). These observations suggest that whole bones can be modeled as composite structures consisting of both a solid phase of mineralized bone tissue and a fluid phase of blood marrow and nerve tissue (McElhaney et al., 1976). The distribution of pores throughout the whole bone contributes to the apparent density distributions which are observed radiographically. The pore geometry and orientation contribute to the structural anisotropy which is evident in both trabecular and cortical bone.

Recently some workers have attempted to view trabecular bone as a porous structure comprised of bone tissue with the same microscopic mechanical properties as compact bone (McElhaney et al., 1970; Pugh et al., 1973; Townsend et al., 1975). McElhaney and co-workers (1970) considered a porous block model which consists of a number of small cubical aggregates arranged to form a larger transversely isotropic porous cube. The primary assumption upon which this model is based is that all

bone has the same physical properties in the small, i.e., bone of different types has the same microscopic properties. In dealing with the varying structure, it is further assumed that local mechanical responses, like the modulus of elasticity, are proportional to the local apparent density raised to some power (n), with n determined empirically. This provides a means of incorporating in the model many of the structural elements that influence the response but are too complex to be included in detail.

The porous block model shows that the modulus of bone is approximately proportional to the third power of the apparent density. Thus, small porosity changes in bone of low relative density result in only small changes in strength and modulus, while small porosity changes in bone of high relative density result in large changes in strength and modulus. Carter and Hayes (1976) extended the porous block model to be applied also for compact bone, confirming the hypothesis that all bone can be mechanically viewed as a single material of variable apparent density. Compression tests of human and bovine bone specimens conducted by Carter and Hayes (1976,1977) spanned a wide range of apparent densities over a wide range of applied strain rates. By analyzing the obtained data with reference to the values of the mechanical behavior of compact and cancellous bone reported in the literature, they obtained empirical relationships between

the apparent density and strain rate and the compressive strength and modulus. In that study, the compressive modulus of bone tissue was approximately proportional to the cube of the bone density, confirming the theoretical relationship developed by McElhaney (1970) in his porous block model. These power relationship which was shown to hold for all bone in the skeleton, allows meaningful predictions of bone tissue stiffness based on in-vivo density measurements such as regular rentgenographic measurements or computed tomography. The compressive elastic modulus of human cortical and trabecular bone tissue can now be determined using an empiric relationship developed by Carter and Hayes (1977):

$$E = C \cdot \dot{\epsilon}^{0.06} \rho^3$$

where $\dot{\epsilon}$ is the applied strain rate, ρ is the apparent density and C is a constant number obtained experimentally. It should be noted that the influence of strain rate is relatively small compared with the influence of apparent density.

The second independent constant for an isotropic material, the Poisson ratio, is the ratio of strain in a direction perpendicular to that of a uniaxial stress, to the strain in the direction of uniaxial stress. The reported values of Poisson ratio in human compact and cancellous bone are difficult to compare due to the different variables including specimen type, moisture,

and strain rate during the relatively low number of experiments conducted for this purpose. McElhaney and co-workers (1970) used a strain gauge glued to the specimen surface for strain measurement in perpendicular direction during compression tests conducted on human cancellous bone specimens. The tests were repeated in three directions, yielding the Poisson ratio for three orthogonal axes. Lang (1970) used an ultrasonic technique with wet bovine bone to obtain Poisson ratio values at the upper extreme of physiological strain rate. Reilly and Burstein (1974) tested a transversely isotropic model to determine five independent elastic constants for human compact bone tissue. The high values for Poisson ratio reported by Reilly and Burstein (1974) have raised the question of whether the human compact bone is incompressible. Mahanian and Piziali (1985) who investigated the incompressibility for a transversely isotropic material in general and the human compact bone in particular, showed that the values reported by Reilly and Burstein are in the acceptable range, below the incompressible limit.

It is generally accepted by many authors that the Poisson ratio is related to some bone physical properties such as the level of moisture in the tested bone tissue, the microscopic architecture, the applied strain rate and more. However, no attempt has been found in the literature to correlate the Poisson ratio of human compact

or trabecular bone to any of these physical properties. Instead, experimental values of Poisson ratio have been obtained for various types of bone tissues and topographic locations in the long bones.

1.3 Finite Element Method in Orthopedic Biomechanics

The finite element (FE) method is a numerical procedure for solving a continuum mechanical problem with an accuracy acceptable for engineers. In practice, most problems are too complicated for a closed form mathematical solution. A numerical solution is required, and a versatile method that provides it is the finite element method. A finite element model, whether it is two- or three-dimensional, consists of "finite elements" of quadrilateral, triangular or other geometry, and "nodes" where elements are connected to one another. A "mesh" is an arrangement of nodes and elements in a specific model.

Versatility is an outstanding feature of finite elements. The method can be applied to various problems: The region under analysis may have arbitrary shape, loads and boundary conditions. The mesh may mix elements of different types, shapes and physical properties. This great versatility is often contained within a single computer program in which a user-prepared input data control the selection of problem type, geometry, boundary conditions, element selection and so on. Another feature of finite elements is the close physical resemblance between the mesh and the actual structure. The finite element method also has disadvantages: There is no closed-form expression that permits analytical study of the problem, reliable computer and program are

essential, many input data are required and voluminous output data must be sorted and interpreted.

The finite element method is implemented in the computer environment, using the theory of elasticity and numerical methods. The "stiffness method" or the "displacement method" is the most popular form of the finite element implementation in structural mechanics. In this method, the displacements are the primary unknowns to be computed. Stress is a secondary variable, computed from the displacements (Cook, 1981).

Considering a single element, and defining a degree of freedom as a displacement or rotation of a node, the stiffness equation can be formed:

$$[k] \times [d] = [r]$$

where $[k]$ is the element stiffness matrix, $[d]$ is the element nodal displacement vector and $[r]$ is the vector of element nodal loads. The matrix and vector dimensions depend on the number of degrees of freedom in the element nodes. In the finite element program, the solved system is:

$$[K] \times [D] = [R]$$

which consist of the same terms used in the previous equation except that "global" replaces "element." This equation can be solved for $[D]$. Hence, because $[d]$ for each element is contained in $[D]$, deformations of all elements are known. From deformations, the stresses are computed at the model elements.

In general, considering the theory of elasticity, if a stress or displacement field satisfies equilibrium, compatibility and boundary conditions, then a solution has been found. This relates to finite element analysis in a sense that if elements are based on displacement fields, so that nodal displacements are the primary unknowns, then the compatibility condition is satisfied within elements. Suitably chosen fields also provide compatibility between elements and satisfy displacement boundary conditions. Equilibrium equations and boundary conditions on stress are satisfied only approximately. The approximation improves as more degrees of freedom are used and, barring computational difficulties, the exact solution is achieved in the limit of infinitely refined mesh.

The first engineering computer program based on the finite element method was developed in the mid-fifties, following the paper by Turner and others (1956) presenting a stiffness and deflection analysis of complex structures (Cook, 1981). Since then, several commercial finite element software packages have been produced and marketed, being used in several engineering areas, such as heat-transfer, fluid-flow and more extensively in stress analysis. The input in static finite element stress analysis programs consists of the model geometry, discretized into a finite element mesh (nodes and elements), the mechanical properties, such as the elastic modulus

and Poisson ratio assigned to the model elements, and of boundary conditions, loads and initial displacements of nodal points. Commercial finite element software packages, such as SAP IV, GIFTS, ANSYS, NASTRAN and SUPERTAB are mostly based on the stiffness method and differ in their program features such as the available analysis types, element variety, input-output organization, interactive access, efficiency, pre- and post-processing and more.

Traditionally, interest existed in orthopedics and orthopedic-related sciences with respect to stresses and strains in loaded bones, specifically concerning the relationship between architecture and load-bearing function. The mathematical tools available for stress analyses in classic mechanics, however, were not very suitable for the highly irregular structural properties of bones. Hence, the powerful finite element method became the logical choice to fill the gap due to its unique capability to evaluate stresses in structures of complex shape, loading and material behavior. New questions and new methods have created a stimulating environment for the utilization of the finite element method in orthopedic biomechanics, and its applications have grown rapidly in the last fifteen years (Rybicki, 1980). Finite element analysis is presently used to investigate the stress-related architecture of bone remodelling processes, to test and to optimize artificial implant designs and fracture fixation devices,

and to study the mechanical behavior of all types of bone tissues and cartilage.

Many authors focused during recent years on the mechanical behavior of the load bearing long bones, utilizing the finite element method. These studies, reviewed by Huiskes (1983), used various types of two- or three-dimensional models, assuming a certain level of anisotropy, assymetry and homogeneity in their model. A two-dimensional finite element model of forty-two curvilinear elements of the femoral head was developed by Brown and Ferguson (1978). Nonhomogeneous elastic properties of trabecular bone based on experimental data were included in this study that was aimed at investigating the influences of trabecular bone non-homogeneity and of geometrical alterations on the stress distribution. Stresses in the trabeculae of the bone structure itself were studied with the finite element method of Pugh and co-workers (1973) using simple plate elements. The aim of this analysis was to correlate local bone loading with trabecular failure. A similar but more sophisticated two-dimensional model was later proposed by Williams and Lewis (1982) to predict the elastic constants of trabecular bone as a continuum material from the non-continuous trabecular structure and properties. The theoretical results were verified by experimental data. Using a two-dimensional finite element model and an iterative algorithm, the unbonded

elastic contact problem between femur and tibia in the knee joint was analyzed by Chand and co-workers (1976). Results correlated favorably with those of two- and three-dimensional photoelastic analyses. Hayes and his associates (1978) presented an axisymmetric finite element analysis of the upper tibia with non-axisymmetric loading. The ring elements used in this analysis are special in the sense that the loads and displacement fields can be represented by Fourier series in the circumferential direction. Recently, a three-dimensional FE analysis of the upper tibia was conducted by Little and co-workers (1986) and compared with strain-gage tests and other analyses from the literature.

Besides investigations aiming at stress analysis of various long bones, a number of finite element analyses of bones have been designed for problems of fracture and fracture fixation, including problems of bone remodelling (Vichnin et al., 1977; Askew, 1981). Artificial joint design and fixation is probably the most popular application of the finite element method in orthopedic biomechanics. Two- or three-dimensional models were analyzed by Rohrle and his associates (1980), Murase (1981), Askew and Lewis (1981), Murase and co-workers (1982), Little and co-workers (1985) and others. Comparing results obtained by these studies is difficult due to vast differences in element types, mesh density, geometry, material properties and loading.

In some finite element analyses, linear elasticity, isotropy and homogeneity of cortical and trabecular bone were assumed (Hight et al., 1975; Piziali et al., 1976; Valiappan et al., 1977; Harris et al., 1978; Hayes et al., 1978). Studying the torsional stress of a human tibia by finite element method, Adamovich and Yanson (1981) used a distribution of the shear modulus by zones of the cross section of the bone. Murase (1981) developed a three-dimensional model of the proximal tibia, divided to ten different material regions. The elastic constants were estimated from the literature (Pugh et al., 1973; Evans, 1973; Goldstein et al., 1980) for each region in the bone. Askew and Lewis (1981) used a two-dimensional axisymmetric finite element model to determine the stresses around a knee prosthesis in the proximal tibia. This model was considered transversely isotropic and the five elastic constants were determined using a combined experimental analytical method. In general, the elastic properties for finite element models were determined by different authors according to the purpose of the analyses, the assumed anisotropy, the desired accuracy and the experimental data available. Although the correlation between the apparent density of human cortical and trabecular bone to the elastic properties was accepted by most authors, only a few finite element analyses used x-ray radiographs to determine mechanical properties in the bone regions (Gordon, 1971; Murase, 1981; Murase et al., 1982).

An advanced technique such as the computed tomography provides the tool for determining the local apparent densities in any scanned bone tissue and, thereby, to determine the mechanical properties in different regions of the bone.

Modelling long bones for finite element analysis requires determining the bone geometry. Accurately determining long bone boundaries is difficult due to the bone intricate geometry. Moreover, due to the variations in long bone geometries, determining the boundaries of a specific bone will not necessarily allow generalizing it in a finite element model valid to other bones of the same type. Previous finite element analyses of long bones used various methods to determine the bone geometry. Hight and co-workers (1975) and Piziali alone and with co-workers (1976,1980) described femurs, tibias and fibulas three-dimensional boundaries utilizing cross sectional information. Each bone was cast in clear epoxy resin and then thin transverse sections were cut at approximately one inch intervals. The geometry of each section was established using an optical digitizer or an optical comparator. The cross sectional information was utilized to develop three-dimensional finite element models. Brown and DiGioia (1984), Chand and co-workers (1976), and Murase and associates (1981,1982) used x-ray photographs of a live long bone to determine the boundaries for a three-dimensional finite element model. Hayes and

co-workers (1978), Stein and Granik (1979), Askew and Lewis (1981), Minns and his associates (1975), Little and co-workers (1985) and others used a combination of physical bone section and x-ray techniques to determine long bone geometry for two- or three-dimensional models. In this method, the bone was cut into several sections which were then radiographed. The x-ray photographs were enlarged and reproduced in positive form, and the cross sectional geometry was physically measured and digitized from them. Lovejoy and Burstein (1977) used non-destructive laminography to obtain geometrical properties of bone sections. A laminogram was obtained for each specimen using a Picker conventional laminographic unit. The measured data were compared to the geometrical properties obtained by physical sections and x-ray tomography method for the same bone specimens. Barton (1980) proposed a simple method for obtaining geometrical properties of bone sections utilizing a radial grid which is superimposed over an enlarged photograph of a section or a laminogram tracing.

With the development of the computed tomography (CT), it is now possible to use this method to obtain outlines of bone structures which may be utilized for bone modelling in finite element stress analyses. Huang and co-workers (1980) reported on a discretization procedure of anatomical structures based on CT scans which can be used for subsequent finite element analysis. In their study,

gross cross-sectional CT scans were obtained for a whole human body, the outlines and inertial properties of each cross section were obtained by picture processing techniques. Mayott, Langrana and Alexander (1983) utilized CT scans of tibia cross-sections to calculate the area and mass properties along the entire length of the bone. In their study, a computer aided procedure was developed to access the CT data file, eliminate unnecessary information such as air and soft tissues, and compute the area and mass properties. Woolson and associates (1984) developed stereoscopic CT techniques to display a three-dimensional image of bone, using a series of CT cross sectional scans of the bone. The CT data was analyzed automatically by computer to extract the three-dimensional anatomy of the skeletal structure on a computer graphic terminal screen. Garg and Walker (1985) used CT data file for a two-dimensional finite element model in a comparison of interface stresses for cemented and uncemented tibial implant components. The geometry and elastic modulus were determined for the two-dimensional model using an experimental correlation between the elastic modulus and the CT number. Nelson and co-workers (1985) used computed tomography to reconstruct the cross-sectional anatomy of individual femurs. A contour detection algorithm was used to transform these data into a three-dimensional model which was then used as input for a computerized implant design program.

In addition to the discretized model and the mechanical properties, the boundary conditions, the applied loads and displacements, are provided to the finite element program as input for each problem stress analysis. In modelling load bearing long bones such as the tibia, the boundary conditions may be determined from bio-engineering analysis of force actions at the hip and knee joints during normal or pathological gait. Human locomotion is a highly complex phenomenon. The fact that walking is a three-dimensional activity creates major difficulties in the analysis of force actions transmitted between limb segments. Although the main effects of locomotion are in the plane of progression, the saggital plane, neglect of lateral and rotatory displacements in the coronal plane will introduce major errors in joint force computations.

Several investigations have been made to calculate joint forces using static analytical methods and experimental gait analyses. Force actions transmitted at the hip have been calculated by Paul (1965) and at the knee by Morrison (1968) using a non-invasive experimental technique. With this method, a force plate was used to define the position, magnitude and direction of the resultant ground-to-foot force. From photographic records taken from the front and side of the subject, the spatial alignment of limb segments and the position of joint centers are determined for successive time intervals.

The resultant joint force at the hip or knee is calculated by considering the appropriate limb segment as a free body at conditions of equilibrium. Kettlekamp and co-workers (1970,1972) described a method of determining force distribution on the tibial plateaus of a standing subject and showed the effect of the angle of the tibio-femoral mechanical axes on force distribution. Harrington (1976) described a simplified analysis for the determination of force actions at the knee joint for normal and pathological gaits in which the stance phase of the gait only is considered and gravitational and inertia forces are excluded from the analysis. Johnson and co-workers (1980) used gait analysis to determine the way in which the load in the knee is shared between the medial and lateral compartments of the tibia plateau during normal walking. Minns (1981) studied the effect of anatomical variations on the medial and lateral compartment contact forces. Moeinzadeh and co-workers (1973) developed a mathematical dynamic model of the two-dimensional representation of the knee joint. The profiles of the joint surfaces were determined by x-ray films and represented by polynomials while joint ligaments and muscles are modeled as nonlinear elastic springs of realistic stiffness properties. Nonlinear equations of motion, coupled with nonlinear constraint conditions were solved numerically to provide forces and contact point

locations between femur and tibia. Nisell and co-workers (1986) constructed a two-dimensional model of the tibio-femoral joint using the results of cadaver knee dissections together with radiographic landmarks on healthy knees loaded at various angles of flexion. The model presented was used for quantifying tibio-femoral forces during knee extending activities.

The knee joint is capable of large flexion in the saggital plane only. With the exception of positions of acute flexion, rotations about the long axis of the shank and in the coronal plane are restricted to a few degrees by restraint due to the ligaments of the joint. For most activities, therefore, the mechanics of the knee joint can be compared to a simple hinge (Kurosawa et al., 1985). Rotations at the knee, i.e. changes in relative angular position of the shank and thigh, are controlled by forces developed in the muscles acting across the joint. These muscles may be classified into three main groups: Quadriceps femoris, Hamstrings and Gastrocnemius. To obtain a solution for force action at the knee joint, a functionally equivalent simplified muscle and ligament system was devised in the light of the experimental information and analytical techniques available. This simplified system consisted of the three muscle groups as defined and the four ligaments which act across the joint: the anterior and posterior cruciate ligaments, and the medial and lateral collateral ligaments.

To measure the force between ground and foot, a force plate is generally used. Forces acting on the top plate are registered by a system of semiconductor strain gauges attached to four columns which support the plate. Using force plate to calculate the force system acting at the knee joint in normal gait, results indicated a maximum loading at the joint of 3 to 5 times body weight (Paul, 1965; Moeinzadeh et al., 1973; Harrington, 1976).

The complexity of the boundary conditions, together with the intricate bone geometry and the anisotropic, nonhomogenous, viscoelastic mechanical properties all strongly affect the accuracy of conventional finite element stress analyses of long bones. Moreover, the variations in specimen geometrical and mechanical properties prevent accurately generating one general long bone finite element model. The large number of studies aiming at long bone stress analyses and the wide range of results support the need for improved modelling methods for long bones. Such a method can use the computed tomography for the finite element stress analysis of long bones.

1.4 Computed Tomography in Bone Assessment

The development of Computed Tomography (CT) began in the early sixties. The initial idea was to pass successive x-rays through an object to obtain the x-ray absorption coefficient at the center. Oldendorf (1961) and Cormack (1963) were the first to realize that passing successive x-rays through an object at different angles could be used to measure the x-ray absorption coefficients in small points of the entire body. Using a Fourier convolution analysis, a complete two-dimensional profile of absorption coefficients could be calculated. The first commercial instrument developed using this process was the EMI scanner built by Hounsfield in 1969. This early device required that the scanned object be surrounded by water and that no gas be present in the scanned field. Since air could not be present, the only images obtained at that time were of the head. Twenty years of progress in CT and computer tomography created fast, efficient and accurate CT scanners which can provide high-resoluted cross sectional images of scanned organs.

In a CT system, the image is not formed directly by the x-ray beam, but it is a multistep process of scanning, data processing and graphical image reconstruction. Most CT systems contain three functional units: Scanning unit, computer and viewing unit. In addition, these systems contain one or more data storage devices such as

magnetic discs and tapes which store the image data and the computer programs.

The first step of the process is to scan the body section with one or more small cross section x-ray beams. After penetrating through the body, the x-ray energy is intercepted by a radiation detector which produces an electrical signal that is proportional to the intensity of the x-ray beam. This intensity is determined by the penetration of the body section, depending on the attenuation coefficients of its material. By either moving the x-ray beam or using a large number of parallel beams, a penetration profile of the body section is obtained. In order to form a CT image, penetration profiles taken at different angles through the body section are required. These are obtained by rotating the x-ray beam and detector assembly around the scanned body.

A digital computer within the system forms the CT image from the penetration profile data by a process which is generally referred to as image reconstruction. The development of the equations used for image reconstruction were first developed by Radon (1917). The early reconstructive process used "back-projection" technique which summed the inverse of the intensity of the attenuation to reconstruct the image. The images reconstructed were fuzzy and prone to producing a star shaped pattern if the density at the center of the image was high. Iterative techniques such as matrix relaxation

and simultaneous iterative reconstruction are currently used today (Smith, 1982). In this technique, a two-dimensional matrix of attenuation values is reconstructed and the sum of each row and column is compared to the attenuation at that position. The matrix values are then changed to effect a "proper guess" of the sum of each row and each column. Sums are then made and checked against the original attenuation values. This is continued until the actual sums equal the values in the matrix. The image created by the computer is a numerical image with specific values for each "pixel" within the image, while the image area is divided into an array of square pixels with dimensions in order of one square mm.

A numerical value is calculated for each pixel within the image, referred to as CT numbers. The numbers are related to the attenuation coefficient values of the materials within the scanned body section, since the diminution or attenuation (by absorption or scatter) of an x-ray beam as it traverse the object is dependent on the local linear attenuation coefficients of the object (Katz, 1981). Arbitrary scales for CT values have been devised, most of them use water as a reference material and assign it a value of zero. The value of CT number for a specific material is given by:

$$N = \alpha \frac{\mu - \mu_w}{\mu_w}$$

where μ and μ_w are the attenuation coefficients of the

measured material and water respectively, and α is the scaling (contrast) factor for the scanner being used (Katz, 1981). The scaling factor " α " determines how many CT numbers will be assigned between the linear attenuation of air and of water. Many systems now use Hounsfield units where the scaling factor is 1000. This produces CT values of -1000 for air, zero for water and an ambiguous upper scale end of 1000 for compact bone. For Hounsfield units, the "contrast scale" or the change in N per Hounsfield unit is 0.1 percent change (McCullough, 1975). Other systems such as General Electric CT scanners use water and plexiglass phantom as reference materials to calibrate the scanner with a scale of 0 to 4095. This range of positive integers was selected to represent the CT numbers scale due to eight bit (half word) limitation of the system computer (CT/T manual, 1980; ECLIPSE line computers, 1973).

Mathematical procedures are used to reconstruct the scanned cross sectional image from the CT numbers of its pixels. The numerical image is converted into a video type signal which is displayed on a graphic terminal screen. Permanent images are obtained by photographing the screen. The scanned image data may be stored in most systems on an archive magnetic tape for later use.

Currently, there are several limitations to the accuracy and precision of CT generated density and geometry measurements. These include noise, non-linearity,

and drift of detectors, partial volume artifacts, motion artifacts and the beam hardening artifact (Joseph and Spital, 1978; Boyd et al., 1979; Zatz, 1981).

Noise is the random variations of attenuation values in an image of uniform material and it gives the CT image a mottled or grainy appearance. Another type of noise is tissue noise, which is defined as the regional variation in CT numbers for a given tissue type (McCullough, 1977). Noise can be reduced by increasing the radiation dose and thereby increasing the number of detected photons.

Non-linearity of x-ray detectors is caused by the extraordinary demands a CT system places on radiation detectors. Ideally, the function of a detector is to produce an output current that is exactly proportional to the intensity of the radiation striking it (linear detector). Causes of non-linearity in detectors include leakage current, saturation, hysteresis and afterglow (Joseph and Spital, 1978).

Partial volume effects are another cause of CT errors. Each picture element (pixel) in the CT image represents a volume element (voxel) of the object scanned. The CT numbers of each pixel represent the average linear attenuation coefficient of the material within the voxel. The voxel can be comprised of different materials, such as bone and soft tissue. Perception of low contrast objects may be decreased by their attenuation being averaged with other tissues within the voxel. This is

the partial volume or volume averaging effect. Volume averaging is particularly apparent when a portion of a high attenuation material such as bone is within the voxel. Such an effect is deleterious to the quantification of soft tissues but is not as important in the quantification of bone (Turnier et al., 1979).

Motion of the scanned object during the process has caused in the past some scan views to be geometrically inconsistent with other views. However, with the increased scanning speeds of modern scanner (several seconds), patient motion artifacts are rarely a problem. This is especially true with regards to the CT imaging of bones.

Scan to scan variations are also due to system drift. Scanner drift is caused by changes in the scanner system over time. Causes include detector drift, x-ray tube aging and hardware or software changes. McCullough (1977) noted that this problem is easily overcome by including an object of known composition (CT numbers) in each scan. Cann and Genant (1980) recommend the use of calibration phantom which is scanned along with the patient. They suggested a "standard" phantom consisted of dipotassium hydrogen phosphate (K_2HPO_4) solutions of known concentrations. In this way, system drift is not a significant problem for serial scan studies, since the true densities can be determined from the known densities of the scanned standard.

The major inaccuracy in quantitative CT is the beam hardening artifact which is the error in the measurement of the true linear attenuation coefficient caused by the polyenergetic x-ray beam (Brooks and DiChiro, 1976). Linear attenuation coefficients depend on the composition of the tissue components and the photon energy distribution of the x-ray beam. Hence, an object measured with two different x-ray spectra will give two different linear attenuation coefficients. This is further complicated by the fact that the energy spectrum that exists at an interior point of the scanned object is not the same as that which emerges from the x-ray tube (Joseph and Spital, 1978). The reason for this phenomenon is that all substances attenuate low energy x-rays more strongly than high energy ones. The strong absorption of low energy x-rays leaves remaining rays of the heterogeneous beam which contain a greater proportion of high energy rays. The beam is now more penetrating or "harder". The end result is that the path integral of attenuation is a non-linear function of distance, even for a uniform substance. This spectral non-linearity creates a distortion of scan projection which mainly affects bone imaging by reducing its attenuation coefficients (Brooks and DiChiro, 1978). There are few types of beam hardening corrections: Preprocessing, which includes prefilteration and scanning in a water bath, which mitigates but not eliminates beam hardening artifacts (Brooks and DiChiro, 1978). Post-

processing, which is a second order correction procedure to correct the measured projection data ray by ray in order to reconstruct a second, corrected, CT image (Joseph and Spital, 1978; Robertson, 1983). Dual energy and mono-energy (radionuclides) methods which use different energy sources to eliminate beam hardening artifacts (Alvarez and Macovski, 1976; Avrin and co-workers, 1978; Ruegsegger et al., 1978, 1980; Boyd and associates, 1979; Hemmingsson et al., 1986).

Quantitative CT assessments include the determination of bone mass, apparent density and geometrical sizing. Some authors used various methods involving CT measurements to evaluate the bone mineral content of human bones in normal and pathological conditions (Reich et al., 1976; Genant and Boyd, 1977; Bradley, 1978; Orphanoudakis, 1979; Cann and Genant, 1980; Banks and Stevenson, 1986). Other studies aimed at mass and geometrical assessments in long bones using the CT method. Blanton and Biggs (1968) used CT to determine the density of fresh and embalmed human compact and cancellous bone. Huang and Wu (1976) and Huang and Suarez (1983) used CT to evaluate the cross-sectional geometry and mass density distributions in the human body. Mayott, Langrana and Alexander (1983) calculated area and mass properties along the entire length of long bone utilizing CT scans.

Recently, some workers used the computed tomography in bone modelling process (see Section 1.3).

Huang and co-workers (1980) reported on a discretization procedure of a whole body model which can be used for finite element analysis. Woolson and co-workers (1984) developed a stereoscopic technique to display a three-dimensional image of bone, using a series of CT cross sectional scans. Nelson and co-workers (1985) used CT scans to reconstruct the three-dimensional anatomy of a human femur and used it as input to a computerized implant design program. Garg and Walker (1985) used computed tomography for two-dimensional finite element model of tibial implant components.

In conclusion, computed tomography is the best method available for performing non-invasive bone density and geometry measurements. The high resolute consecutive cross-sectional images obtained by scanning a long bone can be utilized for generating a three-dimensional finite element model of the bone.

1.5 Objectives

The objective of this study is to develop a computer aided analysis method which, together with a finite element program, determines the stress-displacement pattern in a long bone section, utilizing a computed tomography (CT) data file for the geometry and radiographic density information. The geometry, together with mechanical properties and boundary conditions, loads and initial displacements, comprise the input to the finite element computer program. The output of the program is the stresses and displacements in the bone.

Human bones are complex structures in geometry and composition. For such structures, numerical procedures such as the finite element method, are often the best way to realistically analyze stresses and deformations. One of the major difficulties in utilizing finite element methods in bone stress analyses has been accurately determining the geometrical and mechanical properties of these structures. Previous two- and three-dimensional finite element analyses of bones used various methods of physical measurements and x-ray radiographs in order to determine the model boundaries. The bone properties, elastic modulus and Poisson ratio, have been empirically evaluated for the regions of cortical and trabecular bone. These finite element models were limited in generality and accuracy and the wide range of long bone finite element stress analysis results in the literature emphasize the need

for an improved modeling method.

In this study, a CT data file will be used to provide the bone geometry, and the CT radiographic density will provide the elastic modulus. The CT method is an excellent approach for this purpose for several reasons:

A. There is very little distortion between the bone section and its CT images.

B. CT images are stored in digital format; therefore, no analog to digital conversion is needed when relevant data is extracted from CT cross-sectional images.

C. The CT image of a cross section has a spatial resolution in order of one square mm. This relatively high spatial resolution is adequate for generating a finite element model of bone.

D. The radiographic density information (CT numbers) of the image pixels can be related to the mechanical properties of bone. This provides the finite element model with the elastic properties necessary for the stress analysis.

E. The CT facilities are generally available in hospitals and the current use of the method is safe and routine.

F. The CT method is feasible for determining the in-vivo cross sectional geometry of human bones.

The three-dimensional stress analysis model generated in this study is accomplished by auxiliary software, a pre-processor, for a selected finite element

stress analysis program. The pre-processor reads a CT data file of a scanned long bone section, detects its boundaries and automatically generates a three-dimensional finite element mesh, formatted into a readable finite element input file. The output of the finite element program, the stresses and displacements in the model elements and nodes, will be sorted and displayed by a developed post-processor to provide resultant values of stresses and displacements. The analysis at this stage is limited to the tibia diaphysis (shaft section) since the long bone properties at the epiphysis and metaphysis (the tibia proximal end) are highly anisotropic and difficult to determine by CT methods. The model generation method may be verified by applying the procedures to an object of simple geometry and properties comparing the computer aided analysis results to the analytical solution of the same model with the same boundary conditions. A convergence test may be applied to find the optimal number of selected elements for the three dimensional mesh.

The pre- and post-processors provide an automatic, versatile, non-invasive and relatively accurate tool for long bone modeling and analysis. The processors, together with the finite element program, serves first as an analysis tool towards improved understanding of bone function and remodeling. At this stage, actual long bones, such as load bearing tibiae or femurs, may be scanned and analyzed under applied loads, determined from existing

gait analyses. The stress-displacement patterns thus obtained may be used for studying the biomechanical behavior of specific cases such as long bones with implants or bones with mineral related diseases such as osteoporosis. As a second stage, this processor may be extended to serve as a research and diagnostic tool for analyzing the biomechanical response of a specific patient's long bone by utilizing the in-vivo CT measurements of the specific bone as input to the computer aided automatic stress analysis procedure of this study. A gait analysis study of this patient provides the boundary conditions input required for the analysis. This provides an automatic non-invasive procedure for in-vivo stress analysis of long bones.

2. METHODS

2.1 The Design of Auxiliary Software for a Finite Element Program

The development of pre- and post-processors for a finite element program utilizing a CT data file is a special purpose auxiliary software for the finite element program. The designated processors perform such functions as geometry definition, geometry discretization (mesh generation), model display and verification, model editing, node and element renumbering as well as load and boundary condition definition, and result interpretation.

Several commercial organizations are developing and marketing software packages aimed at finite element manipulations. The development of such commercial pre- and post-processors directed research efforts to some fundamental points associated with mesh generation such as algorithms for geometry definition, discretization of irregular shapes and a newer subject, grid optimization. Some packages attempt a large measure of generality while others are designed with special load requirements in mind.

The process of model definition in preparation for a finite element analysis, comprises several distinct stages. First, a mathematical definition of the geometry is accomplished, and then the discretization process may

be carried out. In creating the geometrical model, mathematical methods for the representation of curves and surfaces in three dimensions typical to those used in computer aided design may be employed. Mathematical methods such as the "Bazier method" of surface representation in parametric form, and methods based on "spline functions" involve the fitting of a piecewise continuous curve through a finite number of points in space (Gordon, 1971; Cavendish, 1974; Durochen and Gasper, 1979; Kamel, 1980). The second stage of the mesh generation employs mathematical methods for the automatic subdivision of complex geometrical configurations. A typical example is the case of three-dimensional solid continua, where a volume, bounded by continuous surfaces, may be subdivided into a number of tetrahedron or brick-type elements.

It was mentioned before that model creation involves both, mathematical definition in continuous form and subsequent discretization into finite elements (subspaces). The procedure by which this may be accomplished is not unique. One way is to proceed from a continuous curve directly to a discrete surface form without necessarily providing a continuous surface definition. Another approach evolves from disregarding the natural geometrical hierarchy, and proceeding directly to the definition of the surfaces in continuous form.

Auxiliary software packages such as PATRAN and SUPERTAB pre-processors utilize the above mathematical

procedure to generate a three-dimensional finite element model. The model generator allows the user to define the geometry of his model with points, lines, arcs, splines, edges, surfaces and volumes. The resultant continuous surfaces and volumes are then subdivided by the mesh generator to define nodes and elements.

In this study, the model geometry of a long bone section is defined using a given (scanned) set of pixels. The high resolution pixel data of the scanned bone carry radiographic density information (CT numbers) in addition to the geometry information. The large number of approximately one by one mm pixels, which comprise the scanned cross sectional images of the bone, yield discrete and still very accurate surfaces. Utilizing a commercial mesh generator to form continuous surfaces, which will then be subdivided back into the discrete format of three-dimensional mesh, is not applicable without losing the CT radiographic densities of most of the image pixels. The radiographic densities of the image pixels are used in this study to calculate the elastic moduli of the three-dimensional elements in the model.

A special purpose mesh generator was developed as a part of the pre-processor CTPRO to generate the finite element discrete mesh directly from the discrete image obtained from the reconstructed cross sectional pixel images. Avoiding the definition of continuous surfaces as a preliminary stage for the model boundaries definition

permits a later use of the radiographic densities of the image pixels. In addition, this procedure avoids discrete-to-continuous and continuous-to-discrete conversions which saves computations and increase the accuracy of the generated model.

The designated auxiliary software for the SAP IV finite element program includes the pre-processor CTPRO which reads a CT data file of a scanned long bone, and creates a three-dimensional finite element model, used as an input file for the finite element program. In addition, a post-processor POST was developed to search and sort the stress analysis results in the SAP IV output file to print and display the resultant stresses and deformations at desired locations. A block diagram of this procedure is displayed in Figure 1.

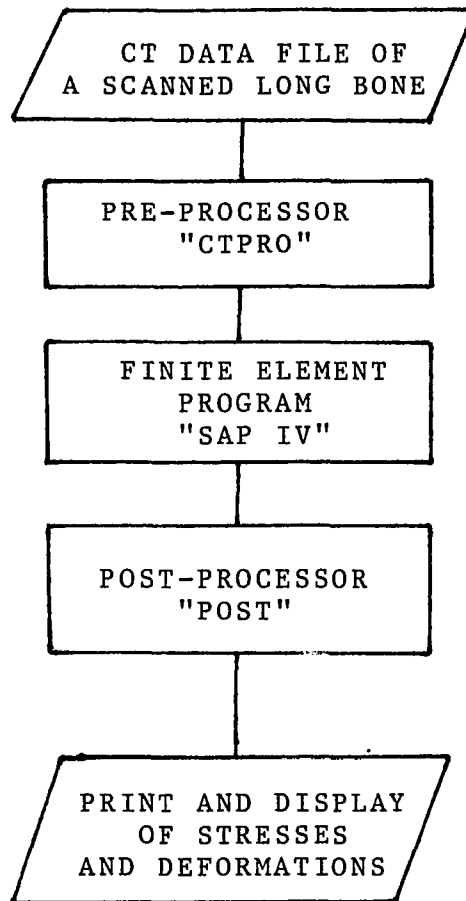


Figure 1: A General Block Diagram of the Designated Auxiliary Software for the FE Program

2.2 Scanning a Long Bone

A male human tibia was dissected out of an embalmed cadaveric limb at the Orthopedic Research Department of New Jersey Medical School in Newark, New Jersey, in March 1984. The tibia was separated from the femur and the fibula and cleaned of external soft tissues. The tibia was scanned in April 1984 by a General Electric CT/T 8800 scanner at the University Hospital, New Jersey Medical School.

2.2.1 Preparation for Scanning

A plastic container was prepared to assemble the tibia during scanning. Two steel wires with a diameter of 0.7mm were assembled in parallel along the longer dimension of the plastic container with a distance of 38.0 ± 0.5 mm between them. The wires were used as a geometric reference in order to verify the bone dimensions calculated from the scanned cross sectional images. The tibia was assembled in the plastic container parallel to the pair of steel wires (Figure 2). The container was filled with water which surrounded the bone to minimize the beam hardening effects in the cortical bone scanning. The water container, including the tibia, was placed on the moving table of the CT scanner with the long axis of the bone aligned with the scanner table motion direction. A "standard" phantom of Dipotassium Hydrogen Phosphate

(K_2HPO_4) was scanned together with the bone to later determine the relationship between the CT radiographic densities of the scanned image pixels and the apparent densities in the bone (Cann and Genant, 1980). The "standard" which consisted of four plastic cylindrical containers with K_2HPO_4 solutions in the amounts of 0, 249, 332, 415 gr/liter, was mounted in parallel to the water container on the scanner moving table (Figure 3).

A typical reconstructed cross sectional image as described, including the bone cross section surrounded by water, two dots indicating the parallel steel wires which were perpendicular to the cross sectional images, and four circular cross sections of the standard solutions (Figure 4). The bone, the container, and the standard were assembled to the scanner table in a manner which prevented sliding of the scanned bone due to the table motion during the scanning procedure. The consecutive cross sections were viewed and scanned by the control graphic terminal of the CT/T 8800 scanner (Figure 5).

2.2.2 Scanning Procedures

A General Electric CT/T 8800 scanner was used for this study. The CT scan data are produced using a dedicated Data General S/200 ECLIPSE mini-computer with 256 Kbytes of memory, a 50 Mbyte disk and an 800 byte-per-inch (BPI) tape drive. The scan data are stored in the main memory and then transferred to the computer disc. The disc can store the data of approximately 300 cross



Figure 2: The Container Assembled With the Steel Wire Indications and the Tibia

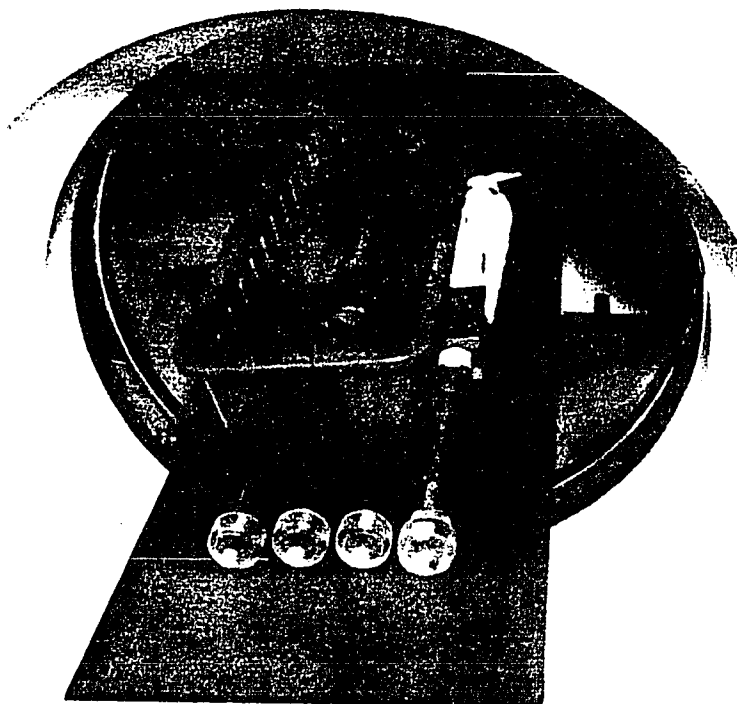


Figure 3: The Assembled Container With the Tibia and the Standard on the CT Scanner

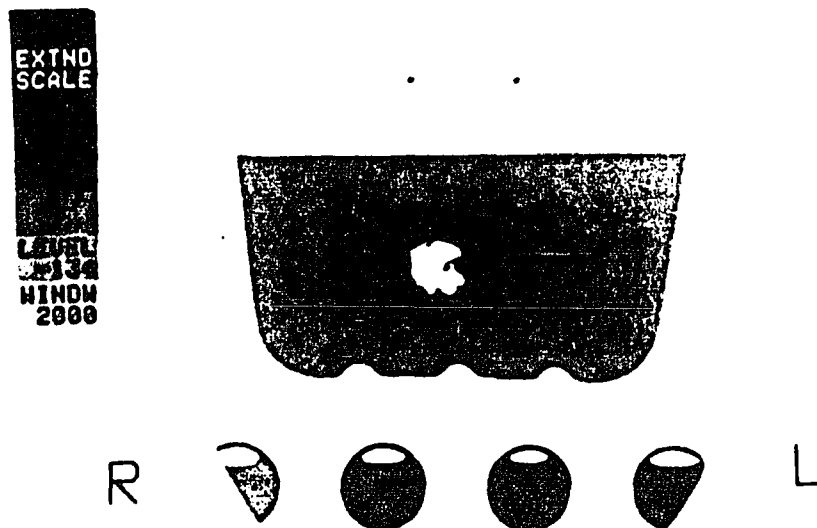


Figure 4: A Typical Scanned Cross Sectional Image of the Tibia, Container and Standard as Obtained by the CT/T 8800 Scanner

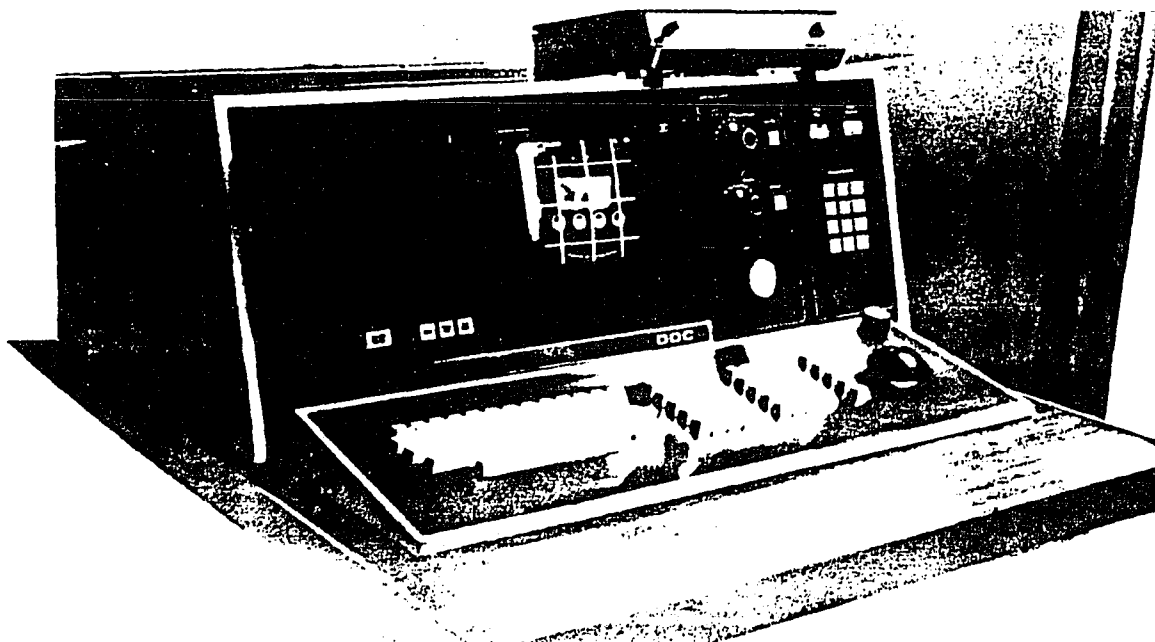


Figure 5: The Control Terminal of the CT/T 8800 Scanner During the Tibia Scanning

sectional images of about 100,000 pixels each, before it is archived onto a magnetic tape. Scans can be viewed on a separate graphics terminal directly connected to the CT system.

The CT/T 8800 scanner provides high spatial resolution in the scan plane, simultaneously with high resolution perpendicular to the scan plane due to its relatively narrow nominal 1.5mm slice thickness (CT/T continuum; evaluation criteria, 1980). The spatial resolution of the scanned images in this study provided 0.8 by 0.8mm pixels by the selected "Head" scan option of the CT operator. Each scanned cross sectional image consisted of 61,284 image pixels of 0.8 squared mm (Appendix C).

The tibia, together with the "standard", were scanned, using the automatic scanning procedure, starting at the proximal end, scanning cross sections in designated spaces of 2.5mm towards the tibia midshaft. The first data file produced, containing 44 scanned cross sections, was processed by the ECLIPSE computer and archived onto a magnetic tape. A bone section, 110mm long, containing the proximal tibia section, was stored on this tape in the form of 44 equally spaced cross sectional images in terms of digital information. This digital information, together with other parametric information stored in the tape directories, permit later reconstruction of the scanned images. The pixel data (CT numbers) indicating

the pixel radiographic densities, are represented in the CT data file by positive integers in the range of 0 (for air) to 4095 (for maximum density cortical bone). These integer values are stored by the ECLIPSE computer in two-byte words, each byte consists of 8 bits.

The CT output data file is formatted on the tape in 4096 word physical records (blocks) which are organized in consecutive files, separated by end-of-file marks. The first is a tape directory file, followed by a dummy file of approximately 30 inches length of blank tape, followed by a number of display files. The file organization allows retrieving and reconstructing scanned cross sectional images by the ECLIPSE software routines which are used for displaying and examining a scanned object from an archive tape on the scanner graphic terminal.

A typical CT archive tape consists, in general, of two main parts: tape directories and display files (Appendix A).

A. Tape Directories

Contain information on the display data files and consist of a main tape directory and display file directories.

B. Display Files

This section contains several display files, each consist of a file header and the CT data of up to 45 slices, each slice starts with a slice header.

The file header contains information regarding the display file, such as the number of slices and thickness, pixel size, x and y diameters of the reconstructed area and more details used for later reconstruction and display of the scanned object. The slice header contains information regarding the given slice, such as its number and relative location. The image pixel data, CT numbers are stored next to the header in 2-byte words, one word for each pixel. This information occupies the major part of the CT archive tape.

Appendix B includes the tape and file directories of the scanned tibia as printed out by the developed pre-processor CTPRO.

2.3 Designating a Pre-Processor for the Finite Element Program

The main task of the pre-processor is to read a CT data file of a scanned long bone section and create a three-dimensional finite element model (mesh) which is formatted to use as an input file for a selected finite element program. The pre-processor CTPRO consists of the major program sections as follows and shown in Figure 6:

A. Image Reconstruction and Display

The cross sectional images are reconstructed by computer routines and displayed by the VAX/11 line printer. The displayed cross sections are used to examine the scanned images and design the edge detector and mesh generator.

B. Edge Detector

The cortical (compact) bone boundaries of the scanned cross sections are detected and stored.

C. Mesh Generator

This section includes the routines which create the three-dimensional finite element mesh of the scanned long bone. The mesh consists of nodes and elements which are assigned with material elastic constants.

D. Model Display

Two-dimensional plots of the model cross sections and three-dimensional display of the bone section model are produced for user examination of the model.

E. Generating a Finite Element Input File

The mesh information of the three-dimensional model is formatted to create an input file which can be read by the selected finite element program according to the program requirements.

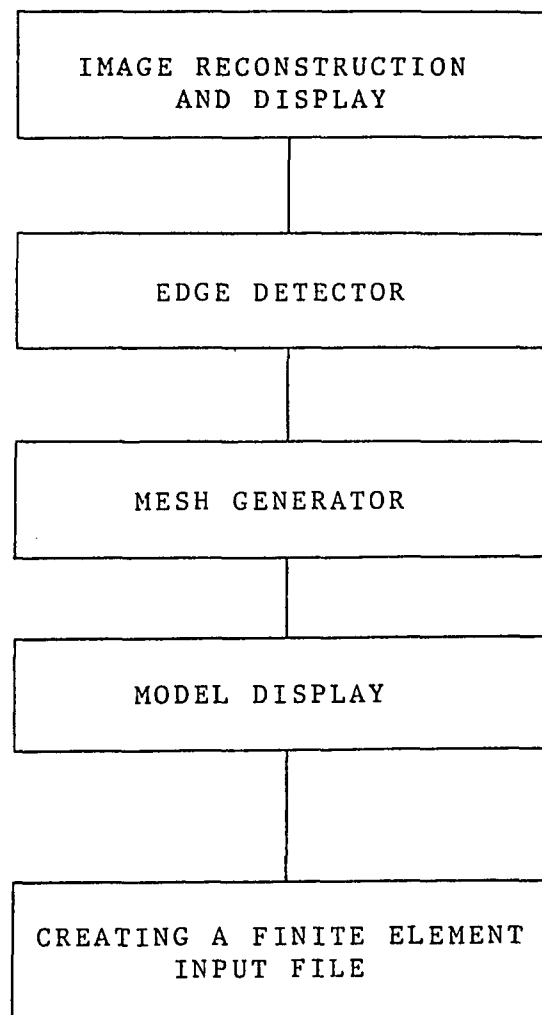


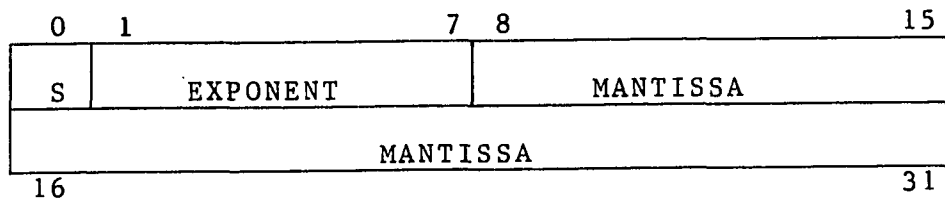
Figure 6: A Block Diagram of the Designated Pre-Processor CTPRO

2.4 Reconstruction and Display of the Scanned Cross Sectional Images

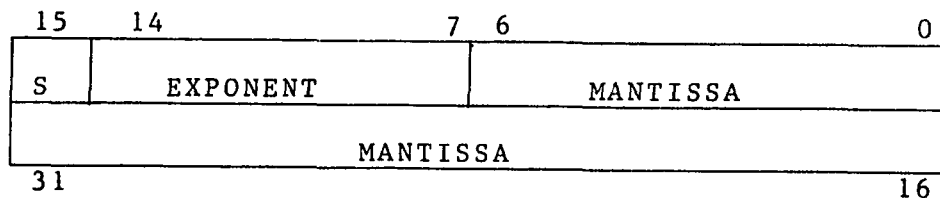
In order to create a finite-element mesh based on the CT file pixel information, a necessary step of reconstructing and displaying the cross sectional images was undertaken. The CT computer procedure is capable of displaying the images on the CT graphic terminal by computer routines which exist in the ECLIPSE computer. The VAX/11 780 mini-computer at the Department of Mechanical Engineering, New Jersey Institute of Technology, was used for the analysis in this investigation. The CT archive tape of the scanned tibia was translated into data storage density of 1600 Bit per Inch (BPI) in order to be read by the VAX tape drive. The usual procedures used for such translation were not accomplished at the NJIT Computer Services Department facilities, probably because of the large size records of information or incompatibility between the two tape drives. The tape was finally translated to 1600 BPI by using different facilities which permit using improved routines for such translation.

The translated CT output file, now on the VAX tape, contains information in a format organization which is specific for the ECLIPSE computer. Integer and floating point data are represented in the ECLIPSE environment in a way that they cannot be simply read from the tape by using usual FORTRAN reading procedures on the VAX computer.

The CT output file contains text information, such as names, dates, and other literal values in ASCII character codes, integer values, such as the CT pixel data, and floating point values such as the pixel size and the x and y diameters of the image reconstruction area. A substantial amount of effort was required in order to find, by trial and error, that the order of the two bytes had to be changed in each word stored by the ECLIPSE computer in order to be compatible with the VAX data storage organization. This conversion had to take place for each two-byte word in the CT data file which is not an ASCII character code, and was performed by library circular shift routines which were used as subroutines in the pre-processor CTPRO. By these routines, for each 16 bit (2 byte) word, 8 bits were shifted out from one end and inserted back in the other end in circular shift. This conversion permitted the reading of the integer data values by FORTRAN reading routines. The floating point values still had to be further converted by similar library bit-shifting routines in order to be readable by the VAX. The ECLIPSE floating point representation consists of a pair of two-byte words as follows:



The VAX floating point representation is as follows:



The significant difference between the two floating point representations required creating a conversion routine to be applied to each floating point value read from the CT data file. The CT data, integer and floating point values has now been revised to a format as required by the VAX computer.

The CT data of any cross sectional image are stored in 256 word records and may reconstruct 320 image lines. The number of pixels in each of the 320 reconstructed lines is determined by the "MAP" array which can be calculated by the values of the following parameters, stored in the file header:

- the pixel size
- the x diameter of the reconstructed area
- the y diameter of the reconstructed area

The MAP array contains 320 entries (one word for each image line) where each entry equal one half the number of pixels reconstructed for that line. The reconstructed image line is symmetrical about an imaginary center line between picture elements 160 and 161 (Figure 7). For example, assume that the pixel values in the image data file consist of the sequence of values:

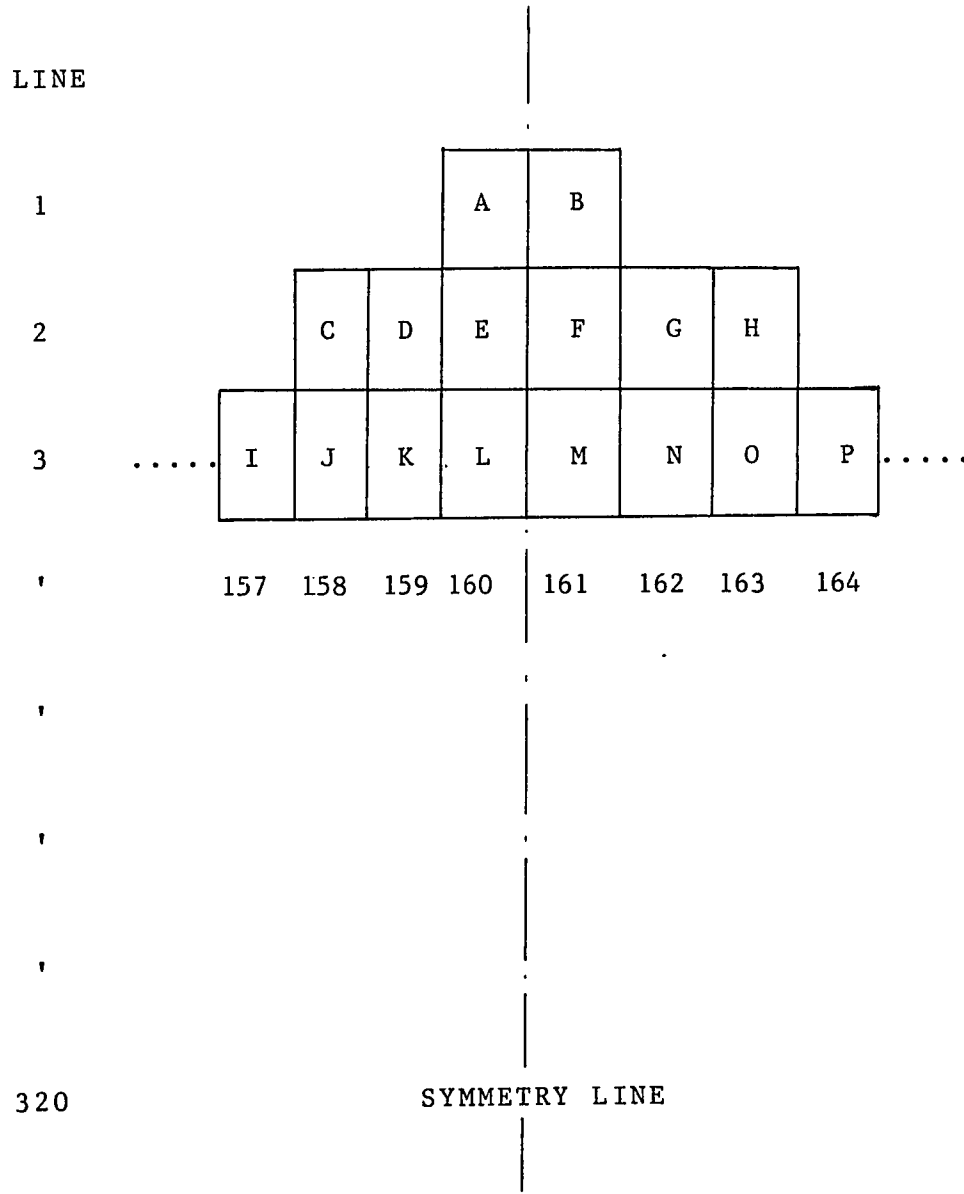


Figure 7: The CT Reconstructed Image Using the MAP Array

A B C D E F G H I J K L M N O P Q ...

If the MAP array contains the following values:

MAP (1) = 1

MAP (2) = 3

MAP (3) = 4

the image will be reconstructed as in Figure 7.

The routine WPIX, developed at General Electric, is used in CTPRO as a subroutine to calculate the values of the MAP array, using the converted display file header information as input for this calculation. The MAP array of the tibia section scanned for this study is given in Appendix C.

In the ECLIPSE environment, the MAP array is used to display the reconstructed image on the CT graphic terminal screen.

In the VAX computer, new computer procedures were developed to display the image using the MAP array. The reconstructed image provides the cross section geometry and the intensity of each pixel of the image, that is its radiographic density, represented by the pixel CT number. The objective of the developed image display routine is to produce image plots which exhibit the pixel densities and the cross sectional geometry. Two methods were considered for this purpose: One was a high-resolution color graphic terminal on which color variations represent the variations in density of the cross section pixels.

The main disadvantage of this method was unavailability of a fast color graphic copier which was necessary for obtaining a hard-copy of the color cross sectional images. The method selected to display the images used the VAX line printer for this purpose. The basic method was to display the image, line by line, using character codes to represent the radiographic density range of each pixel of the image. The printer line contains 132 characters while the size of a reconstructed image line may contain 320 pixels. This requires bounding the bone cross section within each scanned image by a pre-set window. This window bounds only the desired portion of the image and, thereby, eliminates air, soft tissue and other unnecessary data.

The character codes were selected to be numerals where lower values such as "1" represent a lower density range, and higher value numerals represent higher radiographic density ranges of the compact bone. The character code images are versatile in the number of density ranges represented by the pixel character codes, and determined by the control parameter "RANGES" in CTPRO pre-processor. The pre-set window which bounds the displayed images can be designed to bound any desired portion of the scanned image by changing the control values $Nx1$, $Nx2$, $Ny1$, $Ny2$ in CTPRO (Figure 8).

The reconstruction and display computer routine in CTPRO pre-processor is characterized by the following

features:

- A. An adjustable geometric 'window' sets the x and y location of the desired portion of the image display.
- B. The subroutine NCODE assigns a character code "1", "2", etc. to N selected radiographic density ranges.
- C. The user has the option to display any selected number of slices from the CT data file of the scanned bone.

The image reconstruction and display routine (general outline in Figure 9) starts with a subroutine which calculates the MAP array, based on the image file header information. An estimated window size is designated which may later be adjusted to contain the bone cross section. The radiographic densities (CT numbers) of the image pixels are read consecutively in 256 word records into a buffer, limited by the designated window. The image lines of each cross section are filled by character codes which are assigned by the program subroutines according to the CT number of each pixel in the image. The character codes representing pixel data are stored one by one in a character array LINE of a length which is calculated individually for each line, based on the MAP array information. Each image line of characters is printed individually after its formation by the VAX line printer until the image cross section is completed (Figure 10). The maximum number of displayed pixels in each line is limited by the 132 characters a line of the VAX printer. Since the size of the scanned bone cross sections occupied

about 15 percent of the total reconstructed area, the printer character code lines provided a complete image display of each tibia cross section. The image is reconstructed and displayed line by line for a number of cross sections selected by the user (Figure 10).

An additional routine creates a new three-dimensional matrix $NCT(K,L,M)$, which organizes the CT numbers of the image pixels (bounded by the designated window) by their location: cross section (K), Line (L), and pixel location in line (M). This form of data organization eliminates a substantial amount of unnecessary data of the scanned tibia surrounding and yields a direct access data structure for the next manipulation rather than the consecutive data file obtained from the CT computer which could be accessed only by inefficient searching methods.

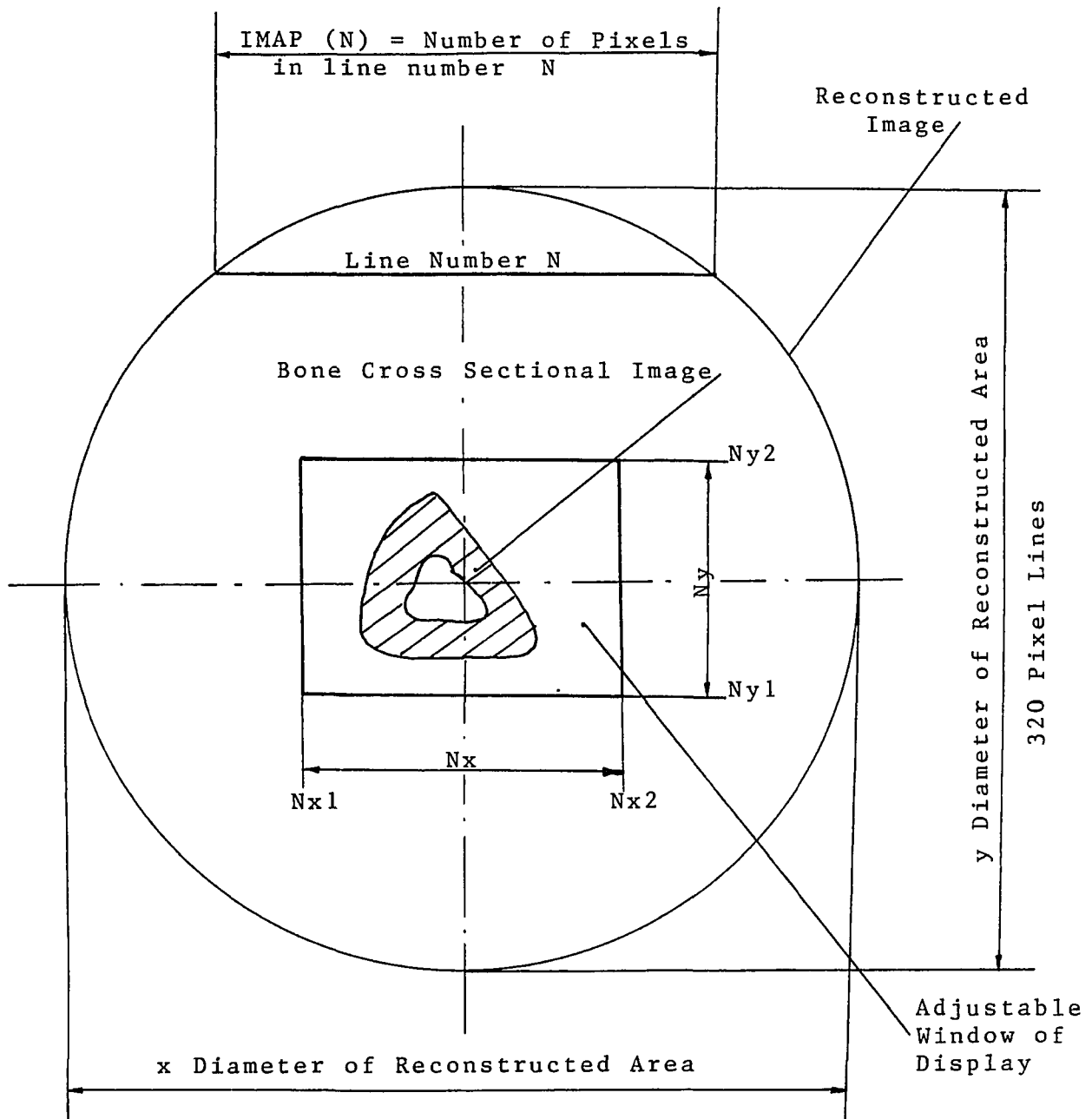


Figure 8: Orientation of Reconstructed and Displayed Area of the Scanned Cross Sectional Image

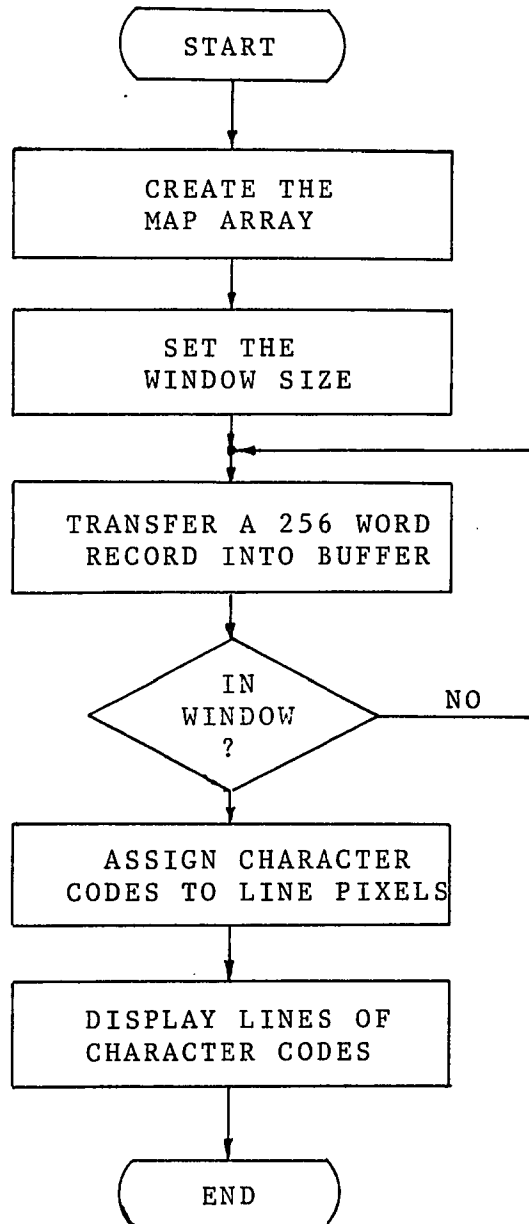


Figure 9: Outline of Image Reconstruction and Display Routine

SCANNED CROSS SECTIONAL IMAGE 42

REAL LOCATION OF CROSS SECTION RELATIVE TO PROXIMAL END : 95.0 [MM]

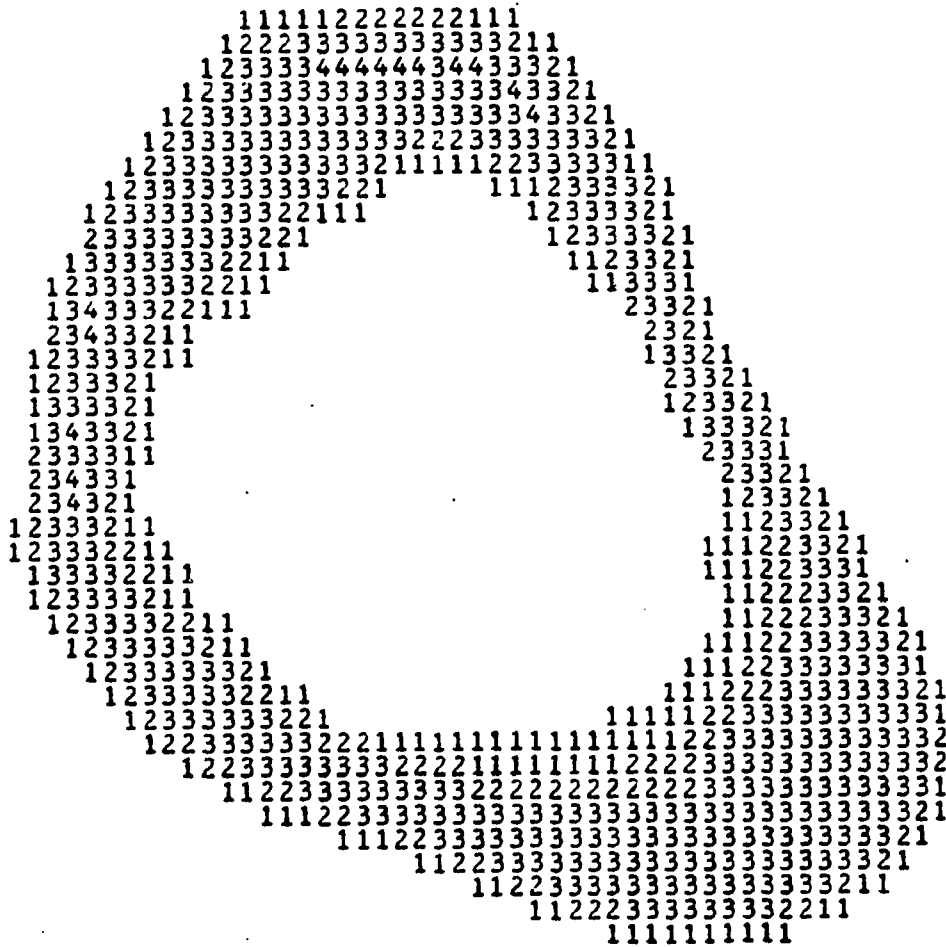


Figure 10: A Character Code Cross Sectional Image Displayed by VAX Line Printer

2.5 The Edge Detector

The displayed character code images are used for several purposes: To observe the cross sections geometry and their local densities in the scanned bone; to adjust the window size of the reconstructed area; to verify the contents of the new CT data matrix $NCT(K,L,M)$; and to design the border detection routine and the mesh generation strategy.

The CT data matrix contains the data of the cross sectional image, bounded by the designated window. The boundaries of the cross sectional images in the window will be detected and stored. Because of the cartesian nature of the image pixel lines, an approach of consecutive, cartesian, first order edge detection routine was selected. For each cross section, the pixels are tested consecutively (x direction), line by line (y direction), in comparison to a selected minimum "compact bone" density. The outside and inside borders of the compact bone zone in each cross section are detected and displayed by this routine. The minimum "compact bone" CT number which indicates the cross sectional borders is selected by the user according to the range of the CT densities found in the scanned bone. The CT numbers of the reconstructed images may be displayed and examined for each pixel using a user-selected option in the program. The CT numbers of air and water are easily deter-

mined from the printed data by comparison with the displayed reconstructed character code images. The characteristic water CT number was 1012 ± 12 , while the characteristic CT number of compact bone, which is not as homogeneous as water, was in the range of 1500-1800. The pixels which are on the border line between the water region and the compact tissue of the scanned image, may, therefore, carry any CT number in the range of 1000 to 1800, depending on the proportions of water and compact bone in the scanned pixel. The compact bone CT number, which is selected by the user, determines which border

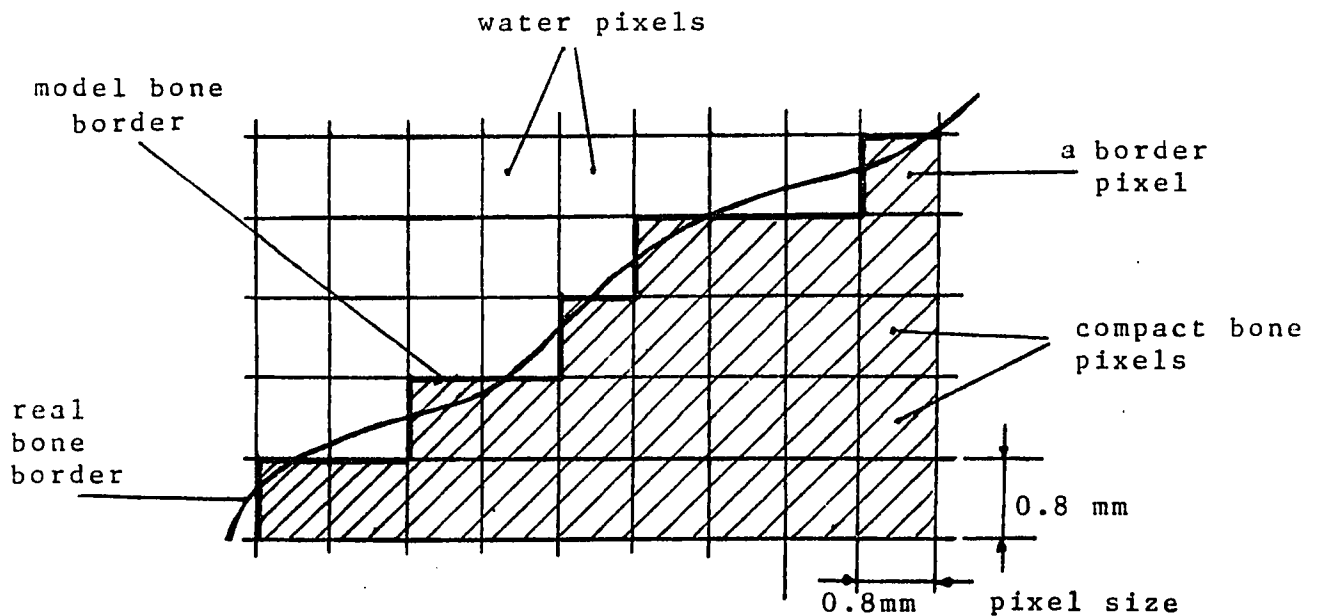


Figure 11: The Cross Section Borders set By the Edge Detector

pixels are excluded, included or partially included in the designed model (Figure 11). The suggested minimum compact bone CT number, which was used in designing the model in this study, was taken as 1500 to include the entire compact bone in the model. The typical shape of the bone cross section consists of two concentric border loops, which bound the compact bone zone in between. Therefore, the error of excluding a valid pixel from the model due to the selection of a minimum compact bone CT number can occur, at most, four times along any reconstructed image line (twice at each border loop). The pixel size of the scanned image in this study was 0.8 mm, while a typical cross section line consisted of about 60 pixels at the diameter. Therefore, the maximum possible error in the bone cross sectional area due to the minimum compact bone CT number selection is:

$$\text{ERR} = \left(\frac{A - A_o}{A} \right) (100) \quad \text{percent}$$

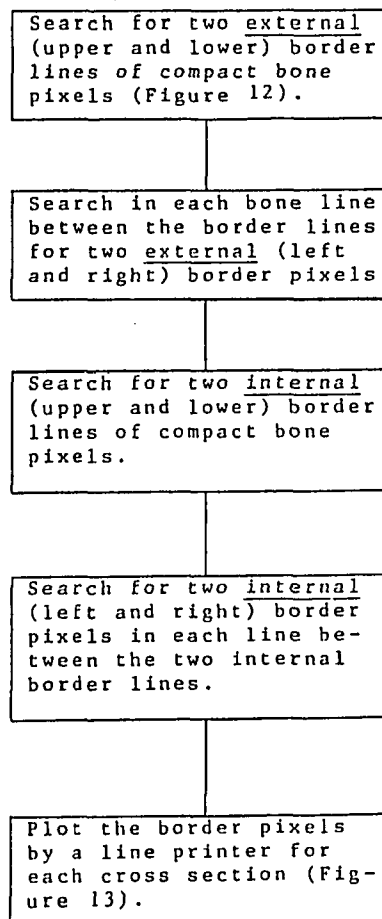
$$\text{where: } A = \left(\frac{N \cdot S - 4 \cdot S/2}{2} \right)^2 \quad \text{the maximum possible area}$$

$$A_o = \left(\frac{N \cdot S}{2} \right)^2 \quad \text{the nominal area}$$

where N is the number of pixels in a typical cross sectional image diameter and S is the pixel size. The maximum calculated error in the cross sectional area is 1.1% and considered negligibly small in a finite element model. Moreover, since the mechanical properties of the model elements will be calculated later based on the CT

information of all the pixels within the compact bone borders, the error in the stiffness due to including a half-bone-half-water pixel in the model is decreased by including also the relatively low radiographic density of this pixel in the calculation of the average elastic modulus of the model. The relatively low modulus assigned to this pixel compensates the geometrical (stiffness) error due to including it in the created model.

The edge detector algorithm in CTPRO pre-processor consists of the following major steps which are applied on each cross sectional image:



The border detection algorithm uses sequential search procedures which are applied in four directions: -x, x, -y, and y, detecting towards the center of the image. The detected border pixels are filed for later manipulations and plotting. The internal and external circumferencial borders bound the compact bone zone in each detected cross section eliminating air, water, soft tissues and spongy bone in the scanned image. This procedure is performed for each cross sectional image with the user option to skip on selected cross sections which will not participate in the designated three-dimensional model. The border detector consists of a main procedure and four searching subroutines for detecting each pixel line in forward (+x) and backward (-x) direction, and for detecting the external and internal border pixels.

The detected bone edges were displayed by the node plotting routine which uses the asterisk character (*) to indicate the border pixels. The routine utilizes the VAX line printer to obtain a hard copy of the cross section borders. The node plotting routine was developed to display the selected finite element nodes of the model and will be explained after the node selection routine section.

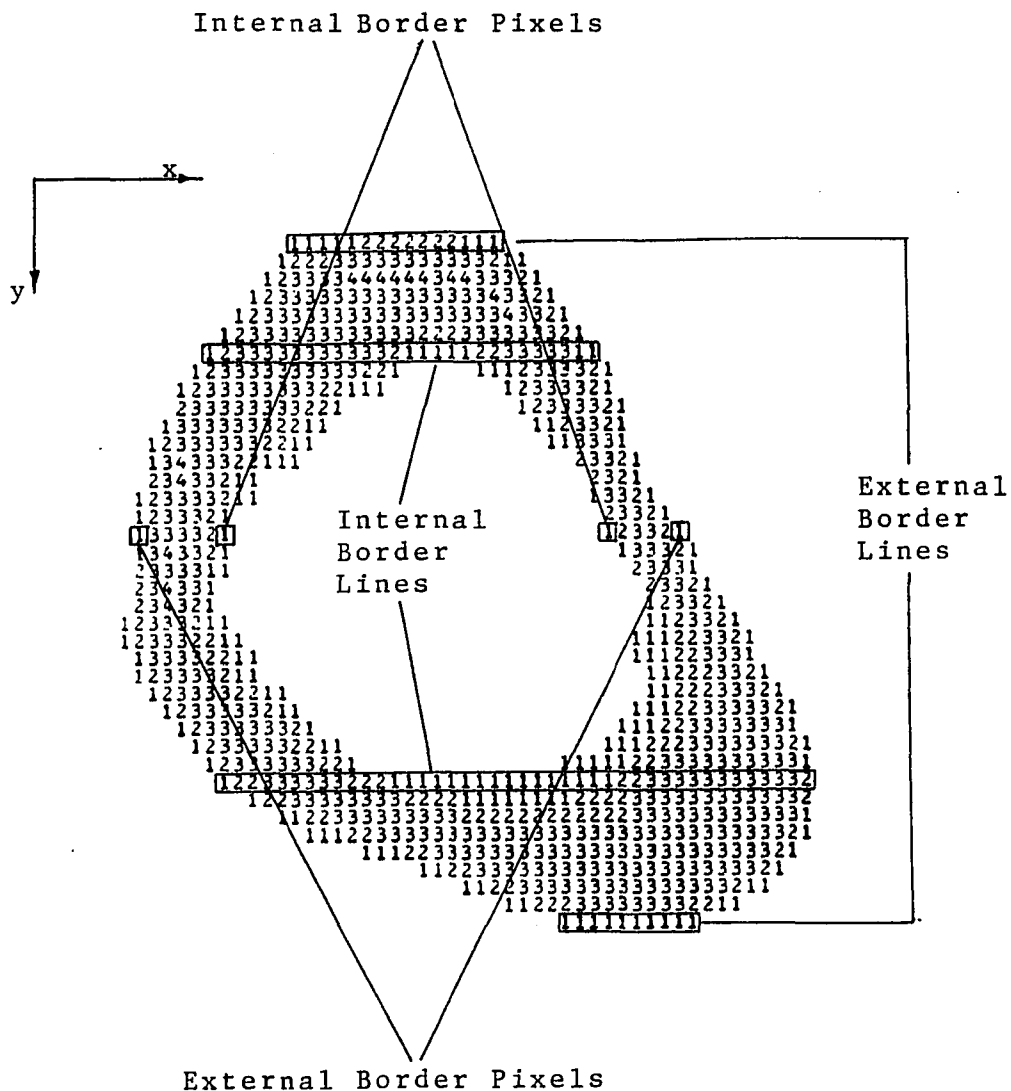


Figure 12: The Cross Section Borders as Defined in the Edge Detector

REAL LOCATION OF CROSS SECTION RELATIVE TO PROXIMAL END : 60.0 [MM]

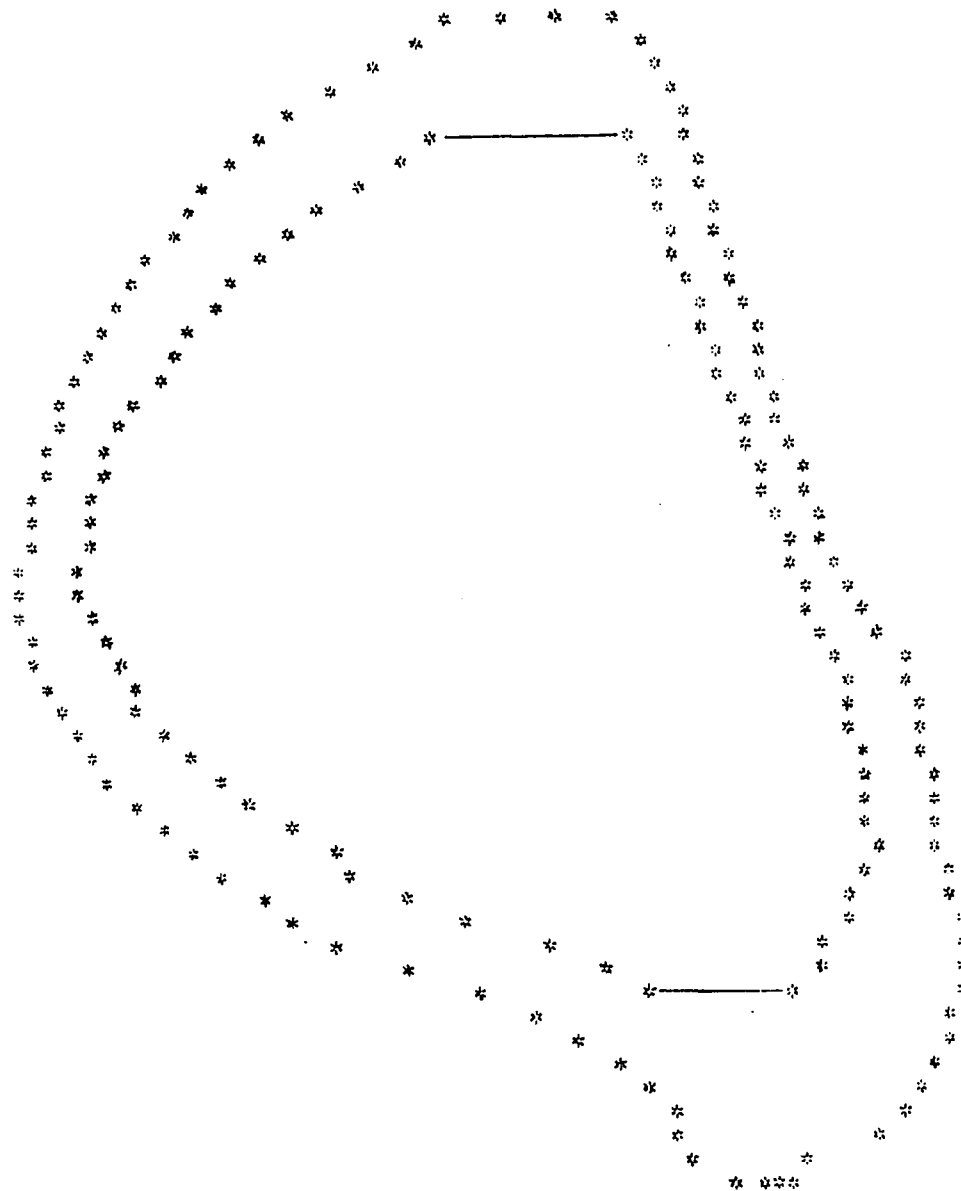


Figure 13: The Borders of a Typical Long Bone Cross Section as Determined by the CTPRO Edge Detector

2.6 The Mesh Generation Strategy

The algorithms which reconstruct, bound, detect, code and plot the cross sectional images provide the display which assists in the design of mesh generation strategy for the finite element model.

A mesh generator is basically a set of computer procedures which discretize given object geometry into a finite element mesh acceptable as input by a finite element program. The mesh is generated in terms of nodes which are defined by their geometrical location in a global coordinate system, and by elements which are directly defined by these nodes. The elastic properties needed for creating the stiffness matrix in the FE program are assigned to the model elements by the mesh generator.

Commercial automatic mesh generators, such as the pre-processors of ANSYS, PATRAN, and SUPERTAB finite element packages, use mathematical methods to define a continuous boundary function of the analyzed model by a given set of points, lines, arcs, curves and surfaces. The two- or three-dimensional model geometry is then discretized by computer procedures to define the model mesh. Such software packages include an element library for the selection of elements geometry (triangular, rectangular, brick, tetrahedral and more). The mesh refinement can often be selected by the user to control the model resolution and accuracy.

As mentioned in Section 2.1, the use of such commercial mesh generators in this study will be inadequate because of the specific structure of the CT cross sectional images. These images consist of pixel matrices which carry CT numbers representing the radiographic density of each pixel. This arrangement yields a discrete structure of 0.8 by 0.8 mm pixels which may be discretized directly into a finite element mesh skipping the usual necessity of continuous geometry definition prior to the discretization stage. The mesh cannot be generated as if it were a continuous and homogeneous structure without losing at least part of the pixel information which is used as an important indication of the local elastic moduli in the model elements. This was the main reason for developing a special purpose mesh generator to create the three-dimensional mesh rather than using a commercial mesh generator for this purpose.

The design of the mesh strategy in this study may be characterized by the following guidelines:

A. The scanned bone section is modeled in the form of a three-dimensional finite element mesh.

B. The mesh may be generated automatically for any bone scanned by the CT/T 8800 scanner.

C. The model size, as well as the mesh refinement, may be determined by the pre-processor user.

D. The generated mesh can be formatted into an input file acceptable by a selected finite element program

after checking it by model display routines.

The geometry is given for this model in terms of two-dimensional parallel cross sections; therefore, the method developed first, creates a two-dimensional mesh in each cross sectional image, and as a second stage generates the three-dimensional mesh by connecting the consecutive two-dimensional cross sections. This method requires the definition of a constant number of selected finite element nodes in each cross section that will later be connected to define the three-dimensional elements.

This method of connecting parallel two-dimensional cross sections suggests using prismatic three-dimensional elements formed by connecting the corresponding nodes of each two adjacent cross sections. The other characteristics of the defined elements will be discussed in the section of the element definition routine.

Two approaches were considered for the generation of the two-dimensional mesh in each cross section: Cylindrical and cartesian.

2.6.1 Cylindrical Mesh

The apparently cylindrical shape of the long bone section suggests the approach of dividing each cross section to a constant number of three-node or four-node elements defined by a set of cylindrical coordinates.

By this approach, a center point must be defined for each cross section. This center may be selected as a physical attribute, such as the center of gravity which

may then be calculated for each cross section based on the information of all the bone pixels. The most convenient center point is the axis parallel to the scanner table motion direction. Such an axis may be selected if the scanned bone section is approximately straight, and remain parallel to the table motion during scanning. By this manner, the selected center point will remain around the center of gravity in each cross section. The center point location around the center of gravity in each cross section will form similar size elements for the finite element mesh. The next step would be defining angle steps and discretize the image cross section by arcs and corners into sections which define a two-dimensional "spider net" shape.

The major difficulty in such a procedure is that the pixels are arranged by image lines in a cartesian manner and the pixel data are stored in a three-dimensional matrix which reflects the pixel arrangement of the images in terms of cross sections (K), lines (L), and pixels in the line (M). Therefore, the search for pixel nodes, geometrically formed by cylindrical coordinates, requires conversion procedures for each detected pixel, from cartesian to cylindrical coordinates. The large number of pixels in the model would substantially decrease the mesh generation efficiency, expose the created model to more truncation and roundoff calculation errors and would occupy additional computer memory space.

2.6.2 Cartesian Mesh

The arrangement of image pixel lines which comprise the two-dimensional images and the three-dimensional matrix data storage of the pixel information suggest the approach of cartesian mesh. This approach does not require definition of any geometrical center in the image cross sections. The mesh is generated by defining parallel node lines (the y direction) and then selecting a constant number of nodes in each of these selected lines (in x direction). The selected nodes form four-node or three-node two-dimensional elements in each cross section. This direct approach does not require any coordinate transformations, such as translation and rotation. Each node location is defined in a global cartesian coordinate system parallel to the scanner coordinate system as reflected in the reconstructed images. This method does not require any particular assembly in the bone scanning process and keeping the long bone approximately parallel to the scanner table motion axis is adequate for the formation of the three-dimensional finite element model.

The cartesian method uses the image pixel lines to form the cross sectional mesh. This allows affiliating the procedures which form the cartesian mesh with the routines of the edge detector which sequentially search the image pixel lines to determine the cortical bone boundaries. Such combination of the two routines

increases the efficiency of the mesh generator since the number of searching iterations in the program is decreased. Substantial amount of CPU time is saved by this procedure due to the large number of searched pixels.

2.6.3 The Mesh Generator Structure

The edge detector and the image display routines provide a set of consecutive cross sectional images of compact bone. The designed mesh generator consists of three major sections (Figure 14), which generate the finite element three-dimensional model of the edge detected images. The node selection routine defines and stores the finite element nodes by their location in a global cartesian coordinate system and numbers them. The element definition routine defines eight-node, three-dimensional isoparametric elements of each two consecutive cross sections. The elastic properties definition routine assigns modulus of elasticity and Poisson ratio to each element in the model. The complete model is displayed for user examination and a formatted input file is created for the selected finite element program.

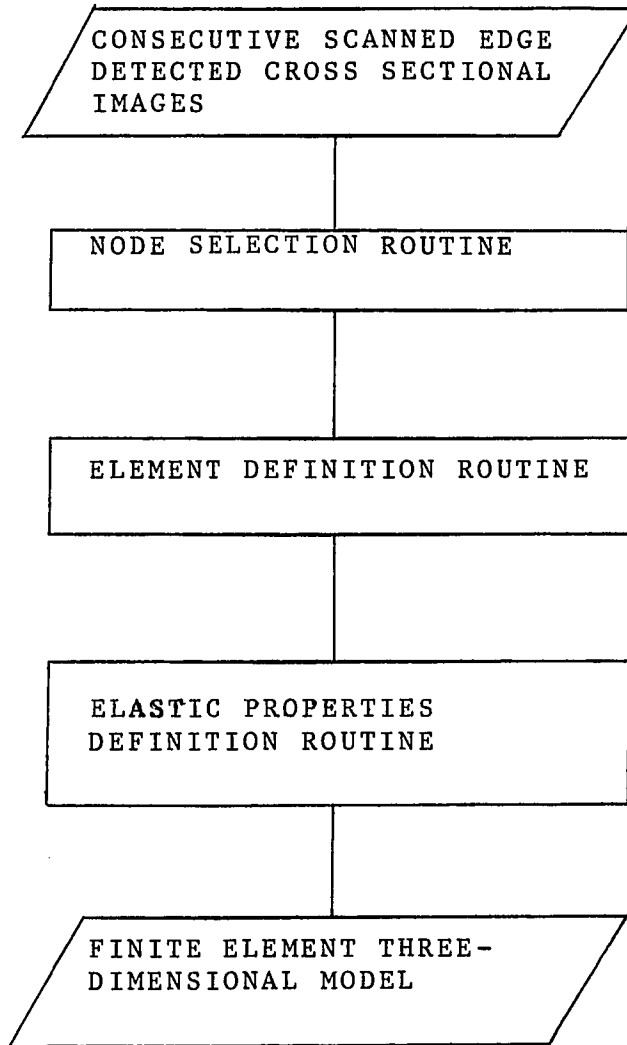


Figure 14: The Mesh Generator:
General Block Diagram

2.7 The Node Selection Routine

This routine is the first section of the mesh generator and its objective is to select and store a user-defined number of finite element nodes in the cross sections. The selected nodes are pixels, defined by their relative location in the image, using a global cartesian coordinate system. The origin of the coordinate system was selected at the upper left corner of the previously designated window which enclosed the borders of the first cross section in the model. The selected coordinate system origin was set for convenience since the window size and location are constant in all the cross sections. By this coordinate system, the image pixel lines are represented top to bottom by the positive y coordinate, the line pixels from left to right by the positive x coordinate, and the consecutive cross sections from first to the last, by positive z coordinate (Figure 15). The pixel data are arranged in a three-dimensional matrix $NCT(K,L,M)$ which reflects the pixel arrangement of the image. Therefore, the coordinate system origin is at the first element of this matrix, $NCT(1,1,1)$.

As mentioned before, the node selection routine is combined with the edge detector for better efficiency. The general step by step description of the routine follows:

A. The desired number of nodes selected in each cross section is set by the user by the "Adjustable Program Parameters" at the pre-processor. The integer values of XGRID, YGRID determine the number of selected nodes in the directions x and y, respectively. Each cross section includes, therefore, a total number of $\text{GRID} = \text{XGRID} \cdot \text{YGRID}$ selected nodes (the nodes are always image pixels).

B. The edge detector routines which have been described in Section 2.6 find two external, upper and lower, border lines (L1, L2) of the compact bone image in each cross section (Figure 16).

C. The range of bone pixel lines (L2-L1) is divided by a discrete dividing algorithm in such a manner that a number of YGRID lines are selected in distances as equal as possible between each other. These lines are the "selected node lines" of a two-dimensional mesh, generated for each cross section.

D. The YGRID number of selected node lines are stored by their line number in an array LINES(LINDEX) with indices computed by the expression:

$$\text{LINDEX} = 1 + (\text{N} - 1) \cdot \text{XGRID}$$

where: N = 1 to YGRID (for each node line).

For example, if the grid selected by the user is:

$$\text{XGRID} = 6$$

$$\text{YGRID} = 12$$

and the external, upper and lower, border lines found by

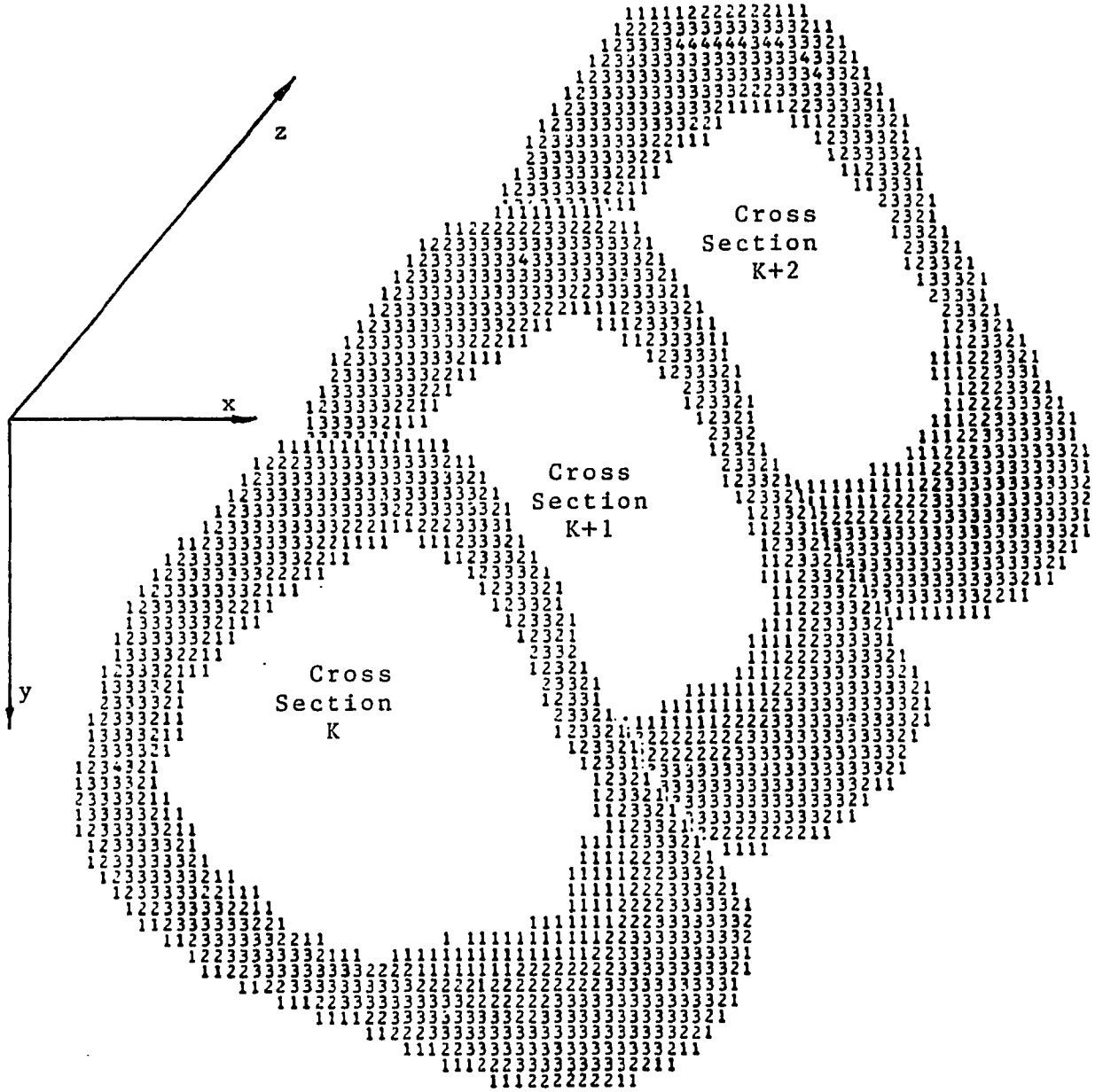


Figure 15: The Global Cartesian Coordinate System of the Finite Element Three-Dimensional Model

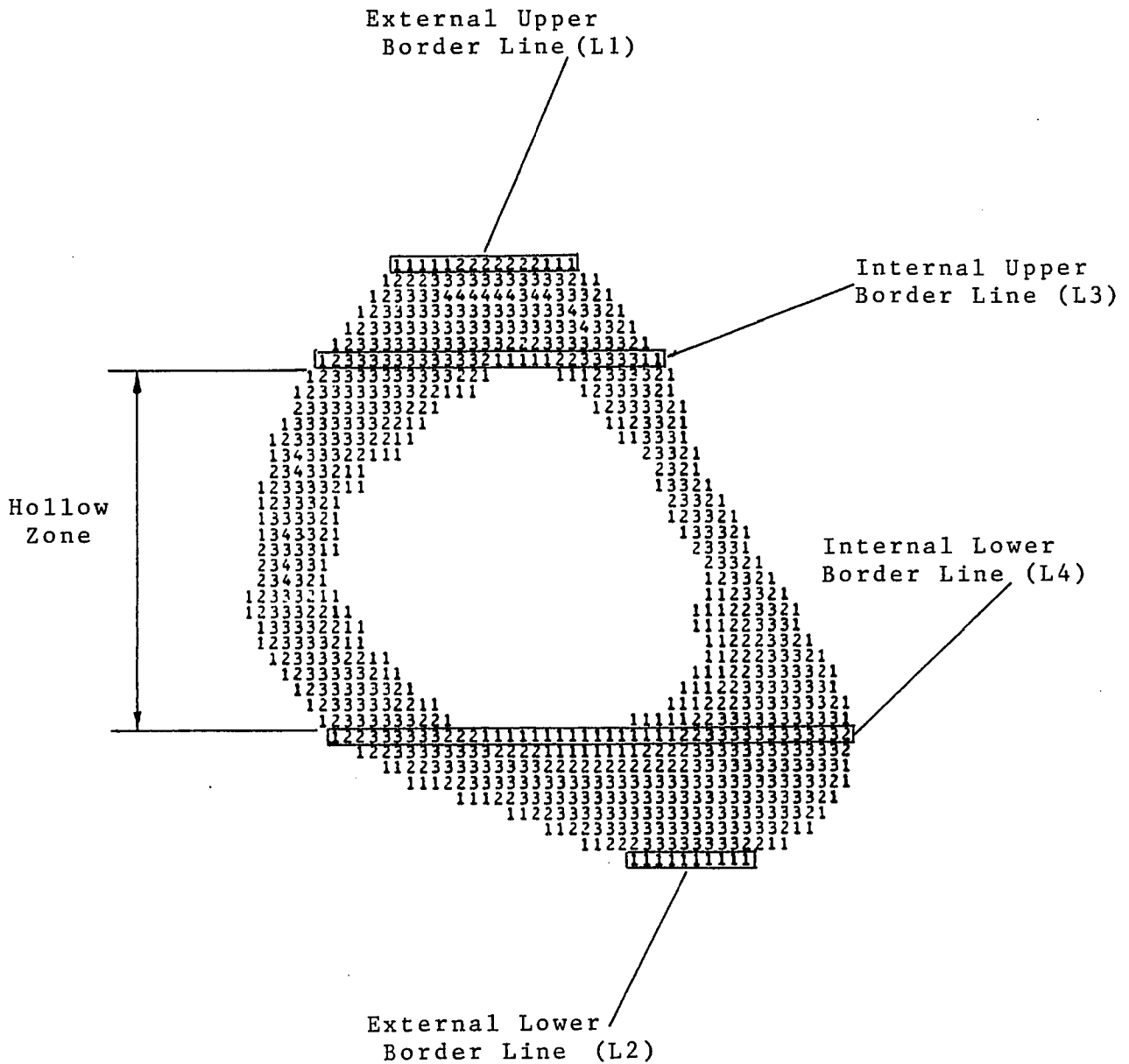


Figure 16: Definition of Border Lines in the Model Cross Sectional Images

the edge detector routines:

L1 = 34

L2 = 73

the selected node lines are determined by the discrete division algorithm and the indices are computed by the LINDEX expression to form the LINES array:

LINES(1) = 34

LINES(7) = 38

LINES(13) = 42

,

,

,

LINES(66) = 70

LINES(72) = 73

This method of data structure is inherent with the node numbering method which provides a systematic procedure for the definition of the model elements and explained later.

E. The edge detector routines find two internal, upper and lower, border lines (L3, L4) of the compact bone image (Figure 16). The detected internal border lines do not necessarily lie on the selected node lines determined by the discrete division algorithm. Therefore, another routine corrects the contents of the LINES array by inserting the two internal border lines instead of the closest adjacent selected node lines in each cross section. The LINES(LINDEX) array now contains the internal, upper

and lower, border lines in terms of "selected node lines", to ensure that the internal compact bone boundaries will not change by selecting a different set of x-y grid.

F. The number of YGRID selected node lines have now been obtained. Applying the forward and backward search routines of the edge detector on each selected node line defines the border nodes on the boundaries of the cortical bone image (Figures 12, 16). In the hollow zone, between the internal upper and lower border lines, four border nodes are found and stored in each selected node line, while in the rest of the bone only two external border nodes are defined in each line.

G. Each selected node line is now divided by a discrete dividing algorithm in such a manner that a number of XGRID nodes are defined in distances as equal as possible between each other in the cortical bone zone of each node line.

H. The above steps are applied on each selected cross section comprising the model, and are numbered by $K = 1$ to $KTOT$.

I. An automatic node numbering procedure assigns the index for each selected node in the model by three nested iterative calculations. The "node index" N is a function of the node location (K,L,M) in the global cartesian coordinate system and calculated by the following expression:

$$N = (K - 1) \cdot KFACT + (L - 1) \cdot XGRID + M$$

where: $K = 1$ to $KTOT$ is the cross section number
(z direction)

$L = 1$ to $YGRID$ is the node line number
(y direction)

$M = 1$ to $XGRID$ is the pixel number in line
(x direction)

The factor $KFACT$ is selected, fulfilling the
condition: $KFACT \geq XGRID \cdot YGRID$

Selecting a round integer such as 100 or 150 for the $KFACT$ value allows faster check to verify the obtained node numbers. However, $KFACT$ is selected only slightly larger than the above expression since its value determines the node index and the size of the node matrix which is related to the required computer memory space.

The selected finite element nodes are stored in a two-dimensional matrix of integer values $NODE(N,I)$, where the node index (N) can have a maximum value of:

$$N_{max} = KTOT \cdot YGRID \cdot XGRID$$

The second matrix index $I = 1,2,3$ was located to store the cross section(K), line(L), and pixel(M) of each selected node in the global cartesian coordinate system. The K, L, M information of each node defines its distance, in terms of number of square pixels from the coordinate system origin in which K, L, M values are zero. The real x, y, z locations of the nodes are calculated and stored by real number values in another two-dimensional matrix $XNODE(N,I)$. The scanned file header information such as the pixel size and the distances between scanned

cross sections is used in this calculation.

The node numbering method is demonstrated in Figure 17 by a display of selected nodes discretized by XGRID = 6 and YGRID = 12. The method can be also demonstrated by a numerical example:

XGRID = 6 nodes in x direction

YGRID = 12 nodes in y direction

Check condition: KFACT \geq XGRID \cdot YGRID = 72

and select: KFACT = 100

The node numbers, N, of the first cross section (K = 1) according to the node index expression are:

1	2	3	4	5	6	first node line
7	8	9	10	11	12	second node line
'						
'						
'						
67	68	69	70	71	72	YGRID node line

The second cross section (K = 2) nodes will be numbered accordingly:

101	102	103	104	105	106
107	108	109	110	111	112
'	'				
'	'				
'	'				
167	168	169	170	171	172

By the same method, KTOT cross sections are numbered and then stored in the matrix NODE(N,I).

For example, if the node number 172 is located in the second cross section $K = 2$, in line number $L = 74$ and the pixel number $M = 41$ in this line, this particular node will be stored in the NODE matrix as follows:

$$\text{NODE}(172, 1) = \text{NODE}(172,K) = 2$$

$$\text{NODE}(172, 2) = \text{NODE}(172,L) = 74$$

$$\text{NODE}(172, 3) = \text{NODE}(172,M) = 41$$

If the scanned file header indicates a pixel size of 0.8 by 0.8 mm and the distances between scanned cross sections are 2.5 mm, the XNODE matrix of node locations will store the following data:

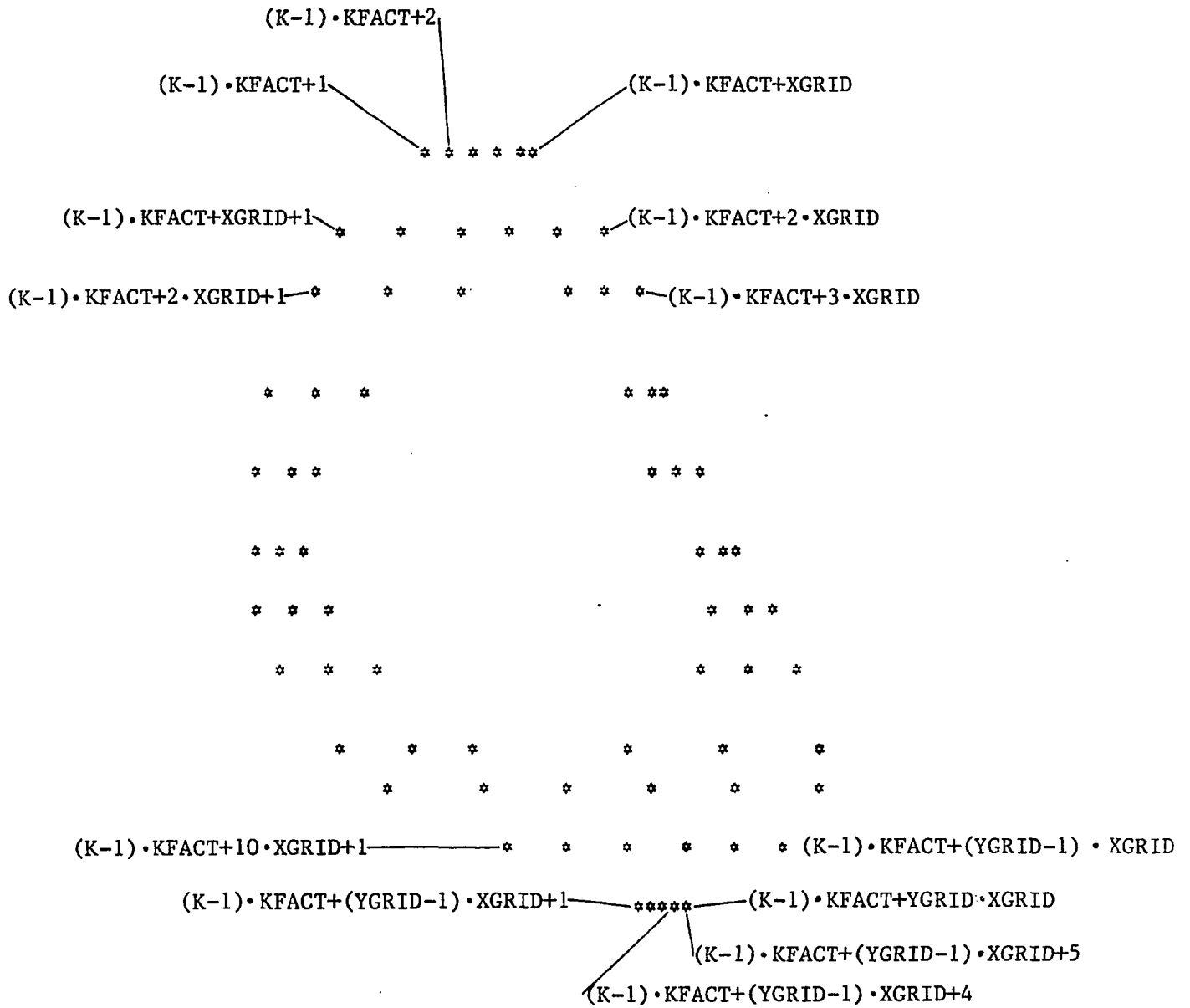
$$\text{XNODE}(172, 1) = 2.5 \cdot (+2) = +5.0 \text{ mm}$$

$$\text{XNODE}(172, 2) = 0.8 \cdot (+74) = +59.2 \text{ mm}$$

$$\text{XNODE}(172, 3) = 0.8 \cdot (+41) = +32.8 \text{ mm}$$

In some cross sections, a selected node line may consist of less than XGRID number of pixels. This may occur in the external upper and lower border node lines (Figure 16) in some cross sections. In such cases, all the pixels in the particular node lines are selected as model nodes. The node numbering procedure assigns more than one number to some of the nodes in order to complete a total number of XGRID selected nodes in this line as well. For example, if $XGRID = 6$ and the first line consists of only five pixels, four of the nodes will be

numbered regularly while the last node will be assigned with two numbers. By this method, when two cross sections will be used later to define the three-dimensional elements, some elements may have two nodes with the same location in space. Another method may be considered to avoid selected node lines with less pixels than requested nodes. Since the shorter pixel lines are always the external, upper and lower border lines (Figure 16), the edge detector can identify such lines while detecting the bone boundaries. The short lines found may be then omitted, or extended by the required number of pixels. If omitted, the next detected pixel line with sufficient number of pixels (greater or equal to XGRID) is selected. Although a smoother mesh is obtained, this method may slightly change the bone geometry as determined by the edge detector.



where K = 1 to KTOT number of cross sections

Figure 17: Demonstration of the Node Numbering Method

2.8 The Node Display Routine

The objective of this section in CTPRO pre-processor is to examine the node selection routine by the display and printout of the selected nodes in the model. The nodes are graphically displayed by character codes, therefore, a hard copy may be obtained by the VAX line printer. The display is followed by the list of node locations as stored in NODE and XNODE matrices. The node display and print is optional and may be omitted once the user has verified the correct formation of the requested mesh.

The routine uses an asterisk (*) character code for the nodes display, and plots the two dimensional mesh nodes for each participating cross section. The cross sections may be examined to verify that they contain a constant number of selected nodes with the same X-Y grid as requested by the user. The node display algorithm uses a vector of characters to represent each selected node line. The characters vector is filled up by asterisk characters where nodes are detected and blank characters in between. The node lines, represented by the characters vector, are printed while the pixel lines between them are skipped. As mentioned before, the user-selected X-Y grid determines the node density in the cross section two-dimensional mesh. Three selected mesh grids of the same cross section are displayed in Figure 18.

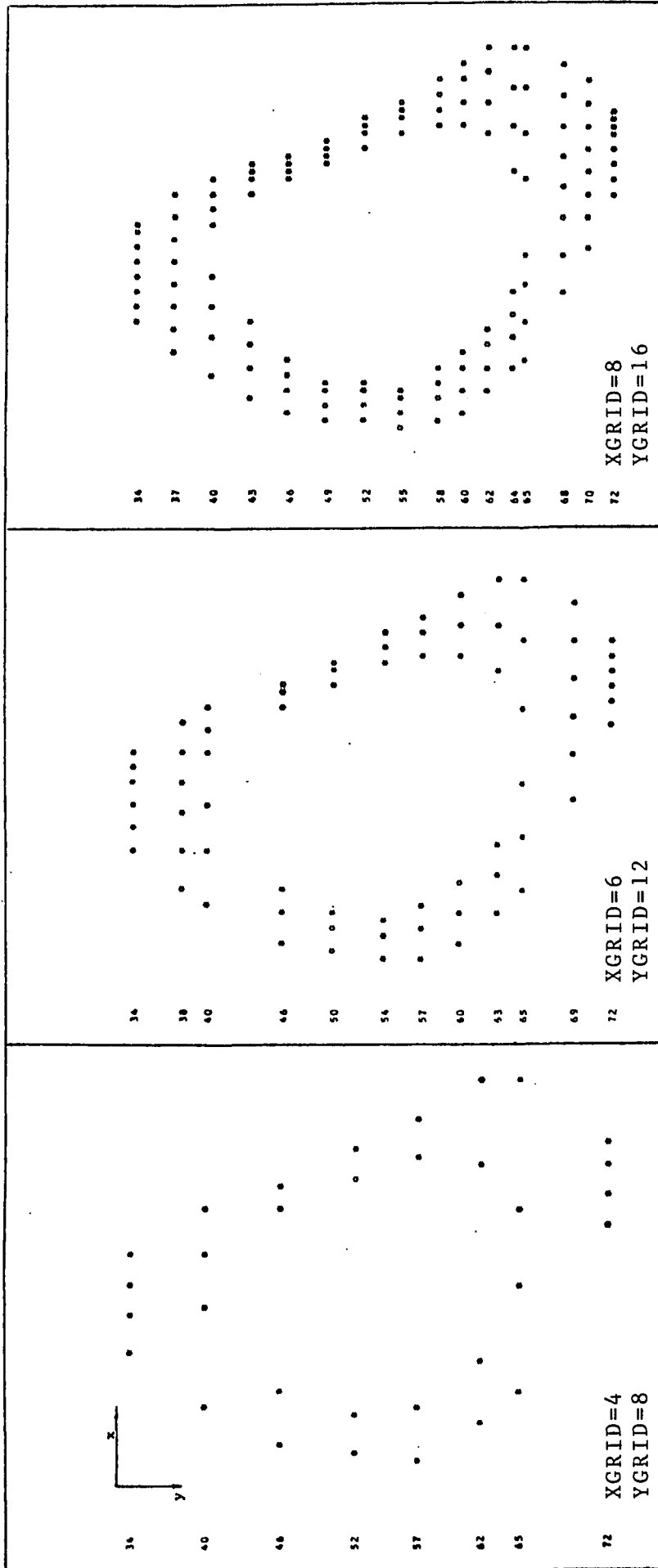


Figure 18: Display of Selected Nodes in Three Different X-Y Grids of Cross Section No. 8

2.9 The Element Definition Routine

The strategy of forming three-dimensional elements utilizing the two-dimensional mesh of the cross sections is coordinated with the node selection and numbering routine. The nodes are connected by the element definition routine to define three-dimensional eight-node isoparametric elements according to the requirements of the selected finite element program for the stress analysis. The definition of the coordinate system of eight node elements in the SAP IV finite element program which was selected for the analysis, is given in Figure 19.

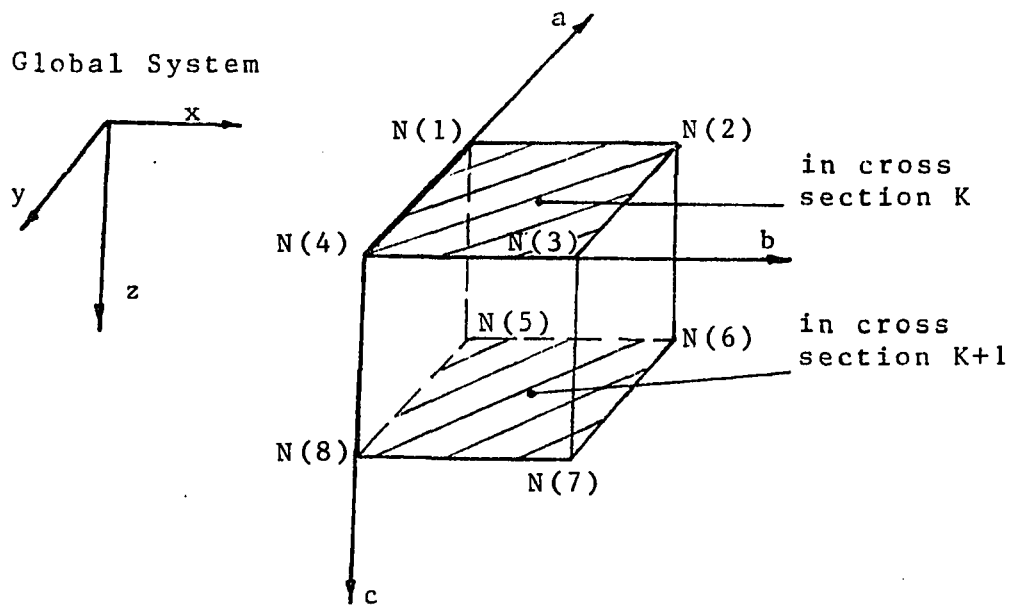


Figure 19: The Coordinate System of Eight Node Elements in SAP IV Finite Element Program

The method of forming the elements is inherent with the node numbering method described in Section 2.7, and is done automatically for each two adjacent cross sections. The node selection routine provides a constant number of nodes in each cross section, and thus insures no free nodes in any cross section after the elements are formed. The element definition algorithm developed takes into account the intrinsic shape of the bone cross-sections and the variations of boundary geometry in the adjacent cross sections in order to create a general procedure for long bone modeling.

The element definition routine starts a sequential procedure for the cross section $K = 1$ to the $K = \text{KTOT} - 1$ in which each adjacent pair $K, K+1$ are utilized to define eight-node elements by the following procedure:

A. Four nodes of cross section K are found as follows:

$$\begin{aligned} N(1) &= (K-1) \cdot K\text{FACT} + (L-1) \cdot X\text{GRID} + M \\ N(2) &= N(1) + 1 \\ N(4) &= (K-1) \cdot K\text{FACT} + L \cdot X\text{GRID} + M \\ N(3) &= N(4) + 1 \end{aligned}$$

are "connected" to the four following nodes of the cross section $K+1$:

$$\begin{aligned} N(5) &= K \cdot K\text{FACT} + (L-1) \cdot X\text{GRID} + M \\ N(6) &= N(5) + 1 \\ N(8) &= K \cdot K\text{FACT} + L \cdot X\text{GRID} + M \\ N(7) &= N(8) + 1 \end{aligned}$$

where: $N(1)$ to $N(8)$ are the element eight nodes according to the coordinate system defined in the SAP IV program (Figure 19).

KFACT is defined at the node selection routine
(Section 2.7).

The above procedure is applied sequentially for:

K=1 to KTOT-1	number of cross sections
L=1 to YGRID-1	number of selected node lines
M=1 to XGRID-1	number of selected nodes per line

B. Each related eight nodes N(1) to N(8) form one eight-node (brick) element by their location at the two parallel adjacent cross sectional planes. Each two such cross sections form, therefore, one three-dimensional slice consisting of eight-node elements. The validity of each element is tested as follows:

If the element lies in the hollow zone of the slice, within the internal compact bone boundaries which were previously defined by the edge detector (Figure 16), it is considered invalid and omitted. Otherwise, it is considered a valid element and filed in the element matrix.

C. The element matrix ELMNT(NE,J) is defined with index NE representing the element numbers assigned sequentially to each valid element. The maximum value of NE is limited by the expression:

$$NE = (KTOT-1)(YGRID-1)(XGRID-1)$$

The index J of the element matrix defines the NE elements by their node numbers:

$$J = N(1), N(2) \dots \dots \dots N(8)$$

2.10 Elastic Properties Definition Routine

The scanned bone cross sectional images consist of 0.8 by 0.8 mm pixels which carry the local radiographic densities by their CT number. Each defined three-dimensional element bounds a finite number of pixels which can be used to calculate a mean value of radiographic density for the element. The radiographic density of a scanned bone can be related to the apparent density of the bone using the "standard" solutions which were scanned together with the bone (see Section 2.2). This provides a linear relationship used to determine the average apparent density of each single element in the model. An empiric relationship between the apparent density and the bone elastic modulus may then be used to determine the average moduli of the elements. These properties are then used in the SAP IV input file.

Recent investigations provide an empirical relationship between the modulus of elasticity of a human bone in compression and the bone apparent density. Such a relationship for the Poisson ratio in human bones was not found in the literature. The Poisson ratio was selected, therefore, constant for the entire model with a value of 0.28 (Reilley and Burstein, 1974). The shear modulus is calculated by SAP IV for each element by its elastic modulus and the Poisson ratio, using the relationship: $G = E / 2(1 + \nu)$. The elastic properties definition routine consists of the

following main steps:

A. The radiographic - apparent densities relationship is determined.

B. The elastic modulus - apparent density relationship is determined.

C. An average radiographic density is calculated for each element in the model.

D. An average modulus of elasticity is assigned for each element by the relationships obtained in steps A and B.

The next sections describe the step-by-step procedures of the elastic properties definition routine.

2.10.1 Radiographic - Apparent Densities Relationship

The four "standard" images (Section 2.2) appear in each reconstructed image as four circular cross sections of gradual grey scale representing the various radiographic densities of the standard solutions (Figure 4). The radiographic densities in two different scans, taken for the same bone, may be slightly different due to the CT scanner drift and calibration prior to the scanning procedure. Therefore, the relationship between the radiographic and the apparent densities is valid only for a specific CT file.

Each of the cross-sectional images taken for this study was examined individually to establish the radiographic - apparent density relationship. This relation-

ship was found to be linear and identical in each cross section and was established as the practical relationship for the whole scanned bone section. A FORTRAN program, STAND, was developed to calculate the radiographic - apparent densities relationship, utilizing the four data points derived from the standard image pixels.

The four data points were obtained by averaging the radiographic density values (CT numbers) of one hundred pixels in the center of each circular image of the standard. The coefficients of the desired linear relationship were obtained by applying a least square method procedure of the first order on these data points. The program STAND takes the following steps:

A. Set a "window" to bound the four circular standard images and display them using the routines developed in the section of image reconstruction and display in CTPRO pre-processor (Section 2.4).

B. Search and read the radiographic density values of one hundred pixels in the center of each circular image of the standard in every cross section.

C. The one hundred pixels are averaged in each circular image to establish the mean CT radiographic density of four data points:

$$(CTD)_j = \left(\sum_{i=1}^m CTD_i \right)_j \quad j = 1, 2, \dots, n$$

where: $m = 100$ pixel radiographic densities

$n = 4$ "standard" images

D. Each of the four scanned solutions has a known mass density according to the concentration of prepared solutions of Dipotassium Hydrogen Phosphate (K_2HPO_4). This determines four experimental points used in a linear curve fitting routine.

E. Apply a least square algorithms to find the linear coefficients of the radiographic - apparent densities relationship. The linear coefficients are calculated by the expressions:

$$A = \left[\sum_{i=1}^m (x_i - \bar{x})y_i \right] / \left[\sum_{i=1}^m (x_i - \bar{x})^2 \right]$$

$$B = \bar{y} - A \cdot \bar{x}$$

where: $\bar{x} = \sum_{j=1}^n \rho$ is the mean value of the standard mass densities

$\bar{y} = \sum_{j=1}^n (CTD)_j$ is the mean radiographic density of each data point

$m = 100$ pixel radiographic densities

$n = 4$ "standard" images (data points)

The linear radiographic - apparent densities relationship which allows the calculation of the density for each pixel is:

$$\rho = (A) \cdot (CTD) + B$$

The coefficients of this relationship determined by program STAND for this study (Appendix D) are:

$$A = 0.9712 \cdot 10^{-3} \qquad B = 0.0$$

F. The linear curve of the calculated relationship was displayed by a Tektronix 4105 graphic terminal and copied by a Tektronix 4611 copier, using PLOT 10 graphic routines (Figure 20). The curve meets the coordinate system origin since the CT scanner was calibrated before scanning to measure the radiographic density of air as zero.

2.10.2 Elastic Modulus - Apparent Density

The average density information obtained from the pixel data is used to find elastic moduli for the model elements needed for the finite element stress analysis. A relationship between the elastic modulus in human bone and the apparent bone density is required.

Recent studies of Carter and Hayes (1976, 1977), and Stone, Beaupre and Hayes (1983) investigate the compressive behavior of bone and the relationship between the bone strength and modulus and the bone apparent density. Compression tests of human and bovine trabecular bone specimens with and without marrow were conducted at strain rates of from 0.01 to 10.0 per second. These experiments showed that the presence of marrow increased the strength, modulus, and energy absorption of specimens only at the highest strain rate of 10.0 per second. In specimens without marrow, the strength was proportional to the square of the apparent density, and the modulus of elasticity was proportional to the cube of the apparent density. Both, strength and modulus, were approximately

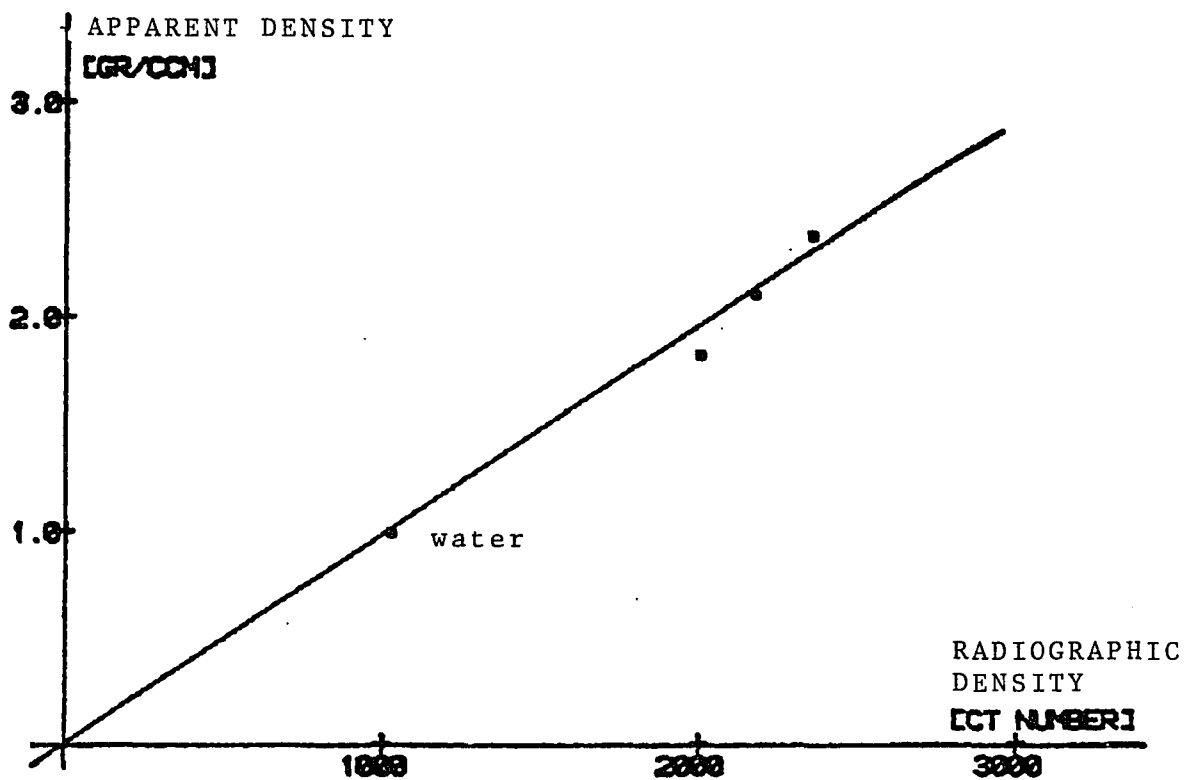


Figure 20: The Radiographic - Apparent Density Curve as Calculated by Least Square Method

proportional to the strain rate raised to the 0.06 power. These power relationships, which were shown to hold for all bone in the skeleton, allow meaningful predictions of bone tissue strength and stiffness based on density measurements as obtained by the bone scan in this study.

The composition and real tissue densities of normal spongy and compact bone tissues are similar (Gong et al., 1964; Galante et al., 1970). In addition, recent work has suggested that the microscopic material properties of trabecular bone are similar to those of compact bone (Martin, 1972; Pugh et al., 1973; Townsend et al., 1975). These observations suggest that whole bones can be modeled as composite structures consisting of both, a solid and fluid phase. The solid phase is the mineralized bone tissue, and the fluid phase is composed of blood vessels, blood, red and yellow marrow, nerve tissue, miscellaneous cells and interstitial fluid (McElhaney et al., 1970). The distribution of pores throughout the whole bone contributes to the apparent density distributions which are observed reontgenographically. The pore geometry and orientation contribute to the structural anisotropy which is evident mainly in the trabecular bone but also in the compact bone tissue.

In order to establish the relationships between the bone strength and modulus and the bone apparent density and strain rate, one hundred cylindrical specimens of human trabecular bone and twenty-four specimens of bovine

trabecular bone were tested under compression by Carter and Hayes (1977). The effect of the apparent density of the specimens on compressive modulus for human and bovine bone at a strain rate of 0.01 per second is shown in Figure 21. The findings of these tests suggest that the compressive modulus of bone is approximately proportional to the cube of the apparent density and to the strain rate raised to the 0.06 power as demonstrated by the empiric relationship:

$$E = E_c \cdot \dot{\epsilon}^{0.06} \left(\frac{\rho}{\rho_c}\right)^3$$

where E = compressive modulus (meganewtons per square meter) of a bone specimen of apparent density ρ (grams per cubic centimeter), tested at a strain rate of $\dot{\epsilon}$ (per second), and E_c = compressive modulus of compact bone with an apparent density of ρ_c tested at a strain rate of 1.0 per second. Finding the compressive modulus of human compact bone tested at a 1.0 per second strain rate allows simplification of the above relationship:

$$E = 3790 \dot{\epsilon}^{0.06} \rho^3$$

This equation shows that the compressive modulus of elasticity is a strong function of bone apparent density and a weak function of the imposed strain rate.

This empiric relationship is used in this study to obtain the modulus of elasticity of the model elements when their average apparent densities are calculated from

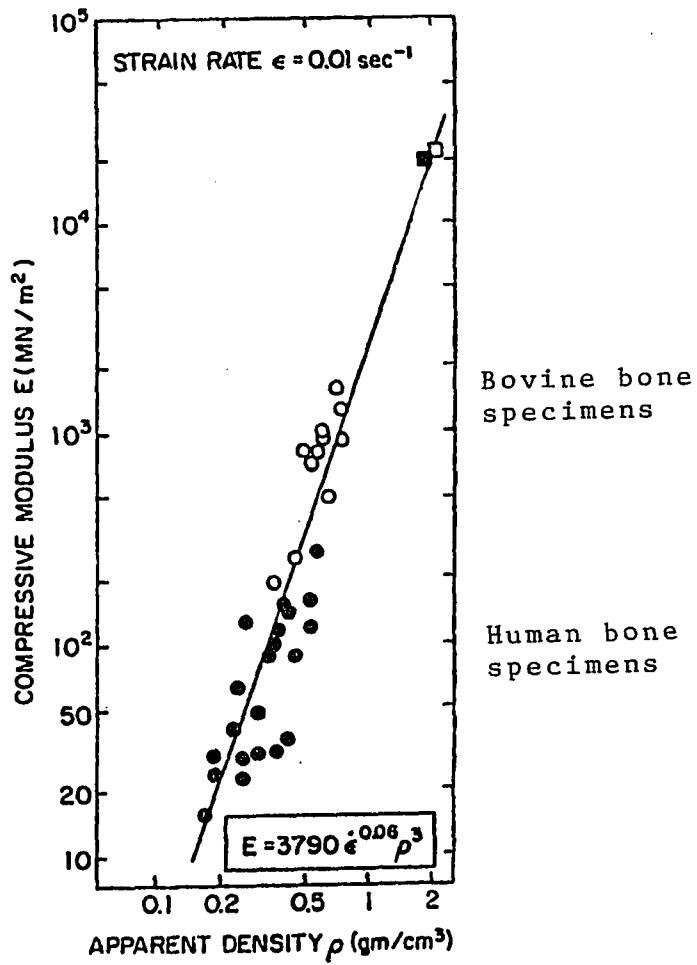
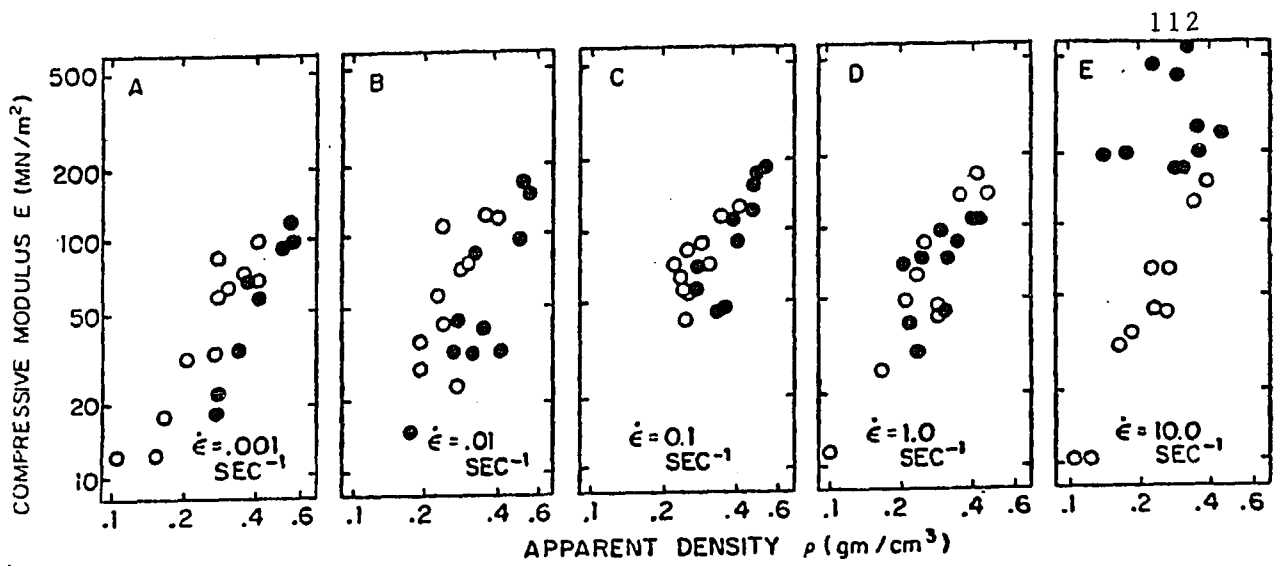


Figure 21: The Effect of the Apparent Density of Specimens on the Compressive Elastic Modulus (Carter and Hayes, 1977)

their pixel data. This particular expression is valid for compression and allows compressive stress analysis of the finite element model generated in this study.

Using gauges bonded to a human tibial diaphysis, Lanyon and Associates (1975) recorded maximum strain rates in the range of 0.002 per second during walking at a rate of 1.0 meter per second, and 0.01 per second during running at a rate of 2.2 meters per second. These strain rate values may be used in Carter and Hayes relationship to calculate the compressive elastic moduli in walking or running.

2.10.3 Average Properties of Model Elements

The average elastic moduli assigned to the model elements in this study are derived from the radiographic densities of all the pixels bounded within the element's borders. The method of element generation creates eight-node elements consisting of two parallel trapezoidal planes which are the pixel images (Figure 22). The pixel information in these two planes is used to calculate the average density of each element. The average elastic modulus is then calculated for each element using Carter and Hayes relationship.

The mean value of the element radiographic density is calculated by summing the CT numbers of all the pixels comprising the element's two parallel trapezoidal planes. The CT number of any requested pixel can be retrieved by the direct-access matrix $NCT(K,L,M)$. The pixels inter-

sected by the element borders are included in the average density calculation in case their relative portion within the borders is larger than the area outside the borders. The sum of CT numbers is divided by the number of pixels included in the calculation to determine the mean value. This procedure is carried out as follows:

The lines L1 to Ln of the element plane in cross section K and lines L1 to Ln of the plane in cross section K+1 (Figure 23) are searched. The pixel CT numbers between the element borders are summed in each line. The pixels intersected by the element borders are tested to find if they are mostly inside the element borders. An intersected border pixel has a trapezoidal shape with bases which can be calculated by the proportions of similar triangles (Figures 23,24):

$$R_o = \frac{IM1}{IL1} * S_o$$

$$R = \frac{IM1}{IL1} * S$$

The area of the trapezoidal shape is proportional to the sum of its bases ($R+R_o$) because the height of the trapezoid is constant in each pixel. This value is examined to determine whether it is larger than the pixel size and, therefore, included in the element pixels. This procedure is applied on each pixel along the element border lines of the two element planes. The average radiographic density is calculated by this method for each three-dimensional

element of the model.

In this study, the scans were taken in distance of 2.5 mm between them. The smallest average elastic modulus obtained for an element was $1.22 \cdot 10^3$ MPa ($1.77 \cdot 10^5$ PSI) and the largest was $53.60 \cdot 10^3$ MPa ($76.70 \cdot 10^5$ PSI), where 1 MPa = 1 Newton per square mm (Appendix E). The overall mean modulus of elasticity of the entire bone section was determined by calculating the element pixel areas and applying it to the following calculation:

$$\bar{E} = \frac{\sum_{i=1}^n E_i A_i}{\sum_{i=1}^n A_i}$$

where \bar{E} is the overall mean bone section modulus, E_i and A_i are the element moduli and areas, respectively. The overall average modulus of elasticity obtained was $4.95 \cdot 10^3$ MPa ($7.18 \cdot 10^5$ PSI). The results are in order of magnitude of compact bone moduli as obtained from experimental studies by McElhaney et al. (1970), Evans (1973), Reilly and Burstein (1974, 1975) and Goldstein (1980, 1983).

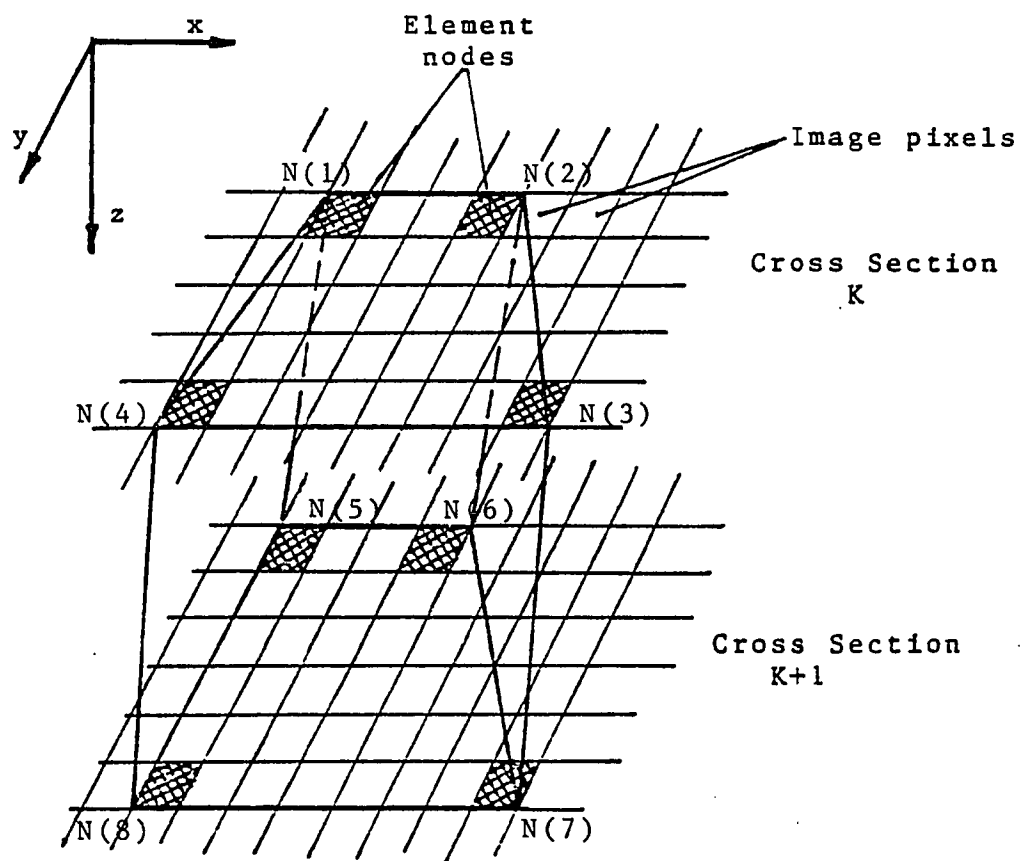


Figure 22: The Eight-Node Three-Dimensional Element Consists of Pixels in Two Adjacent Cross Sectional Images

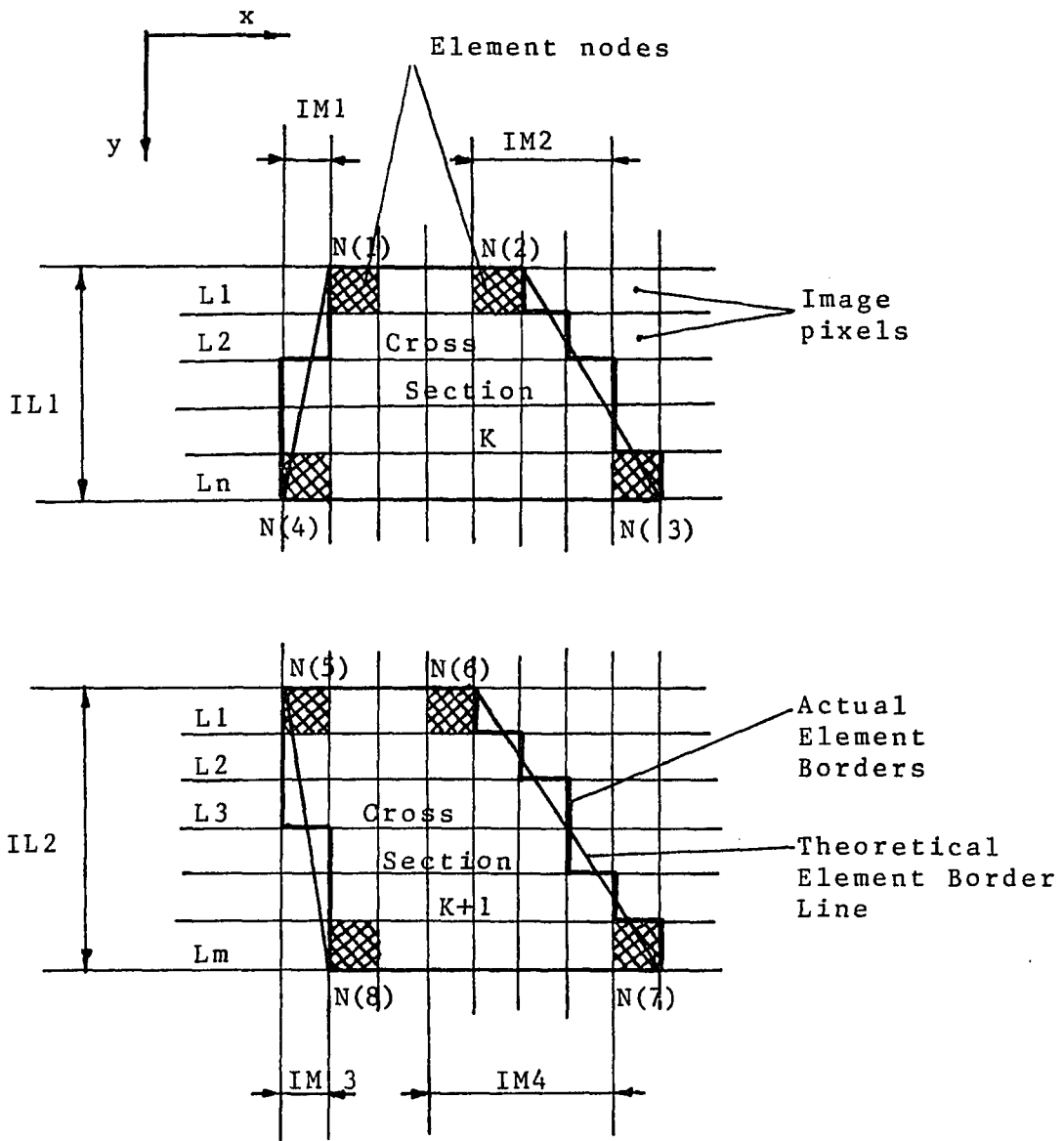


Figure 23: The Element Consists of Two Parallel Pixel Planes

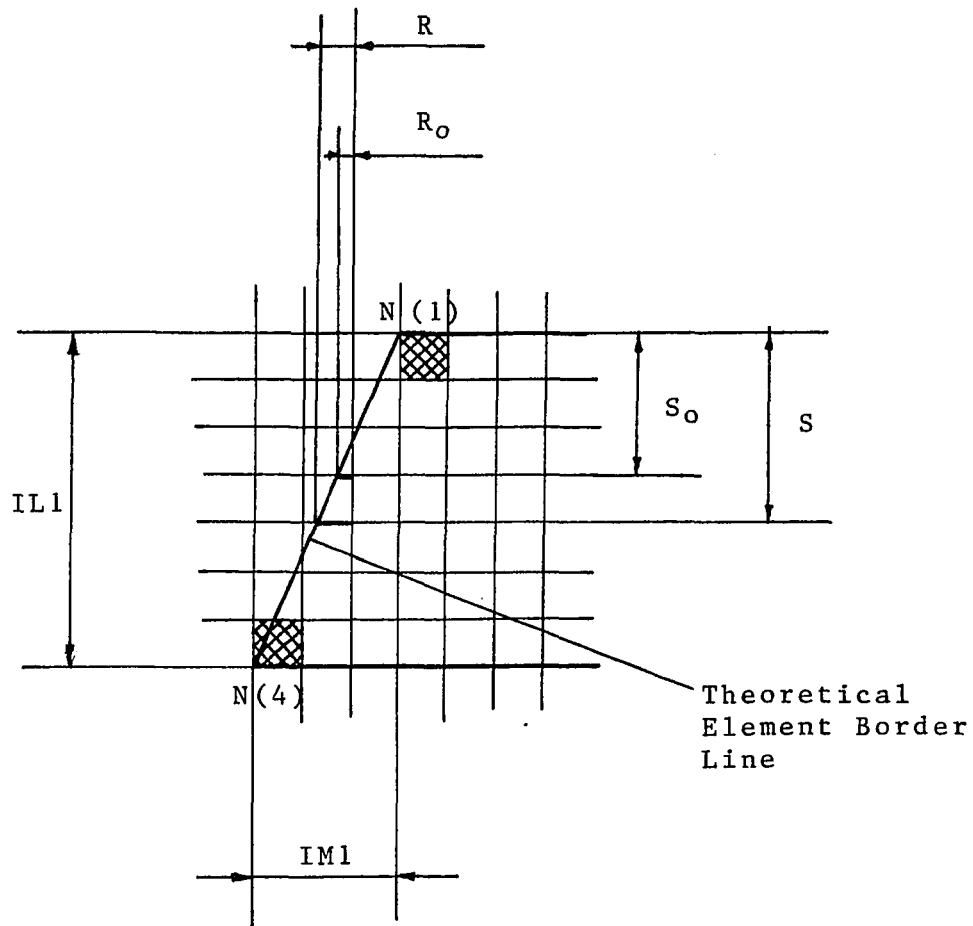


Figure 24: Determination of the Actual Element Borders by Geometrical Considerations

2.11 Generating the Finite Element Input File

The three-dimensional model created by the mesh generator is now formatted to create an input file for the selected SAP IV finite element program. The formatted file must follow the requirements of the finite element program as described by the program manuals (SAP IV User Guide, 1974). The input file consists of a set of numbered nodes and their location in a global coordinate system, a number of elements which are defined by their nodes in certain order due to the local coordinate system requirements, and the modulus of elasticity and Poisson ratio of the model elements. In addition, boundary conditions such as applied loads and initial displacements are applied. The loads may be concentrated forces in any desired direction at the model nodes, or equally distributed loads applied to element surfaces. Displacement boundary conditions are applied by assigning displacement values to desired nodes, where zero displacement defines the fixation of a node. The input file generation routine in CTPRO uses the model information stored in matrices NODE, XNODE, ELMNT and PRPRTY to create the external data file assigned as input to the SAP IV finite element program.

2.12 Display of the Generated Model

Advanced finite element programs include model display routines in their pre- and post-processors. Software packages, such as PATRAN, ANSYS and SUPERTAB have such display capabilities, but the user is not usually provided with access to the program source code. In this study, SAP IV finite element program was selected for the stress analysis primarily because the source code is available to the user. SAP IV model display routines were not sufficient for the two- and three-dimensional model display of this study; therefore, new display routines were developed in the pre-processor CTPRO.

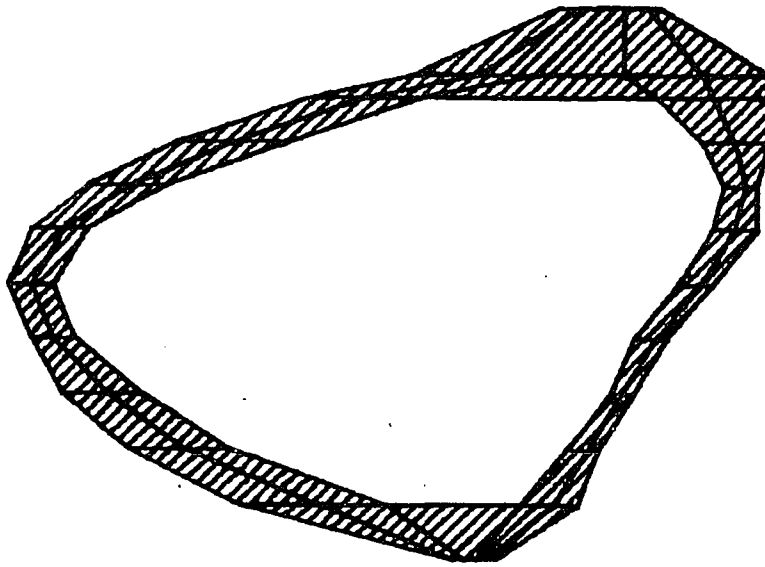
The objectives of the model display procedure were first to examine the model slice by slice to check the compact bone boundaries and the finite element mesh grid in x and y directions. This two-dimensional plotting of the model slices is achieved by using PLOT 10 graphic software which consists of FORTRAN language graphic subroutines. Figure 25 displays the computer output of slice number one of the generated tibia model. The slice display includes the distance of the slice from the tibia proximal end, the finite element mesh grid and the slice number in the model and the number in the scan file. Figures 26 to 28 display the nine slices of the model in grid of 6 by 12 in x and y directions.

The second objective is to visually examine the entire three-dimensional model which consists of the

previously displayed slices. The three-dimensional model display was carried out using the plotting module of ANSYS finite element package. An input file was generated by CTPRO which included the node and element information of the bone model in a format required by ANSYS. The file was read and processed by ANSYS plotting module to provide the three-dimensional display as seen from four directions, front, rear, right side, left side (Figures 29, 30). The slices and the entire model were displayed on a Tektronix 4105 graphic terminal and a hard copy was obtained by a Tektronix 4611 graphic copier.

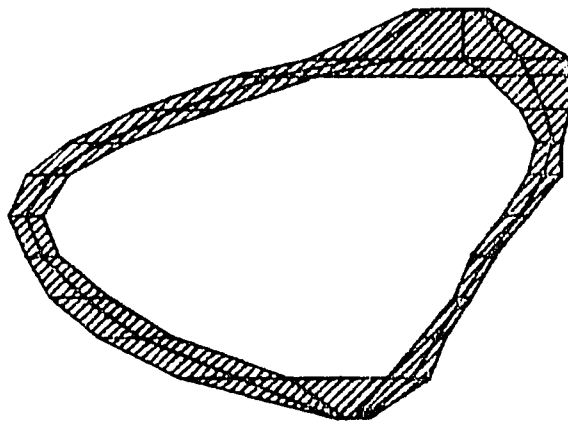
The cross sections display shows that the finite element model generated consists of 10 scanned cross sections of the tibial shaft comprising 9 three-dimensional slices, 5 mm thick. The first model cross section is 55 mm from the tibia proximal end and the tenth cross section is 100 mm from that point. This yields a three-dimensional model of a 45 mm long section of the scanned tibia shaft.

SLICE NUMBER 1
SCANNED SLICE NUMBER 26

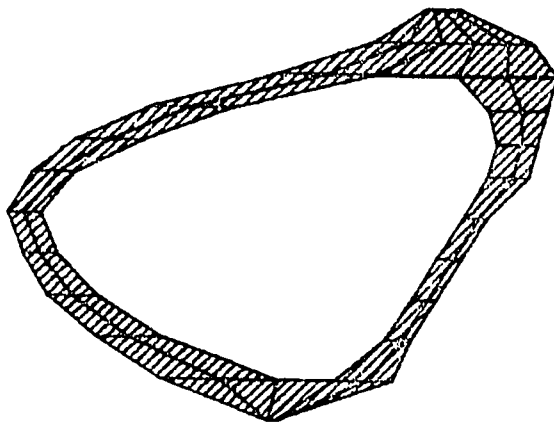


MESH GRID OF SLICE CROSS SECTION IS 8 BY 12 NODES
SLICE LOCATION RELATIVE TO SLICE 1 IN [MM] : 55.00
REAL SLICE DISTANCE FROM PROXIMAL END IN [MM] : 0.00

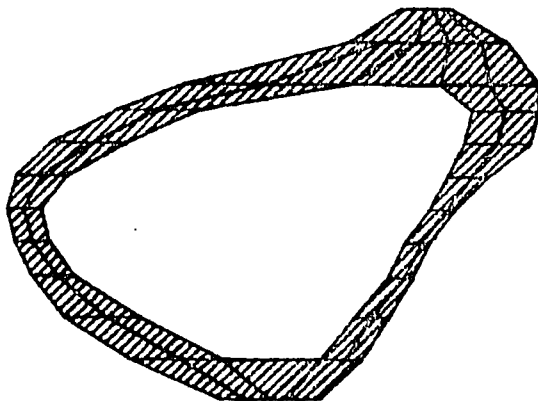
Figure 25: The First Slice of the Three-Dimensional Finite Element Tibia Section Model



Slice: 1
Location: 0.0 mm



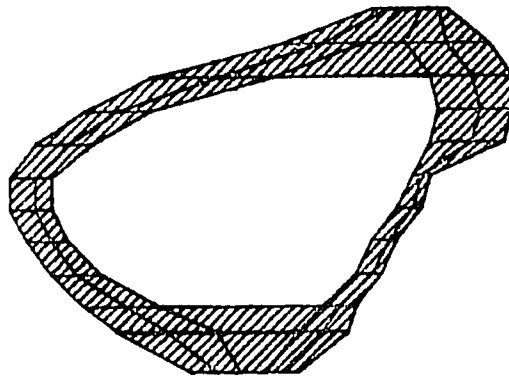
Slice: 2
Location: 5.0 mm



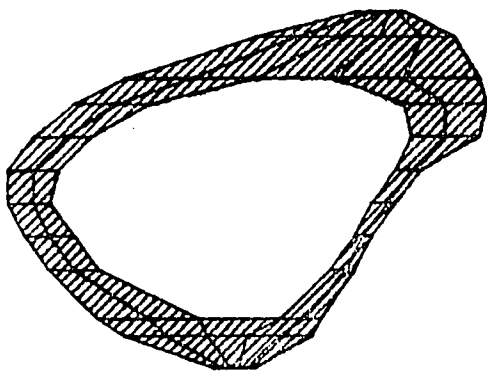
Slice: 3
Location: 10.0 mm



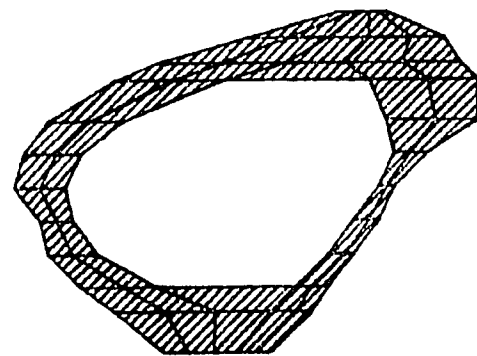
Figure 26: Slices 1 to 3



Slice: 4
Location: 15.0 mm



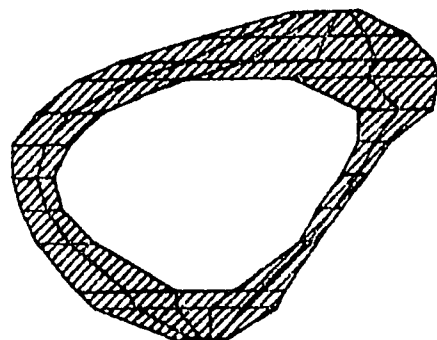
Slice: 5
Location: 20.0 mm



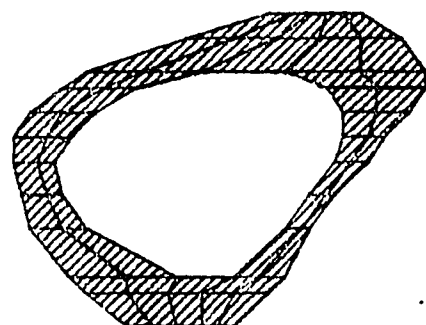
Slice: 6
Location: 25.0 mm



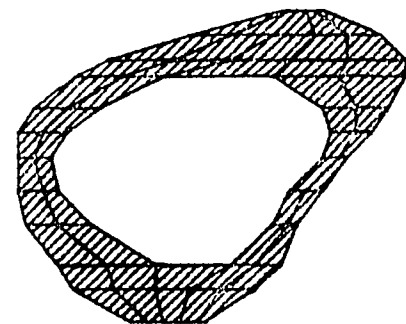
Figure 27: Slices 4 to 6



Slice: 7
Location: 30.0 mm



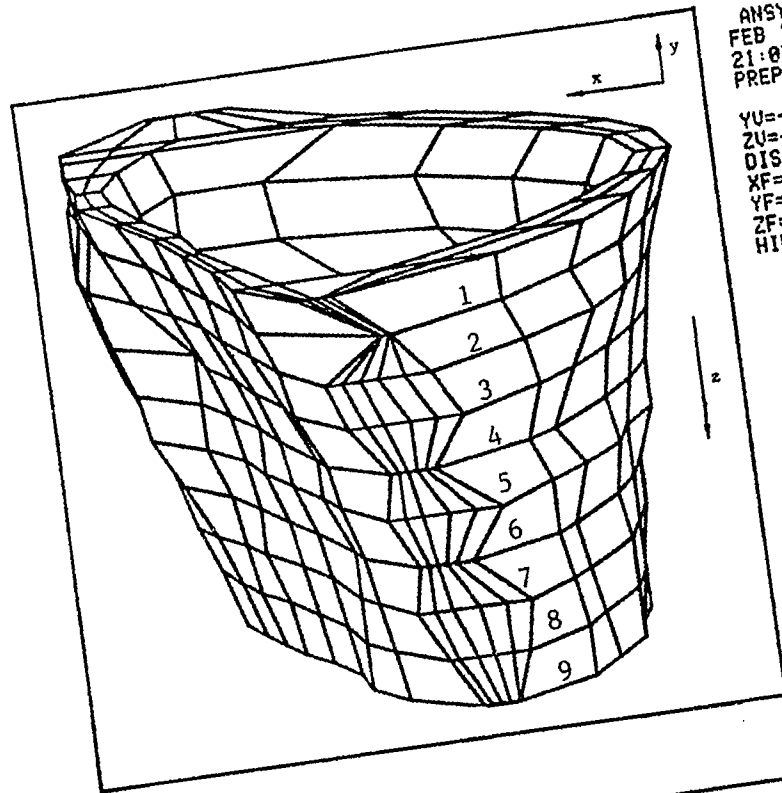
Slice: 8
Location: 35.0 mm



Slice: 9
Location: 40.0 mm

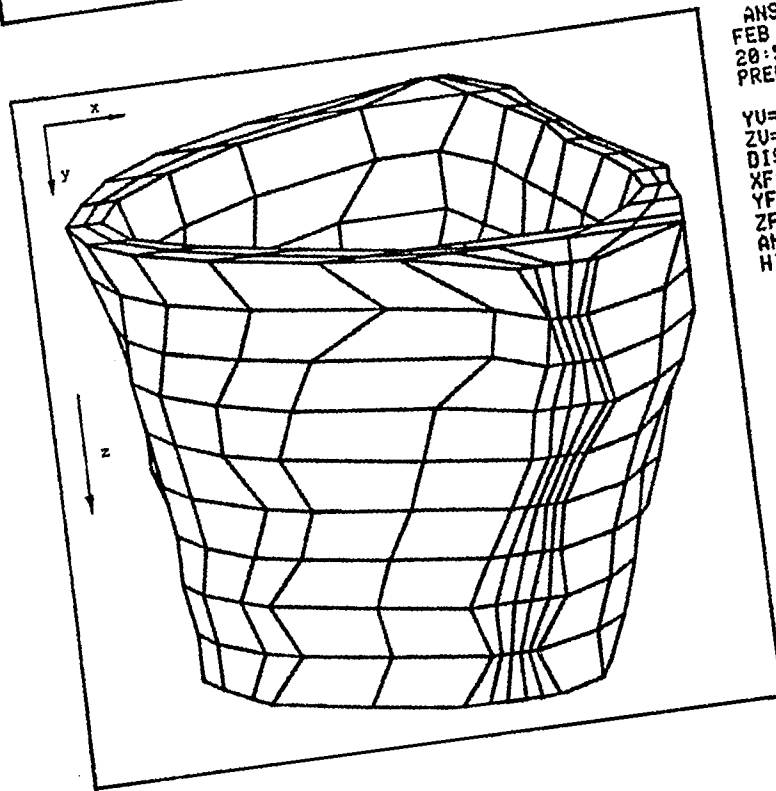


Figure 28: Slices 7 to 9



ANSYS 4.2
FEB 13 1986
21:03:45
PREP7 ELEMENT:

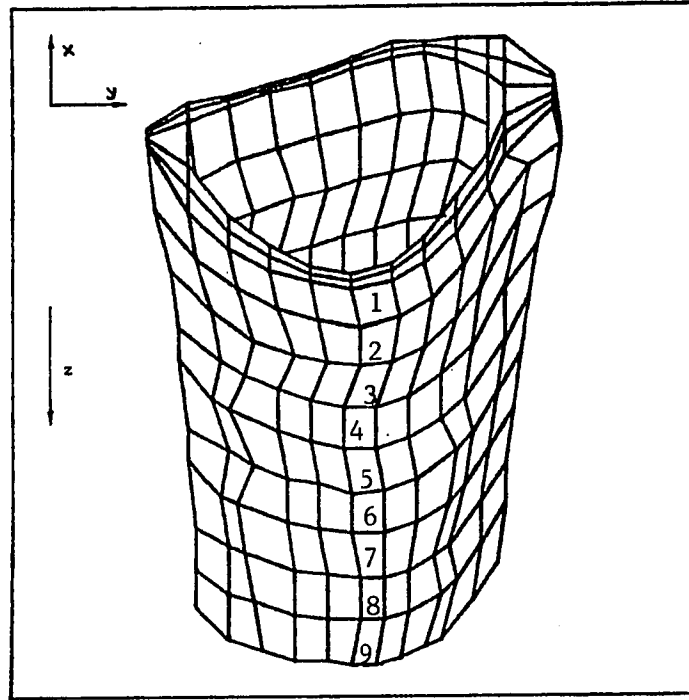
YU=-2
ZU=-1
DIST=30.8
XF=50.4
YF=39.8
ZF=20.4
HIDDEN



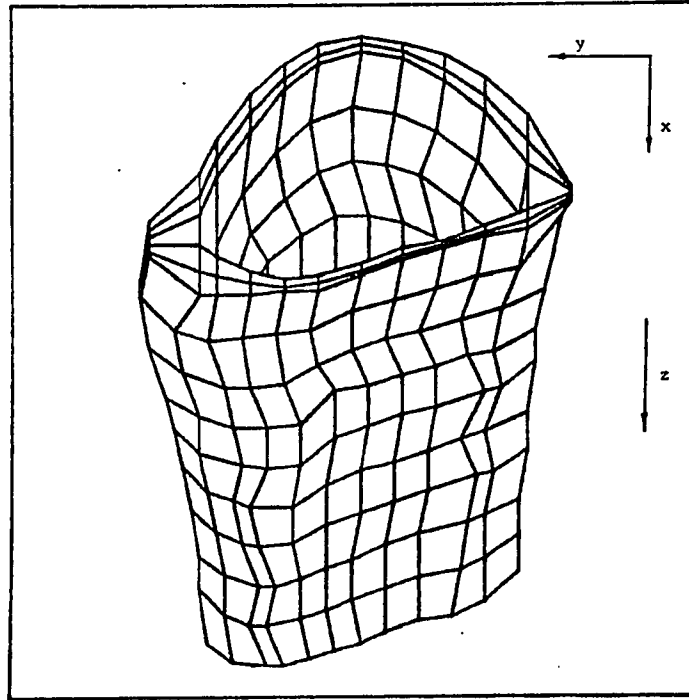
ANSYS 4.2
FEB 13 1986
20:56:46
PREP7 ELEMENT:

YU=2
ZU=-1
DIST=30.6
XF=50.4
YF=43
ZF=20.4
ANGL=180
HIDDEN

Figure 29: The Three-Dimensional Model:
A View from -Y and +Y Directions



ANSYS 4.2
 FEB 13 1986
 21:18:42
 PREP7 ELEMENTS
 XU=-2
 ZU=-1
 DIST=33.7
 XF=46.6
 YF=42
 ZF=18.8
 ANGL=-90
 HIDDEN



ANSYS 4.2
 FEB 13 1986
 21:11:29
 PREP7 ELEMENTS
 XU=2
 ZU=-1
 DIST=32.8
 XF=52.2
 YF=42
 ZF=18.8
 ANGL=90
 HIDDEN

Figure 30: The Three-Dimensional Model:
 A View from -X and +X Directions

2.13 Developing a Post-Processor

Advantages of the SAP IV program are its capability of analyzing large models and the availability of the FORTRAN source code. However, SAP IV does not include a post-processor capable of sorting and displaying the stress analysis results of the model slices. A special purpose post-processor named POST was developed in this study to print and display stresses and displacements obtained from the output of the finite element program.

The SAP IV program was modified in this study to create an additional output file containing the model geometrical data and the resultant stresses and displacements obtained by the finite element analysis, in a special format readable by the developed post-processor. The post-processor sorts the finite element results, finds maximum and minimum values of stresses and displacements, and reveals the cross section, element or node where they occur. The post-processor POST includes the following features:

A. Maximum Displacements in x,y,z Directions

The maximum displacements in the loaded model are searched in x, y and z directions by a sequential search algorithm applied to the nodal displacements δx , δy , δz . The obtained maximum values are printed, including the location they occur: the cross section number and node coordinates (Table 4 in Appendix G).

B. Maximum Resultant Displacement

The magnitude of the resultant displacement of each node is computed by:

$$\delta = (\delta_x^2 + \delta_y^2 + \delta_z^2)^{\frac{1}{2}}$$

where δ_x , δ_y , and δ_z are the displacement components in the global coordinate system. The resultant displacements are then searched to determine the maximum value in the model, the node number and the coordinates where it occurs (Table 4 in Appendix G).

C. Maximum and Minimum Stress

The normal and shear stresses in a small cubic element can be represented by the stress tensor

$$\begin{bmatrix} \sigma_{xx} & \tau_{xy} & \tau_{xz} \\ \tau_{yx} & \sigma_{yy} & \tau_{yz} \\ \tau_{zx} & \tau_{zy} & \sigma_{zz} \end{bmatrix} \quad \text{where} \quad \begin{aligned} \tau_{xy} &= \tau_{yx} \\ \tau_{xz} &= \tau_{zx} \\ \tau_{yz} &= \tau_{zy} \end{aligned}$$

or in tensor notation: σ_{ij} ($i, j = 1, 2, 3$). The stresses in the principal directions are σ_{\max} , σ_{\min} . The stresses in the model elements are searched by a sequential search routine. The maximum and the minimum values of the normal, shear and principal stresses are found with the slice and element of occurrence (Table 5 in Appendix G).

D. Stress Pattern Display

The stress pattern at a bone slice is displayed in four stress ranges using PLOT 10 graphic software sub-routines (Figures 37 to 42). User-selected control

parameters allow displaying various combinations of slice number and stress direction. Options available to the user include:

- (1) Select any slice and display any selected stress σ_{ij} on the slice.
- (2) Select any stress σ_{ij} and display the slice where the maximum (or minimum) value occurs.
- (3) Select a principal stress, σ_{\max} or σ_{\min} , and display the slice where the maximum (or minimum) value occurs.

The stress patterns indicate the stress ranges in the slice plane. The finite element program computes the stress of each element in an "integration point" which is not exactly on the element surface. However, the stresses may be considered in the slice plane, since these distance differences are negligible, especially when the mesh is fine.

2.14 Verification of Model Generation Method

The finite element model generated by the pre-processor can be verified by generating a three-dimensional object of simple geometry, which can be analyzed by analytical methods as well as by the computer aided analysis. The bone model in this study and the procedure of its generation is verified by comparing the numerical results of the computer aided analysis with the analytical solution.

A simple beam with rectangular cross sections was selected (Figure 31). The beam cross sectional CT images were reconstructed using CTPRO pre-processor. The adjustable window, designed to bound the scanned bone image and eliminate unnecessary pixels, was used to bound a rectangular plane of 9 by 6 pixels in each cross section. The 19 participating cross sections form 18 slices 2.5 mm thick to create a 45.0 mm long beam with rectangular cross section of 7.2 by 4.8 mm (pixel size 0.8 mm). The finite element mesh was selected in XGRID of 4 and YGRID of 3 in x and y direction. This provided a three-dimensional finite element model of 228 nodes and 108 eight-node elements. The model was considered to be homogeneous with isoparametric properties, and with modulus of elasticity and Poisson ratio of Aluminum alloy. The beam was fixed at one end as a cantilever and loaded by an equally distributed lateral load of $q=0.2$ Newtons per square mm (290 PSI).

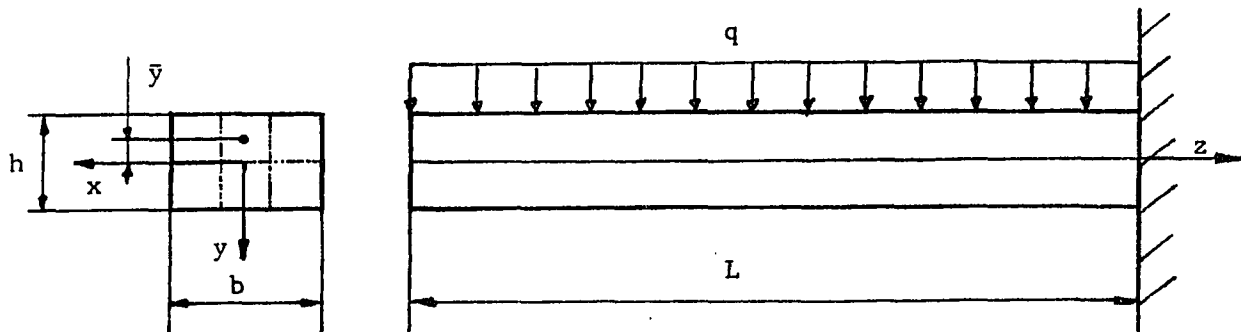
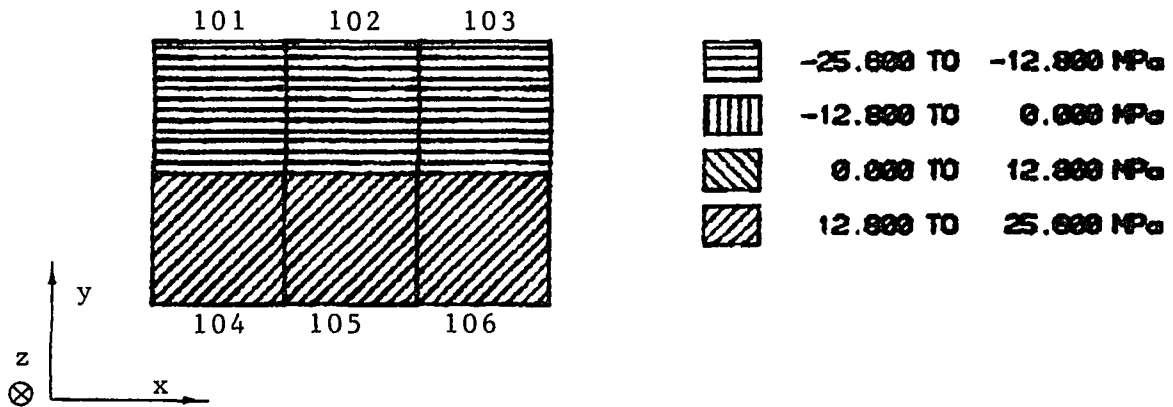


Figure 31: The Geometry and Boundary Conditions of the Verifying Model

The beam model was generated by the pre-processor CTPRO, analyzed by SAP IV finite element program and the obtained results were sorted, printed (Appendix F) and displayed (Figure 32) by the post-processor POST. The maximum deflection in y direction of 0.1567 mm occurred at the free end of the beam (Table 2 in Appendix F). The stress pattern obtained by the computer aided analysis was consistent with bending stress behavior, with fibers above the neutral axis in tension and fibers below the axis in compression (Figure 32). The maximum bending stress (σ_{zz}) occurred, as expected, at the elements at the fixed end of the beam with magnitude of 25.59 MPa (Table 3 in Appendix F).

An analytical solution for the deflection and stresses of the same model and boundary conditions were

SLICE NUMBER 18



SLICE LOCATION IN Z DIRECTION IN [MM] : 42.50 MM
 MAXIMUM STRESS OF 25.800 MPa OCCURS IN ELEMENT 105

Figure 32: The Stress Pattern of σ_{zz} Bending Stress in the Verifying Model as Obtained by POST Post-Processor

calculated as follows:

The maximum moment at the fixed end ($z = L$):

$$M_{\max} = \frac{1}{2} qb^2$$

where: q is the equally distributed load in y direction.

The bending stress due to the maximum moment is:

$$\sigma_{zz} = \frac{M_{\max} \bar{y}}{I} = \frac{6L^2 \bar{y}}{h^3}$$

where: $q = 0.2 \text{ N/mm}^2$, $L = 45.0 \text{ mm}$, $h = 4.8 \text{ mm}$ and \bar{y} is the distance from the neutral axis. The bending stress was calculated at $\bar{y} = \pm h/4$ which is the location of the center of the element compared with the computer aided analysis result:

$$\sigma_{zz} = \frac{3qL^2}{2h^2} = \frac{(3)(0.2)(45^2)}{(2)(4.8^2)} = 26.37 \text{ MPa}$$

The computer aided analysis result of bending stresses at the same location is:

$$\sigma_{zz} = 25.59 \text{ MPa}$$

The variation of the two results in percent:

$$E = \frac{26.37 - 25.59}{26.37} (100) = 2.9\%$$

The maximal deflection is calculated at the free end of the beam in the y direction:

$$\delta_{\max} = \frac{qbL^4}{8EI} = \frac{3qL^4}{2Eh^3}$$

where: $E = 70,000 \text{ MPa}$

$$\delta_{\max} = \frac{(3)(0.2)(45^4)}{(2)(70,000)(4.8^3)} = 0.1589 \text{ mm}$$

The computer aided analysis result of the deflection at the free end of the beam in direction of the applied load q is:

$$\delta_{\max} = 0.1567 \text{ mm}$$

The variation of the computer aided analysis from the analytical results in percent:

$$E = \frac{0.1567 - 0.1589}{0.1589} (100) = 1.4\%$$

The comparison of the stresses and displacements which were calculated for the same model by the analytical method and by the computer aided analysis show a satisfactory agreement. The variations of 2.9% in the stress results and 1.4% in the deflections are typical for engineering purpose stress analysis by a finite element method. The comparison of the above results, therefore, verify the three-dimensional model of the scanned long bone section and the procedure of generating the finite element mesh.

2.15 Convergence Tests

A convergence test for the finite element results has been conducted to test the convergence of nodal displacements with mesh refinements. In a valid finite element model, displacements of the same node location should converge to an asymptotic result when a larger number of smaller elements are selected. The number of model elements may be selected by the user of CTPRO pre-processor by setting the number of selected nodes in x and y directions of each cross section and thus to define the grid of the two-dimensional mesh. The defined two-dimensional grid determines the total number of generated elements in the three-dimensional model of the entire bone section.

The first set of mesh refinements included eight different grid sizes of the 45 mm tibia shaft section with 274 elements of the most coarse mesh, and 1018 elements of the finest mesh (Figure 33). The model was fixed at the lower tibia end as a cantilever, and loaded at the free end by two forces, each of 35 Newton, in y direction and by one force of 50 Newtons in x direction. Due to slight variations of the model borders during the mesh refinements, the finite element results of the generated three-dimensional model showed no convergence of the displacements at several inspected nodes. The displacement values were substantially close to each other but varied in value instead of converging to an

asymptotic result.

The model generation routine of CTPRO was examined to reveal the parameters which do not remain constant during altering the mesh size. As a result of developing a debugging routine as part of CTPRO pre-processor, it was found that the internal borders of the bone model were slightly altered for different mesh sizes. As a result, the generated three-dimensional model stiffness was also slightly altered during mesh refinements and, therefore, the convergence test did not provide the expected results.

In order to keep the borders constant for each mesh size, the edge detector and the node selecting routines were modified. In the original routines, the three-dimensional model was generated together with the border detection for each mesh size. In the modified routines, the edge detector first determines the external and internal compact bone borders in each cross section, then the cross sections are discretized to define the mesh.

The model was generated, loaded and analyzed again for eight mesh sizes. The displacements of selected nodes now converged to asymptotic results. The displacements of four nodal points were plotted as a function of mesh sizes (Figure 34). The location of the nodes remained fixed in space during the mesh refinements (corner nodes) so that their displacement could be compared. The resultant curves demonstrate an acceptable

convergence of the finite element results from the generated model. The selected grid of 6 by 12 nodes in x and y directions gives an acceptable accuracy relative to the asymptotic results and, therefore, is selected as the working grid for finite element analyses.

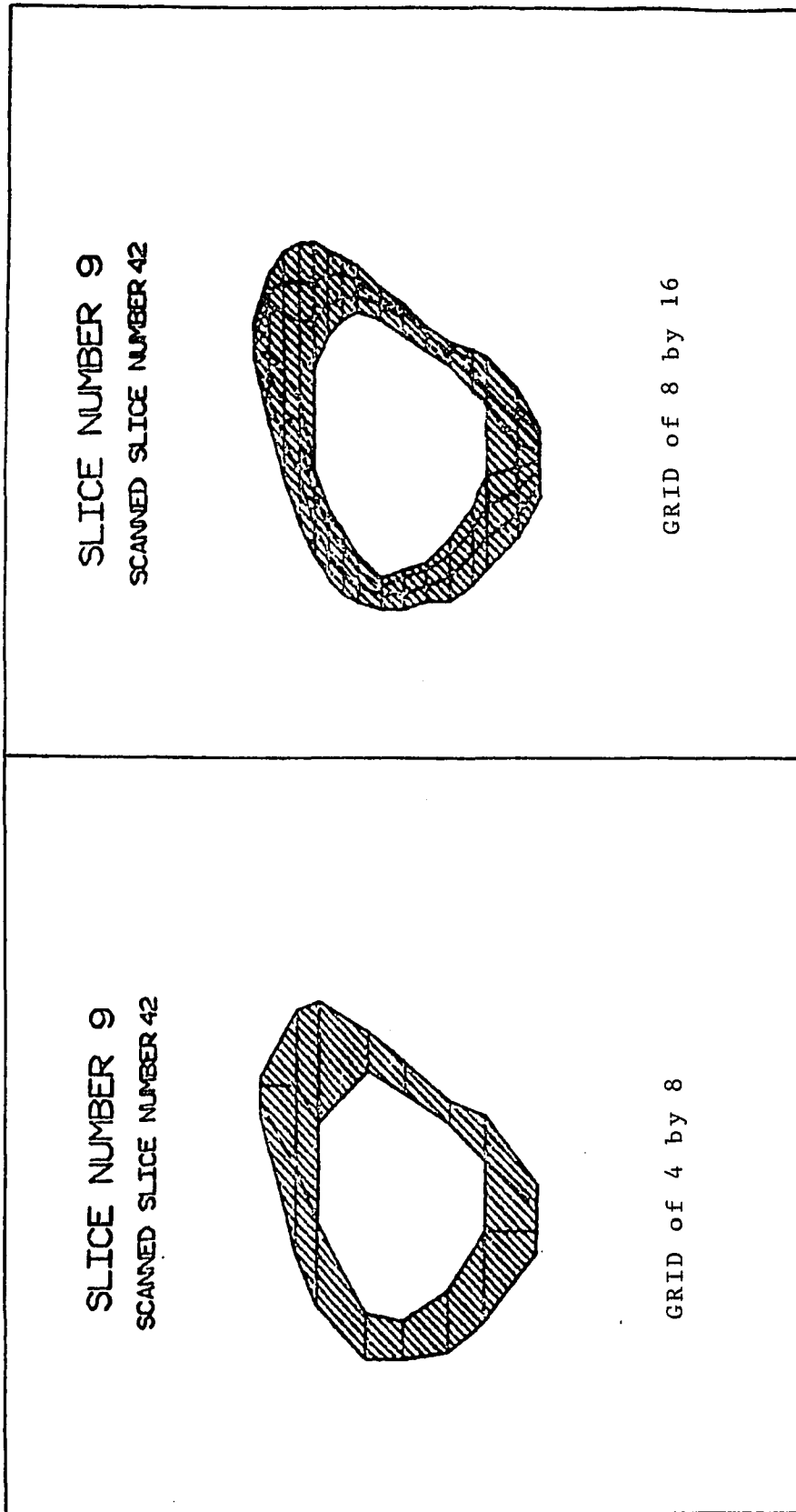


Figure 33: The Finest and the Most Coarse Mesh Sizes for the Convergence Test

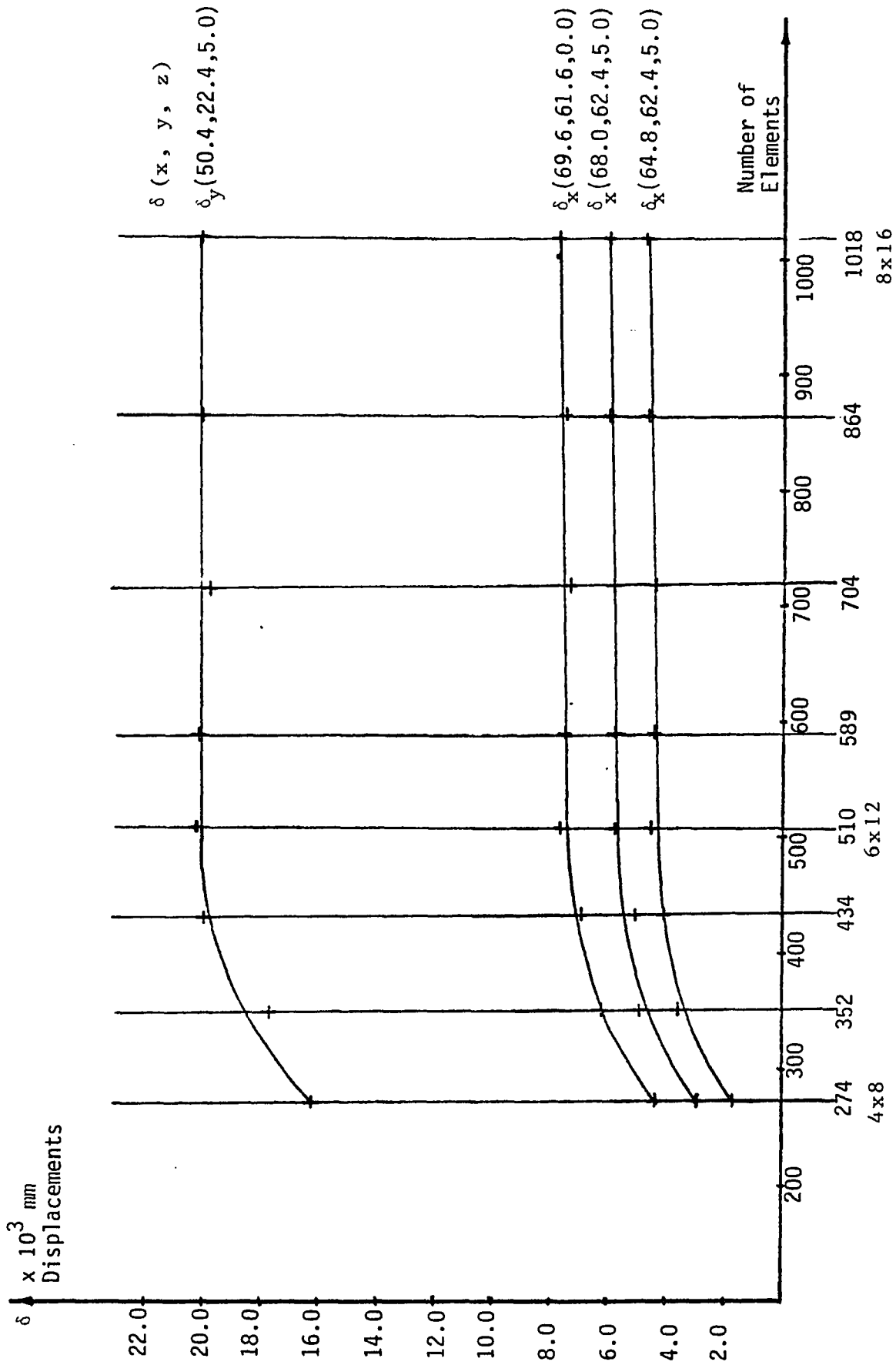


Figure 34: Convergence Test of Node Displacements in Mesh Refinements

2.16 Demonstration Problem Analysis

A sample problem was modeled and analyzed using the computer aided procedures developed in this study to demonstrate the processor's capabilities, using the scanned tibia section as the analyzed model.

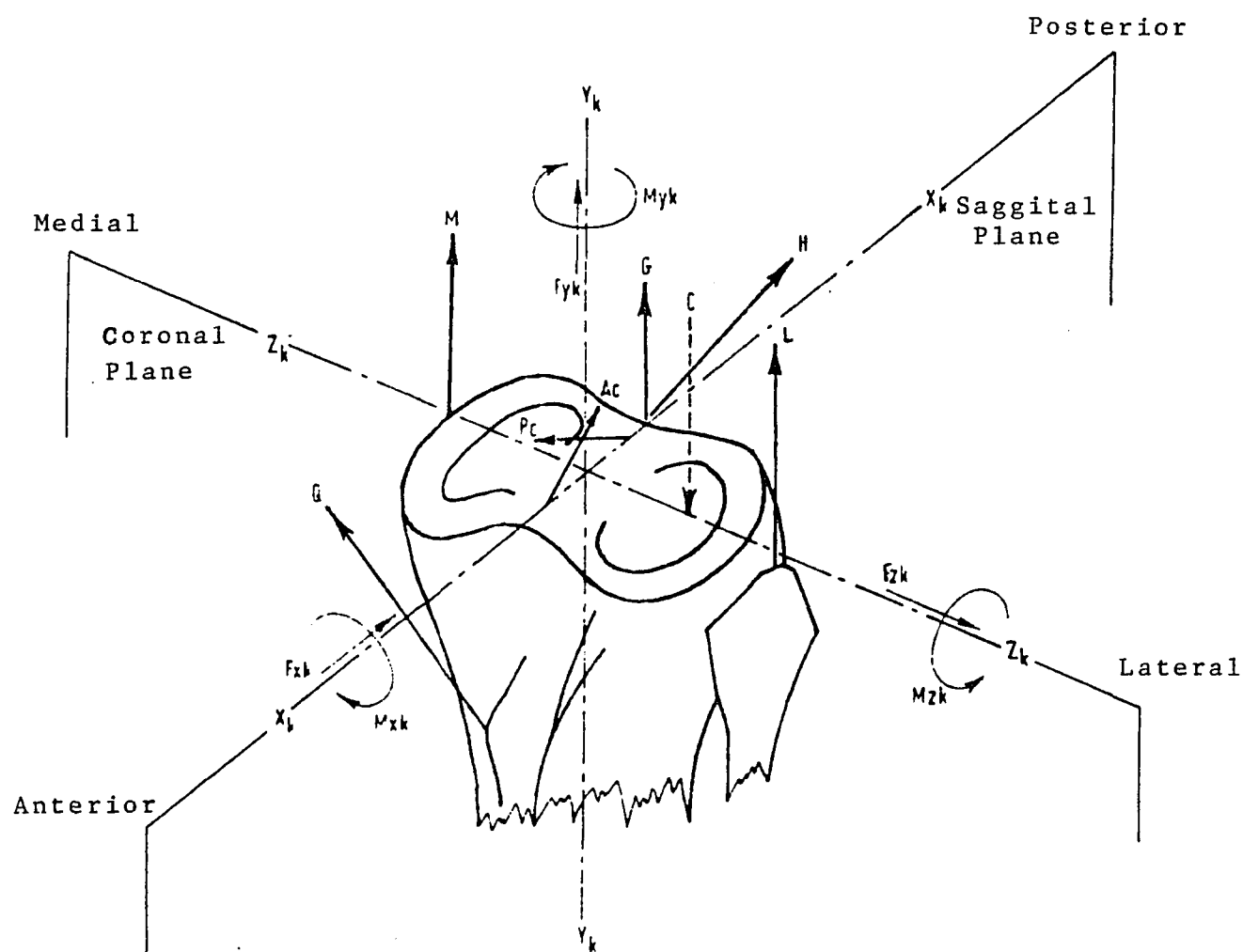
Several investigations have been made to calculate the force actions transmitted by the knee joint (Morrison, 1968; Kettlekamp and Chao, 1972; Harrington, 1976; Minns, 1981; Nissel et al., 1986 and others). The evaluation of the direction and magnitude of these forces was based on the tibial-femoral geometry, contact areas, relative alignments, and experimental force plate results. The resultant forces acting at the knee joint during normal gait depend on several ligament orientations, such as the cruciate and collateral ligaments, and muscle groups such as the quadriceps, hamstrings and gastrocnemii which act on the proximal tibia in various directions (Figure 35). External forces, gravitational and acceleration effects at the knee joint can be represented as three forces and three moments. Equilibrium must be obtained at the knee joint by the direct force between the tibia and femur acting at the bearing surface (the tibial plateau), and by force actions in the muscle and ligament groups. Experimental and theoretical gait analyses show that the dominant loads on the proximal tibia are the compressive loads on the medial and lateral tibia plateau in a maximum value of 3.5 times the body weight (Moeinzadeh

et al., 1973; Harrington, 1976). The difference between the magnitudes of these loads and the asymmetric tibia geometry add moments acting mainly at the coronal plane. Other ligament and muscle groups cause a moment acting in the sagittal plane (Figure 35).

2.16.1 Model and Boundary Conditions

The finite element model generated in this study yields a 45 mm length of tibial shaft starting 55 mm from the tibia proximal end. The compressive loads on the medial and lateral tibia plateau (z direction) may be expressed as uniformly distributed loads in the tibial shaft according to Saint Venant principle of rapid dissipation of localized stresses, which asserts that the effect of forces or stresses applied over an area may be treated as a statically equivalent system when far enough from the applied area causes a stress distribution that follows a simple law.

In order to simulate the loading pattern on the tibial shaft, the generated model was fixed at the lower end (slice number 9 at $z=45.0$ mm) and the loads were applied on the nodes and element surfaces at the proximal end (slice 1 at $z = 0.0$ mm). A uniformly distributed load of 0.365 Newton per square mm (52.9 PSI) was applied on the surface of the proximal end in the z direction (Figure 36). The total force in the z direction was obtained by calculating the slice surface area using the AREA subroutine in CTPRO pre-processor which sums the



Knee joint force model, where F_{xk} , F_{yk} , F_{zk} and M_{xk} , M_{yk} , M_{zk} represent applied forces and moments. Reactive muscle ligament and bearing forces are: M —medial collateral ligament; L —lateral collateral ligament; Ac —anterior cruciate ligament; Pc —posterior cruciate ligament; Q —quadriceps force action; H —hamstrings; G —gastrocnemii; C —bearing force.

Figure 35: Forces and Moments Acting at the Knee Joint in Normal Gait (Harrington, 1976)

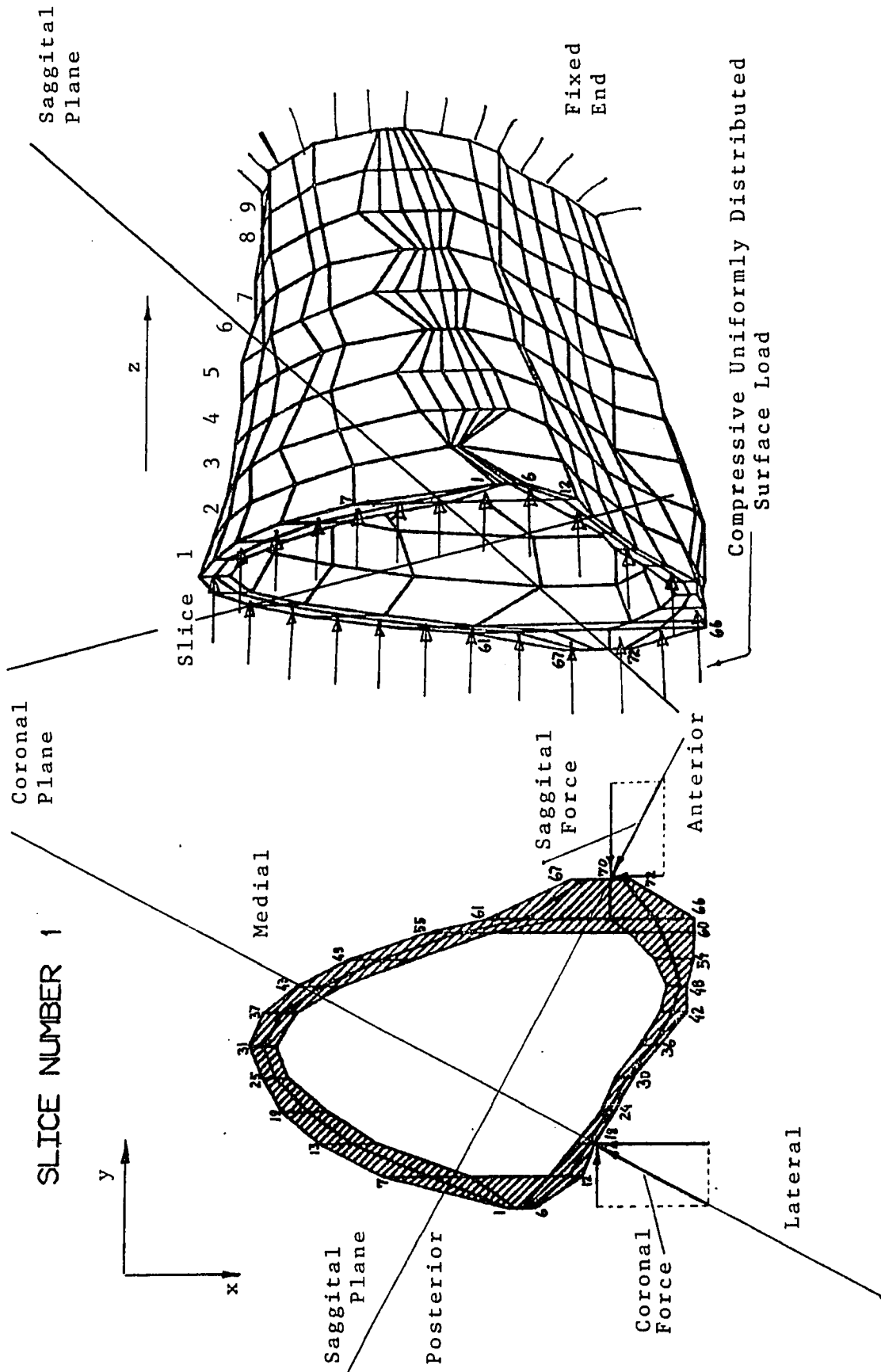


Figure 36: The Loading and Boundary Conditions of the Demonstrating Problem Analysis

element surface areas in a given slice. The resultant load in z direction was 2450 Newtons (551 lb) which is 3.5 times an average body weight of 700 Newton. A force of 180 Newtons (40.5 lb) was applied at the saggital plane on node 70 (Figure 36) to simulate the forces and moments due to the cruciate ligaments and the quadriceps, hamstrings, and gastrocnemii muscle groups action. A force of 145 Newtons (32.6 lb) was applied at the coronal plane on node 18 to simulate forces and moments due to the collateral ligaments and asymmetric effects of the bearing force in z direction (Appendix E).

The model was generated with grid of 6 by 12 in x and y directions. The uniformly distributed load and the concentrated forces were applied to the model and the input file for the SAP IV finite element program was generated. The CTPRO pre-processor generated a nine slice model consisting of 720 nodal points and 434 three-dimensional, isoparametric, eight-node elements. SAP IV finite element program produced an output file containing the displacements of model nodes in the global coordinate system and the stresses in the model elements. The POST post-processor searched and sorted the SAP IV output file to find maximum and minimum values of stresses and displacements (Appendix G). In addition, stress patterns of model slices in which maximum stresses occur were also produced (Figures 37 to 42). The finite element program used 1153 CPU time units to generate the 720 node and 434

element model and solve the 1944 equations of the static analysis (Appendix H).

2.16.2 Analysis Results and Interpretation

The multi-axial loading of a three-dimensional model of complex geometry and material properties, such as the tibia section, allows only general interpretation of the stress analysis results. As mentioned before, the main objective of the sample problem analysis was to demonstrate the processors capabilities rather than performing a practical stress analysis on the tibia section.

The largest resultant displacement of 0.536 mm (Table 4 in Appendix G) occurred at node 36 of slice 1 (Figure 37). This displacement occurred at the free end of the model, at the thin cylindrical wall of the first slice, near the point of the applied coronal force and it is mainly a result of this force combined with the compressive load in z direction. The maximum displacement of 0.296 mm in z direction occurred at the first slice ($z=0$) mainly due to the equally distributed compressive load on the proximal surface.

The maximum stress in x direction ($-\sigma_{xx}$) of -15.4 MPa (-2234 PSI) (Table 5 in Appendix G) occurred in element 13 of slice 1 (Figure 37). The location of this stress is apparently due to the thin cylindrical wall and force component in x direction applied at the coronal plane on node 18 of this element (Figure 36).

The maximum stress in y direction (σ_{yy}) of 19 MPa

(2756 PSI) occurred at element 141 of slice 3 (Figure 38) near the location of the applied saggital force. A maximum stress of $\sigma_{zz} = -68.8$ MPa (-9979 PSI) was obtained at element 434 of slice 9 at the fixed end of the model. σ_{zz} is due to compressive and bending stresses at the fixed end, where the bending moment due to the saggital force is largest at the external fibers, far from the neutral axis.

The maximum shear stress τ_{xy} in the plane of the cross sections occurred at slice 1 in element 40 (Figure 40) with magnitude of -11.3 MPa (-1639 PSI). The shear stress at the cross sections is a result of the superimposed direct shear forces and torsion. The torsion is the result of applying the forces at the saggital and coronal planes which do not necessarily intersect at the center of gravity.

The maximum principal stress σ_{max} of 21.2 MPa (3075 PSI) occurred in element 141 of slice 3 (Figure 41), at the same location of the maximum σ_{yy} (Figure 38). The second principal stress σ_{min} of -23.7 MPa (-3437 PSI) occurred in element 40 of slice 1 (Figure 42), at the same location of the maximum τ_{xy} (Figure 40).

In a recent investigation by Little and co-workers (1986), a three-dimensional finite element stress analysis of the upper tibia was performed. The geometry for the model was determined by casting a cadaver tibia in a polyester resin, slicing it in transverse planes and then photographing and digitizing the slices. The stiffness of the tibia cancellous bone was determined by indentation

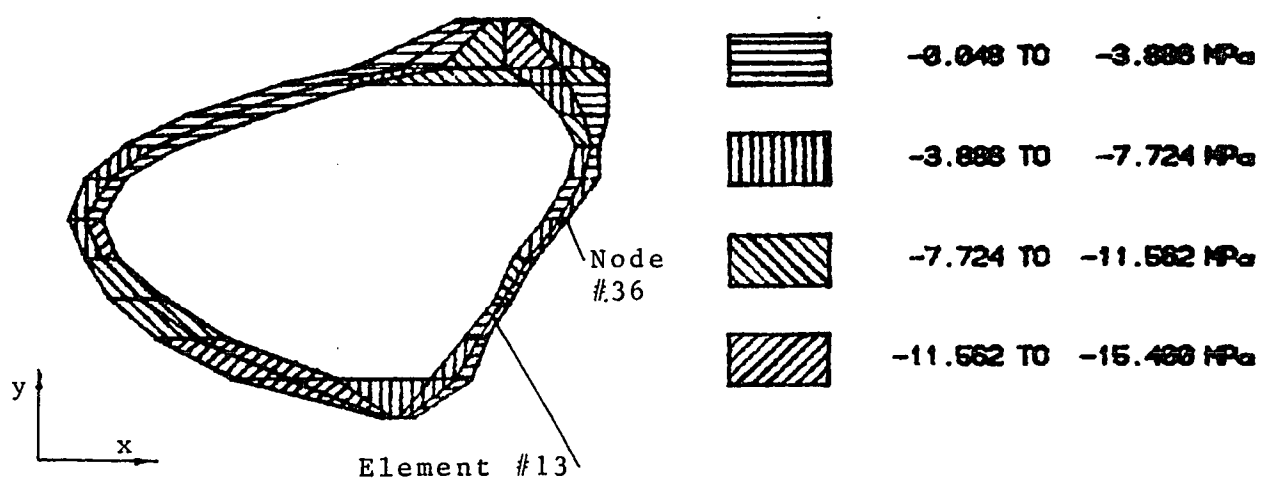
tests, and of the compact bone by values taken from the literature. The model materials were assumed to be linearly elastic, isotropic and heterogeneous. A finite element mesh of three-dimensional eight-node isoparametric elements was generated. The elastic modulus of the compact bone in the cortex was determined from the literature while the cancellous bone elements had individual moduli based on the indentation tests. A Poisson ratio of 0.3 was selected for the entire model based on the literature. An equally distributed compressive load of 2450 Newton was applied at the tibia plateau as occurs during normal gait at the stance phase in near full extension (Harrington, 1976). The stress analysis was performed by the SAP IV finite element program. The results were processed by a post-processor and compared with strain gage tests and with a two-dimensional axisymmetric model, both from the literature.

An additional stress analysis was performed in this study with only one equally distributed compressive load of 2450 Newton (3.5 times average human weight) applied to the tibia plateau (z direction). The similar loading in both analyses provides the common base for comparing the results in spite of the differences in the model geometry and material properties. In the above investigation, a maximum compressive stress of 24.77 MPa was obtained at the compact bone tissue, while in our study the maximum compressive stress was 75.2 MPa (Table 7 in Appendix H).

A maximum nodal displacement of 0.5 mm was reported in the above investigation at the subchondral bone layer, immediately beneath the cartilage. In our study, the subchondral layer was not included in the bone section model and the maximum displacement in z direction due to the compressive load was 0.260 mm (Table 6 in Appendix H). In both studies, the deflections in z direction become smaller far from the loaded tibia plateau. The agreement by order of magnitude in the maximum stress and displacement values is adequate for studies which used two tibiae from different origin for the model geometry and material properties.

SLICE NUMBER 1

σ_{xx} Pattern

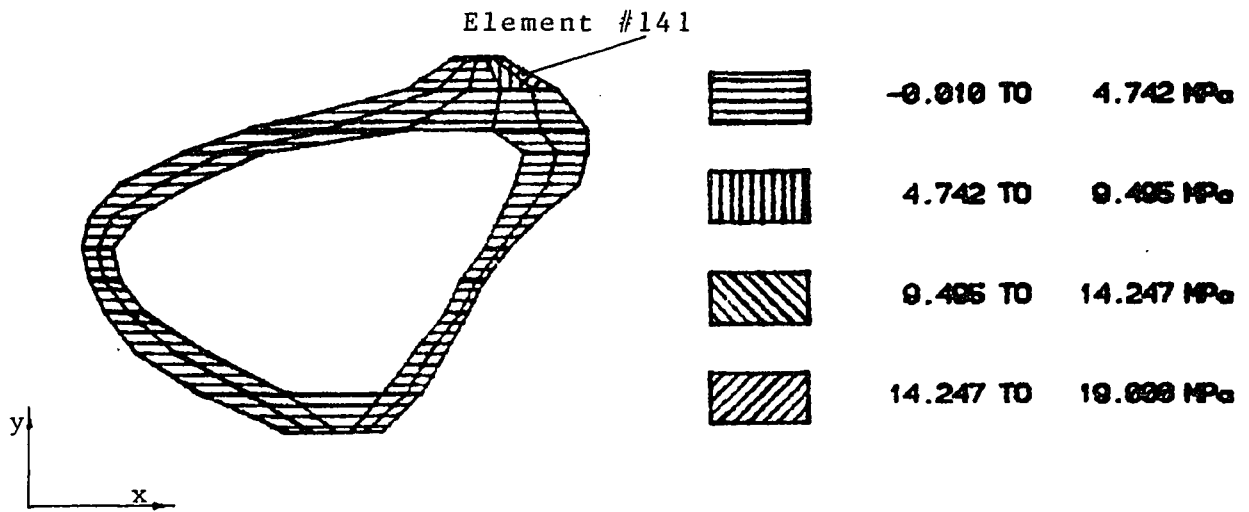


SLICE LOCATION IN Z DIRECTION IN [MM] : 0.00 MM
 MAXIMUM STRESS OF -15.400 MPa OCCURES IN ELEMENT 13

Figure 37: Slice of Maximum Stress σ_{xx} (Element 13) and Maximum Resultant Displacement (Node 36)

SLICE NUMBER 3

σ_{yy} Pattern



SLICE LOCATION IN Z DIRECTION IN [MM] : 10.00 MM

MAXIMUM STRESS OF 19.000 MPa OCCURS IN ELEMENT 141

Figure 38: Slice of Maximum σ_{yy}
(Element 141)

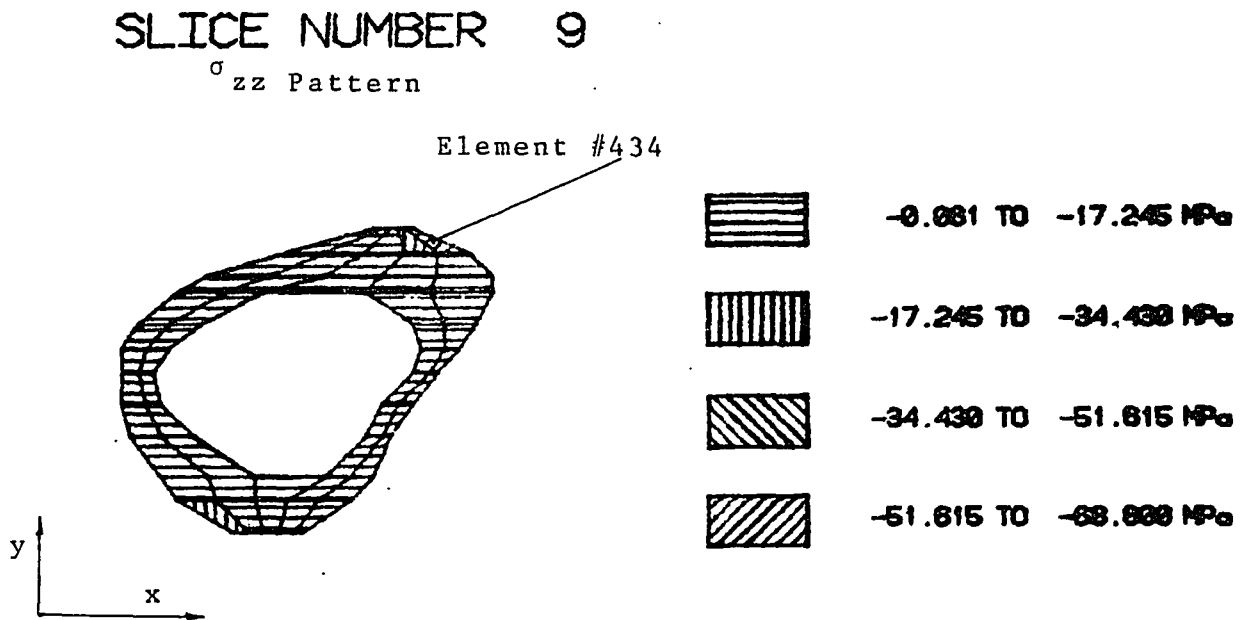


Figure 39: Slice of Maximum σ_{zz}
(Element 434)

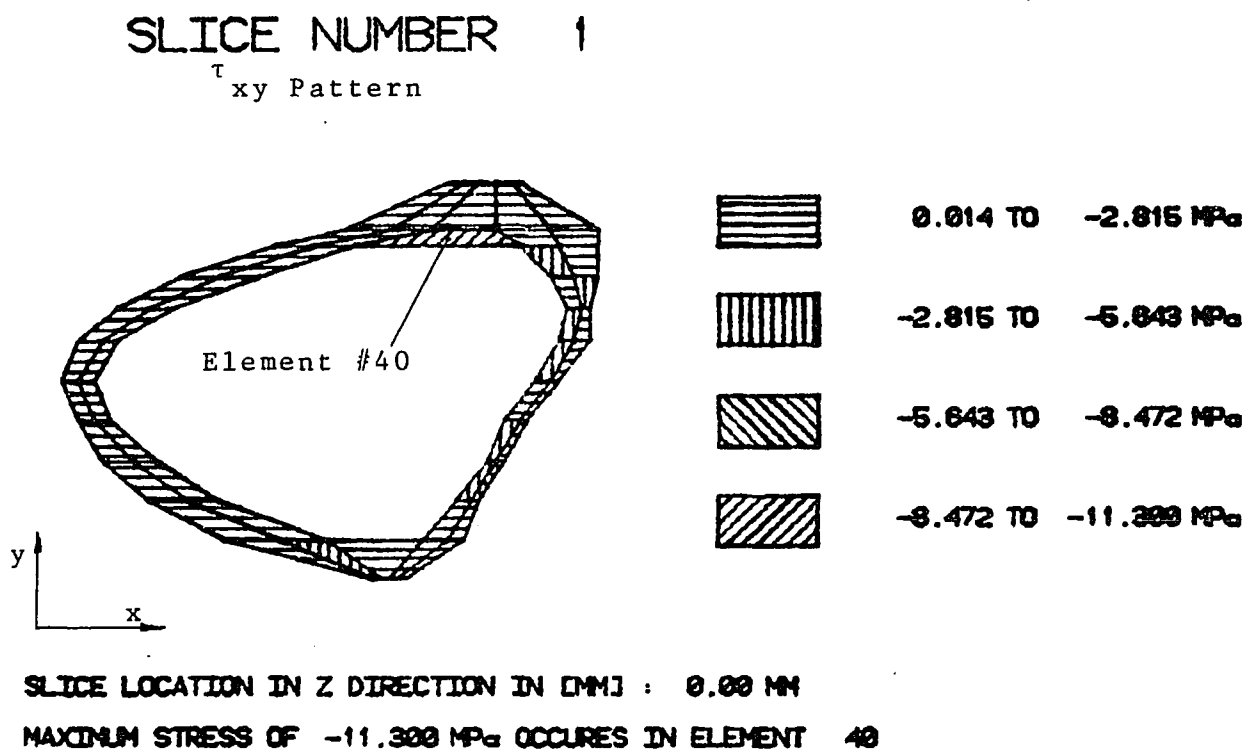


Figure 40: Slice of Maximum τ_{xy}
(Element 40)

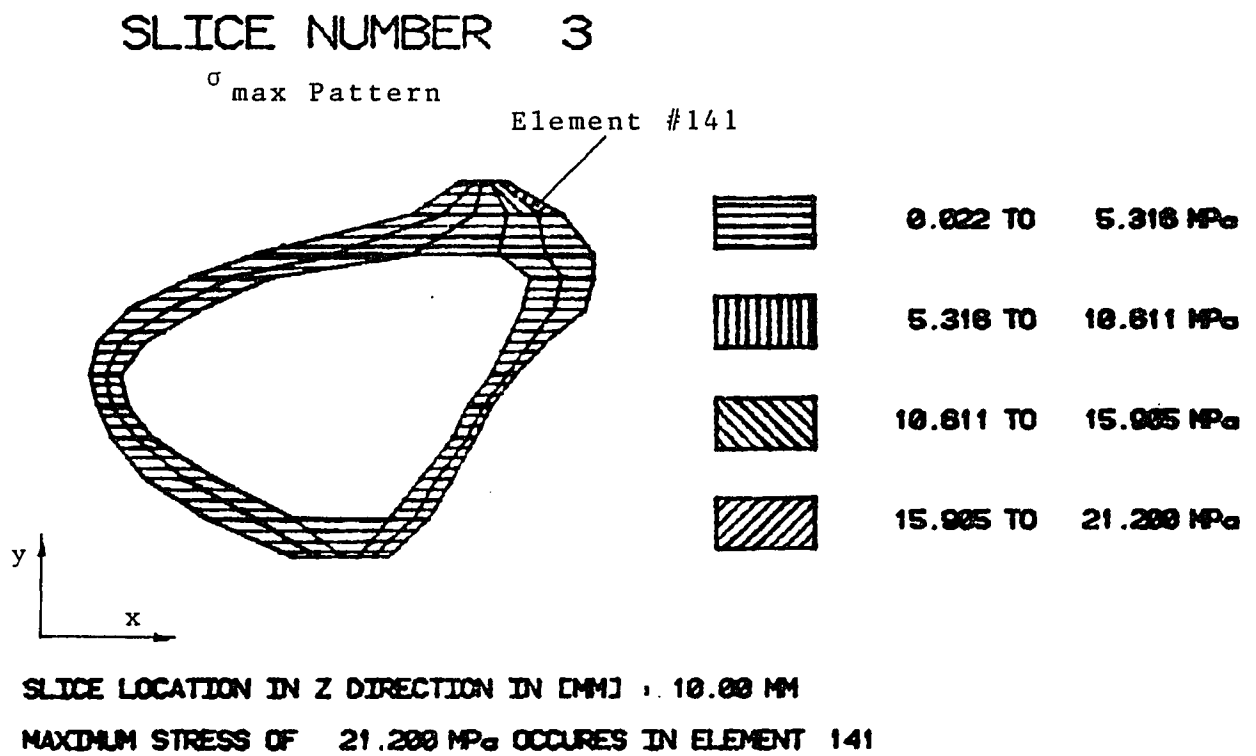
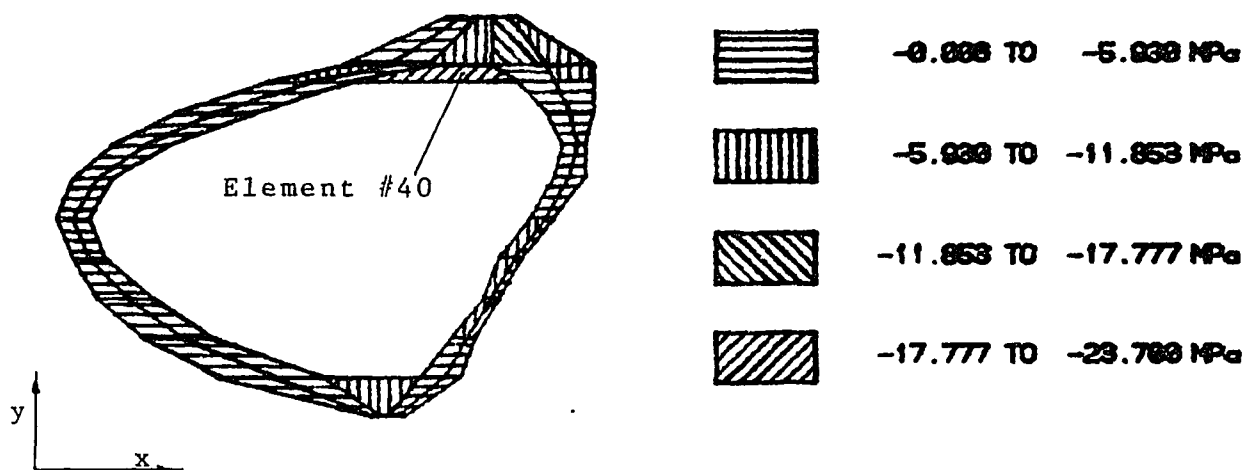


Figure 41: Slice of Maximum σ_{\max}
(Element 141)

SLICE NUMBER 1

σ_{\min} Pattern



SLICE LOCATION IN Z DIRECTION IN [MM] : 0.00 MM

MAXIMUM STRESS OF -23.788 MPa OCCURS IN ELEMENT 40

Figure 42: Slice of Minimum σ_{\min}
(Element 40)

3. SUMMARY AND DISCUSSION

3.1 The Computer Aided Analysis Method

CTPRO has been developed to process a CT data file of a scanned long bone section and create a formatted input file for the stress analysis calculation by the finite element program. The pre-processor CTPRO has the major functions as follows:

A. CTPRO reads a scanned long bone data file which contains the directory files and radiographic density information of up to 45 cross sectional images of the bone. The cross sectional scans are with a constant distance of 2.5 mm from each other. The scan distances may be determined according to the designated model. At the diaphysis (tibia mid-shaft), the spaces between scans may be larger than at the epiphysis and metaphysis in which the geometry changes much faster along the bone main axis. The program can be modified to read consecutive CT data files in order to allow bone section modeling of more than 45 cross sectional images.

B. CTPRO reconstructs the bone cross-sectional images using the directory file information and displays them by a line printer to create the character code images. The obtained images are characterized by high resolution which allow discretizing the cross sections into fine two-dimensional meshes based on the pixel lines.

C. A first order edge detection routine defines the outside and inside borders of the compact bone in the image cross sections. The mesh generator provides continuous closed boundaries of the cortical bone section in the image. The line by line (cartesian) search of the edge detector allows using a first order edge detector. A radial approach would allow using a second order edge detector routine which detects the change in radiographic density rather than comparing it to a minimum breakpoint density. The cartesian approach was preferred due to its higher efficiency and easier implementation.

D. The three-dimensional automatic mesh generator was developed as the main part of the pre-processor and consists of three main sections:

(1) The node selection routine automatically defines a constant number of nodes in each cross sectional image, and stores their location information in a matrix after numbering them by a method which allows automatic generation of three-dimensional elements. The algorithm was designed to select nodes within the borders of the detected cortical bone as defined by the edge detector. Special cases such as demand for more nodes than existing pixels in a discretized region, or a user-selected mesh which is not feasible due to the size of the input scan data, are treated by correction routines or guiding messages.

(2) The element definition routine defines three-dimensional isoparametric eight-node elements from each two adjacent cross sectional discretized images. The method of automatic generation of the elements is inherent with the node numbering method. Some modified finite element programs can discretize a given object into elements of orthotropic or transversely isotropic elastic properties. The use of such programs, when available, would allow more flexibility in long bone modeling.

(3) The mechanical properties generation routine assigns average elastic modulus and Poisson ratio, individually for each element in the model. The average elastic properties were calculated based on the radiographic density information of each pixel within the element borders using an empirical relationship. A relationship from the literature, considered appropriate for this study, relates the apparent density and strain rate to the compressive modulus of elasticity in cortical and trabecular bone tissues. Further experimental work may be aimed at deriving other relationships between the apparent density and other bone mechanical properties which can provide better modeling using computed tomography. In addition, the designed routine calculates the average elastic properties of the entire model which may be compared with experimental measurements.

E. A formatted input file is created for the SAP IV finite element program. The file includes the model

information as obtained by the mesh generator, and applied loads and displacements as defined by the user. The SAP IV program is a long standing program which was selected for this study due to its available source code and large possible model size. The use of modified finite element packages, such as ANSYS, PATRAN or SUPERTAB may provide better efficiency and flexibility in modeling and analyzing, and can be carried out by developing a modified version of the pre-processor of this study. The model display in two and three dimensions was performed in this study using PLOT 10 graphic package and ANSYS plotting module.

The stress analysis results of SAP IV finite element program, stresses and displacements, were sorted and displayed by the developed POST post-processor. The SAP IV source code was available to modify and create an additional output file containing the analysis results in a special format. The dedicated post-processor provides the means to view the stress patterns in the model slices, and examine the maximum values of stresses and displacements at selected elements and nodes in these slices.

The automatically generated three-dimensional finite element model of the long bone section is characterized by the following features:

A. The size (length) of the bone model is determined by the user through selecting the participating scanned slices within the limits of the provided scan information.

B. The cortical bone volume comprising the model is determined by a selected breakpoint radiographic density considered as "cortical bone density" which indicated the participating pixels to the model edge detector.

C. The mesh size is determined by the user through the selection of discretized grid.

D. The model consists of isoparametric eight-node elements, each is assigned with individual elastic properties.

The model generation method was verified by a comparison of the computer aided analysis results with the analytical solution of a generated model of simple geometry. The selected verification model was rectangular and the similarity in both solutions verified the model generation procedures. A convergence test was conducted to determine an optimal mesh size for the bone model. The model displacement values were examined to display convergence to an asymptotic result during mesh refinements. The verification procedure, together with the convergence test, confirm the mesh generation method and the model validity.

The pre- and post-processors of the finite element program may be characterized by the following features:

A. The processors can be applied on any long bone section scanned by a General Electric CT/T 8800 scanner.

B. The processors are affiliated with a SAP IV finite element program version which has been modified in its output generation procedures.

C. The finite element model is generated automatically in a format of SAP IV input file and the results are sorted and displayed by user-selected options which determine the model characteristics as well as the desired results for display.

D. User selected variables determine input-output organization features, such as eliminating redundant information and skipping undesired printout bulks.

E. The processors are coded in FORTRAN 77 computer language. The programs are fully in-line documented and a debugging routine indicates the reason for program stop in cases of improper or insufficient input data file.

A sample problem was modeled and analyzed to demonstrate the processors capabilities. The scanned tibial shaft section was reconstructed and the generated finite element model was analyzed with approximate loads, taken from existing gait analyses. The generated model is displayed in two- and three-dimensions and the resultant stresses and displacements are given by the post-processor in various locations in the bone model. The stress analysis results, stresses and displacements have been compared with results of a recent stress analysis study of the upper tibia (Little et.al., 1986). The model in their study was generated by the conventional method of casting a cadaver tibia, transversely slicing it and then photographing and digitizing the slices to determine the three-dimensional geometry. The material properties of the model were deter-

mined by values from the literature and indentation tests. The generated three-dimensional models of the compared studies differ in the geometry and material properties since analyzing two tibiae of different origin. Both studies were loaded by the same compressive load, determined by Harrington (1976), and agree by order of magnitude in their results.

In summary, this study provides an automatic, non-invasive, versatile and relatively accurate tool for the in-vivo finite element modeling of long bones utilizing a CT data file for the geometry and material properties of the model.

3.2 Future Work

The usefulness of the computer aided analysis method can be enhanced by extending the scope of the present study in the areas of modeling, analysis and applications.

The modeling method in its present state of development generates a non-homogeneous but isotropic three-dimensional model. Combining the processors with a finite element software package including transversely isotropic elements allows the development of a more realistic model with transversely isotropic elastic properties. This feature allows also extending the stress analysis model to the metaphysis and epiphysis where the trabecular bone mechanical properties are anisotropic.

An additional verification problem of cylindrical model with varying geometry and mechanical properties may be analyzed. The computer aided analysis results may be verified by comparing them to the stress analysis results obtained by manual modeling and solving with ANSYS finite element program. This problem analysis may provide an extended verification of the long bone models generated by CTPRO.

The stress analysis of the generated model may be modified by using a more advanced finite element package, which is equipped with various display features and produces more efficient solution. The finite element program used in the future may be selected according to its modeling capabilities and its analysis and post-analysis

features. The pre-processor of this study may be then modified to generate a suitable model and a formatted input file readable by the selected program. An advanced finite element package can provide a stress contour display at the post-processing level to indicate possible failure points.

Applications such as a whole long bone stress studies and long bones with artificial implants may be analyzed by the computer aided stress analysis using the CT data file. A geometric reference, related of the scanned object, can indicate the biomechanical coordinate system which can then be related to the scanner coordinate system. This will allow realistic loads, which may be determined from gait analysis, to be applied to the model generated by the pre-processor. This model analysis may provide more realistic results for the specific scanned models.

A long range goal of this study may be extending this method to serve as a research and diagnostic tool for analyzing the biomechanical response of the long bone of a specific patient. The general procedure of such analysis may be in-vivo scanning of the patient's leg, performing the model generation and stress analysis using the CT data files. Such processors would employ additional methods for eliminating the imaging of soft tissues, isolating the pixel data of the examined bone and relating the scanner coordinate system to the biomechanical system. At

this stage, an interactive version of the processors may be developed with detailed "user friendly" instructions which provide access to the processors by users not expert in computer analysis and coding.

APPENDIX A
TAPE ORGANIZATION

SECTION	SUB SECTIONS	SIZE (2-Byte Word)
Tape Directories	Main Tape Directory	32
	File Directory #1 ‘ ; ‘ ‘ File Directory #N	32 4096 32
Dummy File		30 inch
Display File #1	File Header	256
	Slice #1, Header	256
	Slice #1, data	315x256
	· · ·	
	Slice #N Header	256
	Slice #N Data	315x256
· · ·	· · ·	
Display File #M	· · ·	

Table 1: A CT Archive Tape Organization
in a CT/T 8800 Scanner

APPENDIX B

TAPE AND FILE DIRECTORIES

```
*****  
*  
*          CTPRO PREPROCESSOR FOR SAP IV FINITE ELEMENT          *  
*  
*    STRESS ANALYSIS PROGRAM UTILIZING COMPUTED TOMOGRAPHY    *  
*  
*                   DEVELOPED BY S. MARDM                       *  
*  
*****
```

```
*****  
MAIN DIRECTORY OF SCANNED BONE CT FILE  
*****
```

STARTING POINT : HEAD

REEL NUMBER : 1745

HOSPITAL NAME : UNIVERSITY HOSP UMDNJ

NUMBER OF FILES : 1

SCAN DATE : 7 / 19 / 1984

DISPLAY FILE HEADER

FILE NAME :16867.
PATIENT ID :0
PATIENT NAME :MALE TIB FIB
SCAN DESCRIPTION : MALE CADAVER TIBIA
CONTROL CHARS : SV (SA)VE OR (DE)LETE
HEAD SCAN : 1 (0=NO,1=YES)
NUMBER OF 256 WORD BLOCKS PER SLICE : 1544
SLICE THICKNESS :VT
NUMBER OF SLICES TAKEN : 44
STARTING SLICE : 1
LAST SLICE NUMBER : 44
PIXEL SIZE [MM]: 0.8000
Y-DIAMETER [MM]: 25.0000
X-DIAMETER [MM]: 20.0000
DETECTOR SPACING [MM]: 1.2067
HOSPITAL NAME : UNIVERSITY HOSP UMONJ
DATE OF SCAN : 7 / 19 / 84
DATA TYPE : 3
FILE MODE : 0 (0=NDRMAL,1=SEGMENTED,2=TARGET)

APPENDIX C

MAP ARRAY OF THE CT FILE

 THE MAP ARRAY FOR IMAGE RECONSTRUCTION

IMAP(1) = 1	IMAP(2) = 1	IMAP(3) = 1	IMAP(4) = 1	IMAP(5) = 10
IMAP(6) = 17	IMAP(7) = 22	IMAP(8) = 25	IMAP(9) = 30	IMAP(10) = 33
IMAP(11) = 36	IMAP(12) = 38	IMAP(13) = 41	IMAP(14) = 43	IMAP(15) = 45
IMAP(16) = 47	IMAP(17) = 49	IMAP(18) = 51	IMAP(19) = 53	IMAP(20) = 54
IMAP(21) = 56	IMAP(22) = 58	IMAP(23) = 59	IMAP(24) = 61	IMAP(25) = 62
IMAP(26) = 63	IMAP(27) = 65	IMAP(28) = 65	IMAP(29) = 67	IMAP(30) = 68
IMAP(31) = 70	IMAP(32) = 71	IMAP(33) = 72	IMAP(34) = 73	IMAP(35) = 74
IMAP(36) = 75	IMAP(37) = 76	IMAP(38) = 77	IMAP(39) = 78	IMAP(40) = 79
IMAP(41) = 80	IMAP(42) = 81	IMAP(43) = 82	IMAP(44) = 83	IMAP(45) = 84
IMAP(46) = 85	IMAP(47) = 86	IMAP(48) = 87	IMAP(49) = 87	IMAP(50) = 88
IMAP(51) = 89	IMAP(52) = 90	IMAP(53) = 91	IMAP(54) = 91	IMAP(55) = 92
IMAP(56) = 93	IMAP(57) = 94	IMAP(58) = 94	IMAP(59) = 95	IMAP(60) = 95
IMAP(61) = 96	IMAP(62) = 97	IMAP(63) = 98	IMAP(64) = 98	IMAP(65) = 99
IMAP(66) = 99	IMAP(67) = 100	IMAP(68) = 101	IMAP(69) = 101	IMAP(70) = 102
IMAP(71) = 102	IMAP(72) = 103	IMAP(73) = 103	IMAP(74) = 104	IMAP(75) = 105
IMAP(76) = 105	IMAP(77) = 105	IMAP(78) = 106	IMAP(79) = 107	IMAP(80) = 107
IMAP(81) = 108	IMAP(82) = 108	IMAP(83) = 108	IMAP(84) = 109	IMAP(85) = 109
IMAP(86) = 110	IMAP(87) = 110	IMAP(88) = 111	IMAP(89) = 111	IMAP(90) = 112
IMAP(91) = 112	IMAP(92) = 112	IMAP(93) = 113	IMAP(94) = 113	IMAP(95) = 113
IMAP(96) = 114	IMAP(97) = 114	IMAP(98) = 115	IMAP(99) = 115	IMAP(100) = 115
IMAP(101) = 116	IMAP(102) = 116	IMAP(103) = 116	IMAP(104) = 117	IMAP(105) = 117
IMAP(106) = 117	IMAP(107) = 117	IMAP(108) = 118	IMAP(109) = 118	IMAP(110) = 118
IMAP(111) = 119	IMAP(112) = 119	IMAP(113) = 119	IMAP(114) = 119	IMAP(115) = 120
IMAP(116) = 120	IMAP(117) = 120	IMAP(118) = 120	IMAP(119) = 120	IMAP(120) = 121
IMAP(121) = 121	IMAP(122) = 121	IMAP(123) = 121	IMAP(124) = 122	IMAP(125) = 122
IMAP(126) = 122	IMAP(127) = 122	IMAP(128) = 122	IMAP(129) = 122	IMAP(130) = 123
IMAP(131) = 123	IMAP(132) = 123	IMAP(133) = 123	IMAP(134) = 123	IMAP(135) = 123
IMAP(136) = 123	IMAP(137) = 124	IMAP(138) = 124	IMAP(139) = 124	IMAP(140) = 124
IMAP(141) = 124	IMAP(142) = 124	IMAP(143) = 124	IMAP(144) = 124	IMAP(145) = 124
IMAP(146) = 124	IMAP(147) = 125	IMAP(148) = 125	IMAP(149) = 125	IMAP(150) = 125
IMAP(151) = 125	IMAP(152) = 125	IMAP(153) = 125	IMAP(154) = 125	IMAP(155) = 125
IMAP(156) = 125	IMAP(157) = 125	IMAP(158) = 125	IMAP(159) = 125	IMAP(160) = 125
IMAP(161) = 125	IMAP(162) = 125	IMAP(163) = 125	IMAP(164) = 125	IMAP(165) = 125
IMAP(166) = 125	IMAP(167) = 125	IMAP(168) = 125	IMAP(169) = 125	IMAP(170) = 125
IMAP(171) = 125	IMAP(172) = 125	IMAP(173) = 125	IMAP(174) = 125	IMAP(175) = 124
IMAP(176) = 124	IMAP(177) = 124	IMAP(178) = 124	IMAP(179) = 124	IMAP(180) = 124
IMAP(181) = 124	IMAP(182) = 124	IMAP(183) = 124	IMAP(184) = 124	IMAP(185) = 123
IMAP(186) = 123	IMAP(187) = 123	IMAP(188) = 123	IMAP(189) = 123	IMAP(190) = 123
IMAP(191) = 123	IMAP(192) = 122	IMAP(193) = 122	IMAP(194) = 122	IMAP(195) = 122
IMAP(196) = 122	IMAP(197) = 122	IMAP(198) = 121	IMAP(199) = 121	IMAP(200) = 121
IMAP(201) = 121	IMAP(202) = 120	IMAP(203) = 120	IMAP(204) = 120	IMAP(205) = 120
IMAP(206) = 120	IMAP(207) = 119	IMAP(208) = 119	IMAP(209) = 119	IMAP(210) = 119
IMAP(211) = 118	IMAP(212) = 118	IMAP(213) = 118	IMAP(214) = 117	IMAP(215) = 117
IMAP(216) = 117	IMAP(217) = 117	IMAP(218) = 116	IMAP(219) = 116	IMAP(220) = 116
IMAP(221) = 115	IMAP(222) = 115	IMAP(223) = 115	IMAP(224) = 114	IMAP(225) = 114
IMAP(226) = 113	IMAP(227) = 113	IMAP(228) = 113	IMAP(229) = 112	IMAP(230) = 112
IMAP(231) = 112	IMAP(232) = 111	IMAP(233) = 111	IMAP(234) = 110	IMAP(235) = 110
IMAP(236) = 109	IMAP(237) = 109	IMAP(238) = 108	IMAP(239) = 108	IMAP(240) = 108
IMAP(241) = 107	IMAP(242) = 107	IMAP(243) = 106	IMAP(244) = 106	IMAP(245) = 105
IMAP(246) = 105	IMAP(247) = 104	IMAP(248) = 103	IMAP(249) = 103	IMAP(250) = 102
IMAP(251) = 102	IMAP(252) = 101	IMAP(253) = 101	IMAP(254) = 100	IMAP(255) = 99
IMAP(256) = 99	IMAP(257) = 98	IMAP(258) = 98	IMAP(259) = 97	IMAP(260) = 96
IMAP(261) = 96	IMAP(262) = 95	IMAP(263) = 94	IMAP(264) = 94	IMAP(265) = 93
IMAP(266) = 92	IMAP(267) = 91	IMAP(268) = 91	IMAP(269) = 90	IMAP(270) = 89
IMAP(271) = 88	IMAP(272) = 87	IMAP(273) = 87	IMAP(274) = 86	IMAP(275) = 85
IMAP(276) = 84	IMAP(277) = 83	IMAP(278) = 82	IMAP(279) = 81	IMAP(280) = 80
IMAP(281) = 79	IMAP(282) = 78	IMAP(283) = 77	IMAP(284) = 76	IMAP(285) = 75
IMAP(286) = 74	IMAP(287) = 73	IMAP(288) = 72	IMAP(289) = 71	IMAP(290) = 70
IMAP(291) = 68	IMAP(292) = 67	IMAP(293) = 65	IMAP(294) = 65	IMAP(295) = 63
IMAP(296) = 62	IMAP(297) = 61	IMAP(298) = 59	IMAP(299) = 58	IMAP(300) = 55
IMAP(301) = 54	IMAP(302) = 53	IMAP(303) = 51	IMAP(304) = 49	IMAP(305) = 47
IMAP(306) = 45	IMAP(307) = 43	IMAP(308) = 41	IMAP(309) = 38	IMAP(310) = 35
IMAP(311) = 33	IMAP(312) = 30	IMAP(313) = 26	IMAP(314) = 22	IMAP(315) = 17
IMAP(316) = 10	IMAP(317) = 1	IMAP(318) = 1	IMAP(319) = 1	IMAP(320) = 1

NUMBER OF PIXELS (CALCULATED) FOR EACH SLICE : 61284

APPENDIX D

RADIOGRAPHIC - APPARENT DENSITIES RELATIONSHIP

PROGRAM STAND.FOR OUTPUT

AVERAGE SAMPLE DATA BASED ON ALL 20 SCANNED IMAGES :

CT #	DENS	ERROR(%)
----	----	-----
1026.	1.000	0.4
2000.	1.830	5.8
2174.	2.107	0.2
2356.	2.383	4.2

THE LINEAR REGRESSION COEFFICIENTS ARE :

A = 0.971E-03

B = 0.000E+00

WHERE THE LINEAR REGRESSION RELATIONSHIP IS :

DENSITY = A * CT DENSITY + B

APPENDIX E

CTPRO OUTPUT OF MODEL INFORMATION

434 ELEMENTS WERE FILED IN ARRAY "ELMNT".

9 SLICES , EACH CONSISTS OF 48 ISOPARAMETRIC (BRICK) ELEMENTS
ARE FORMING THE THREE DIMENSIONAL MESH OF THE TIBIA SEGMENT .

THE AVERAGE MODULUS OF ELASTICITY OF THE WHOLE
BONE SECTION IS : 0.4950E+04 [MPa] OR 0.7179E+06 [PSI] .

THE MAXIMUM ELEMENT AVERAGE MODULUS OF ELASTICITY IS : 0.5357E+05 [MPa]

THE MINIMUM ELEMENT AVERAGE MODULUS OF ELASTICITY IS : 0.1220E+04 [MPa]

2 CONCENTRATED LOADS WERE APPLIED IN X DIRECTION :

-123.75 [NEWTONS] AT NODE NUMBER 18

-38.00 [NEWTONS] AT NODE NUMBER 70

2 CONCENTRATED LOADS WERE APPLIED IN Y DIRECTION :

65.00 [NEWTONS] AT NODE NUMBER 18

-162.52 [NEWTONS] AT NODE NUMBER 70

APPENDIX F

POST OUTPUT OF VERIFYING MODEL ANALYSIS

```
*****  
*  
*   POSTPROCESSOR FOR SAP IV FINITE ELEMENT MODEL   *  
*  
*           GENERATED BY READCT PREPROCESSOR       *  
*  
*           DEVELOPED BY S. MAROM                   *  
*  
*****
```

THE READ INPUT FILE INCLUDES NODAL INFORMATION , COORDINATES
AND RESULTANT DISPLACEMENTS , OF NUMNP = 228 NODAL POINTS ,
DEFINITIONS , PROPERTIES AND RESULTANT STRESSES OF NELM = 108 ELEMENTS

THE MODEL CONSISTS OF 18 3-D SLICES .

THE FIRST AND LAST NODES IN EACH SLICE ARE :

SLICE	FIRST ELEMENT	LAST ELEMENT
-----	-----	-----
1	1	6
2	7	12
3	13	18
4	19	24
5	25	30
6	31	36
7	37	42
8	43	48
9	49	54
10	55	60
11	61	66

12	67	72
13	73	78
14	79	84
15	85	90
16	91	96
17	97	102
18	103	108

MAXIMUM DISPLACEMENTS (TABLE 2)

MAXIMUM NODAL DISPLACEMENTS IN THE DIRECTIONS X Y AND Z :

DELTA MAX = 0.698E-03 MM IN NODE NUMBER 216
AT LOCATION (7.20 , 4.80 , 42.50) [MM] .

DELTA MAX = 0.157E+00 MM IN NODE NUMBER 12
AT LOCATION (7.20 , 4.80 , 0.00) [MM] .

DELTA MAX = 0.110E-01 MM IN NODE NUMBER 60
AT LOCATION (7.20 , 4.80 , 10.00) [MM] .

MAX/MIN STRESSES IN MPa : (TABLE 3)

SIGMA	MAX	ELEMENT	AT SLICE	MIN	ELEMENT	AT SLICE
XX	0.13E+02	105	18	-0.13E+02	108	18
YY	0.13E+02	105	18	-0.13E+02	108	18
ZZ	0.26E+02	105	18	-0.26E+02	108	18
XY	0.74E+00	100	17	-0.74E+00	102	17
YZ	0.22E+01	106	18	-0.22E+01	108	18
ZX	0.33E+01	104	18	0.42E-01	5	1
MAX	0.13E+02	105	18	-0.13E+02	108	18
MIN	0.13E+02	105	18	-0.13E+02	108	18

THE DESIRED SLICE , KSTR = 18 WAS PLOTTED AND STORED IN FILE

APPENDIX G

POST OUTPUT OF DEMONSTRATING PROBLEM ANALYSIS

```

*****
*
*   POSTPROCESSOR FOR SAP IV FINITE ELEMENT MODEL   *
*
*   GENERATED BY CTPRO PREPROCESSOR                 *
*
*   DEVELOPED BY S. MAROM                           *
*
*****

```

THE READ INPUT FILE INCLUDES NODAL INFORMATION , COORDINATES
AND RESULTANT DISPLACEMENTS , OF NUMNP = 720 NODAL POINTS ,
DEFINITIONS , PROPERTIES AND RESULTANT STRESSES OF NELM = 434 ELEMENTS .

THE MODEL CONSISTS OF 10 2-D (SCANNED) CROSS SECTIONS ,
EACH OF THEM INCLUDES 6 NODES IN X DIRECTION , AND 12 NODES IN Y DIRECTION
HENCE , THE TOTAL NUMBER OF NODES IN EACH CROSS SECTION IS 72 ,
AND IN THE WHOLE MODEL 720 NODES .

THE FIRST AND LAST NODE IN EACH CROSS SECTION ARE :

<u>CROSS SECTION</u>	<u>FIRST NODE</u>	<u>LAST NODE</u>
1	1	72
2	73	144
3	145	216
4	217	288
5	289	360
6	361	432
7	433	504
8	505	576
9	577	648
10	649	720

THE MODEL CONSISTS OF 9 3-D SLICES .

THE FIRST AND LAST ELEMENTS IN EACH SLICE ARE :

SLICE	FIRST ELEMENT	LAST ELEMENT
-----	-----	-----
1	1	47
2	48	94
3	95	141
4	142	189
5	190	238
6	239	287
7	288	336
8	337	385
9	386	434

MAXIMUM DISPLACEMENTS (TABLE 4)

MAXIMUM NODAL DISPLACEMENTS IN THE DIRECTIONS X, Y AND Z :

DELTA MAX = 0.389E+00 MM IN NODE NUMBER 36
 AT LOCATION (73.60 , 41.60 , 0.00) [MM] .

DELTA MAX = -0.251E+00 MM IN NODE NUMBER 70
 AT LOCATION (67.20 , 61.60 , 0.00) [MM] .

DELTA MAX = 0.296E+00 MM IN NODE NUMBER 36
 AT LOCATION (73.60 , 41.60 , 0.00) [MM] .

MAXIMUM RESULTANT NODAL DISPLACEMENT IS :

DELTA MAX = 0.536E+00 MM IN NODE NUMBER 36

AT LOCATION (73.60 , 41.60 , 0.00) [MM]

WITH DISPLACEMENT COMPONENTS IN X,Y,Z, DIRECTIONS OF :

0.389E+00 -0.221E+00 0.296E+00 [MM]

MAX/MIN STRESSES IN MPa : (TABLE 5)

<u>SIGMA</u>	<u>MAX</u>	<u>ELEMENT</u>	<u>AT SLICE</u>	<u>MIN</u>	<u>ELEMENT</u>	<u>AT SLICE</u>
XX	-0.154E+02	13	1	0.173E-02	356	8
YY	0.190E+02	141	3	-0.170E-02	362	8
ZZ	-0.688E+02	434	9	-0.183E-01	355	8
XY	-0.113E+02	40	1	0.285E-03	246	6
YZ	0.171E+02	287	6	0.821E-02	143	4
ZX	0.103E+02	287	6	0.518E-02	47	1
MAX	0.212E+02	141	3	-0.464E-02	219	5
MIN	-0.237E+02	40	1	-0.374E-02	433	9

THE DESIRED SLICE , KSTR = 6 WAS PLOTTED AND STORED IN FILE "STRESS"

APPENDIX H

POST OUTPUT FOR COMPARISON ANALYSIS

MAXIMUM DISPLACEMENTS (TABLE 6)

MAXIMUM NODAL DISPLACEMENTS IN THE DIRECTIONS X Y AND Z :

DELTA MAX = 0.363E+00 MM IN NODE NUMBER 30
AT LOCATION (70.40 , 37.60 , 0.00) [MM] .

DELTA MAX = -0.199E+00 MM IN NODE NUMBER 24
AT LOCATION (68.00 , 32.60 , 0.00) [MM] .

DELTA MAX = 0.260E+00 MM IN NODE NUMBER 30

MAX/MIN STRESSES IN MPa : (TABLE 7)

<u>SIGMA</u>	<u>MAX</u>	<u>ELEMENT</u>	<u>AT SLICE</u>	<u>MIN</u>	<u>ELEMENT</u>	<u>AT SLICE</u>
-----	---	-----	-----	---	-----	-----
XX	0.157E+02	2	1	-0.310E-02	266	6
YY	0.167E+02	52	2	-0.140E-02	412	9
ZZ	-0.752E+02	434	9	-0.237E-03	351	8
XY	0.416E+01	24	1	0.260E-03	419	9
YZ	0.196E+02	287	6	-0.356E-02	24	1
ZX	0.117E+02	287	6	0.292E-03	185	4
MAX	0.170E+02	52	2	0.164E-02	376	8
MIN	-0.117E+02	3	1	0.327E-02	413	9

APPENDIX I

SAP IV OUTPUT INFORMATION OF DEMONSTRATING PROBLEM

SAPIV STRUCTURAL ANALYSIS PROGRAM

STRESS ANALYSIS OF A LONG BONE UTILIZING COMPUTED TOMOGRAPHY

NUMBER OF NODAL POINTS = 720
NUMBER OF ELEMENT TYPES = 1
NUMBER OF LOAD CASES = 1
NUMBER OF FREQUENCIES = 0
ANALYSIS TYPE = 0
0 - STATIC ANALYSIS
1 - PERIODS AND MODE SHAPES
2 - FORCED RESPONSE ANALYSIS
3 - RESPONSE SPECTRUM (SINGLE)
5 - RESPONSE SPECTRUM (MULTIPLE)

STATIC SOLUTION EXECUTION TIMES

SOLUTION OF EQUATIONS = 881.31
CALC. & PRINT DISP. = 4.76
CALC. & PRINT STRESSES = 9.18

STRESS ANALYSIS OF A LONG BONE UTILIZING COMPUTED TOMOGRAPHY

EXECUTION TIMES

NODAL POINT INPUT = 13.97
ELEM. STIF. FORMATION = 139.70
NODAL LOAD INPUT = 0.90
TOTAL STIF. FORMATION = 103.13
STATIC ANALYSIS = 895.25
PERIODS AND MODE SHAPES = 0.00
FORCED RESPONSE ANAL. = 0.00
RESPONSE SPECTRUM ANAL. = 0.00
STEP BY STEP INTEG. = 0.00

TOTAL SOLUTION TIME = 1152.95

EQUATION PARAMETERS

NUMBER OF EQUATIONS = 1944
BANDWIDTH OF SYSTEM = 240
NO. OF EQUATIONS/BLOCK = 82
NUMBER OF BLOCKS OF EQ. = 24

BIBLIOGRAPHY

- 1 ADAMOVICH, I. S., YANSON, I. M., "INVESTIGATION OF THE STRESS STATE OF A HUMAN TIBIA IN TORSION BY FINITE ELEMENT METHODS", MECHANICS OF COMPOSITE MATERIALS, VOL. 3, 1981, PP. 499-504.
- 2 ALVAREZ, R. E., MACOVSKI, A., "ENERGY-SELECTIVE RECONSTRUCTIONS IN X-RAY COMPUTERIZED TOMOGRAPHY". PHYSICAL AND MEDICAL BIOLOGY, VOL. 21, 1976, PP. 733-744.
- 3 ANSYS ENGINEERING ANALYSIS SYSTEM USER'S MANUAL, SWANSON ANALYSIS SYSTEMS, HAUSTON, PENNSYLVANIA, 1983.
- 4 AVRIN, D. E., MACOVSKI, A., ZATZ, L. M., "CLINICAL APPLICATION OF COMPTON AND PHOTO ELECTRIC RECONSTRUCTION IN COMPUTED TOMOGRAPHY: PRELIMINARY RESULTS", INVESTIGATIVE RADIOLOGY, VOL. 13, 1978, PP. 217-222.
- 5 ASHMAN, R. B., COWIN, S. C., VAN BUSKIRK; W. C., "A CONTINUOUS WAVE TECHNIQUE FOR THE MEASUREMENT OF THE ELASTIC PROPERTIES OF CORTICAL BONE", JOURNAL OF BIOMECHANICS, VOL. 17(5), 1984, PP. 349-361.
- 6 ASKIEW, M. J., "ANALYSIS OF MODEL VARIABLES AND FIXATION POST LENGTH EFFECTS ON STRESSES AROUND A PROSTHESIS IN THE PROXIMAL TIBIA", JOURNAL OF BIOMECHANICAL ENGINEERING, VOL. 103, NOVEMBER, 1981, PP. 239-245.
- 7 BANKS, L. M., STEVENSON, J. C., "MODIFIED METHOD OF SPINAL COMPUTED TOMOGRAPHY FOR TRABECULAR BONE MINERAL MEASUREMENTS", JOURNAL OF COMPUTER AIDED TOMOGRAPHY, VOL. 10(3), 1986, PP. 463-467.
- 8 BARRETT, H. H., GORDON, S. K., HERSHEL, R. S., "STATISTICAL LIMITATIONS IN TRANSAXIAL TOMOGRAPHY", COMPUTERS IN BIOLOGY AND MEDICINE, VOL. 6, 1976, PP. 307-323.
- 9 BARTON, T. J., "A SIMPLE RAPID METHOD OF OBTAINING GEOMETRICAL PROPERTIES FROM SECTIONS OR LIMINOGRAPHIS OF LONG BONES", JOURNAL OF BIOMECHANICS, VOL. 13, 1980, PP. 65-67.
- 10 BEAUPRE, G. S., HAYES, W. C., "FINITE ELEMENT ANALYSIS OF A THREE DIMENSIONAL OPEN-CELLED MODEL FOR TRABECULAR BONE", JOURNAL OF BIOMECHANICAL ENGINEERING, VOL. 107, AUGUST, 1985, PP. 249-256.
- 11 BEHIRI, J. C., BONFIELD, W., "FRACTURE MECHANICS OF BONE - THE EFFECT OF DENSITY", JOURNAL OF BIOMECHANICS, VOL. 17(1), 1984, PP. 25-34.

- 12 BEHRENS, J. C., WALKER, P. S., SHOJI, H., "VARIATIONS IN STRENGTH AND STRUCTURE OF CANCELLOUS BONE AT THE KNEE", JOURNAL OF BIOMECHANICS, 1974, PP. 201-207.
- 13 BENSUSAN, J. S., DAVY, D. T., HAIPLE, K. G., "TENSILE COMPRESSIVE AND TORSIONAL TESTING OF CANCELLOUS BONE", TRANSACTIONS 29TH ANNUAL ORS, MARCH, 1983, P. 132.
- 14 BLANTON, P. L., BIGGS, N. L., "DENSITY OF FRESH AND EMBALMED HUMAN COMPACT AND CANCELLOUS BONE", AMERICAN JOURNAL OF PHYSIOLOGY AND ANTHROPOLOGY, VOL. 29, 1968, PP. 39-44.
- 15 BOYD, D., CANN, C., GENANT, H., "A PROPOSED MULTISOURCE CT SCANNER FOR ULTRAACCURATE TOMODENSITOMETRY THROUGHOUT THE BODY", JOURNAL OF COMPUTER ASSISTED TOMOGRAPHY, VOL. 3, 1979, P. 856.
- 16 BRADLEY, J. G., HUANG, H. K., LEDLY, R. S., "EVALUATION OF CALCIUM CONCENTRATION IN BONES FROM CT SCANS", COMPUTED TOMOGRAPHY, JULY, 1978, PP. 103-107.
- 17 BROOKS, R. A., DICHIRO, G., "BEAM HARDENING IN X-RAY RECONSTRUCTIVE TOMOGRAPHY", PHYSICAL AND MEDICAL BIOLOGY, VOL. 21(3), 1976, PP. 390-398.
- 18 BROOKS, R. A., "BONE CORRECTIONS IN COMPUTER ASSISTED TOMOGRAPHY", JOURNAL OF COMPUTER ASSISTED TOMOGRAPHY, VOL. 1, 1977, P. 267.
- 19 BROOKS, R. A., DICHIRO, G., "SPLIT-DETECTOR COMPUTED TOMOGRAPHY: A PRELIMINARY REPORT", RADIOLOGY, VOL. 126, 1978, PP. 255-257.
- 20 BROOKS, R. A., MITCHELL, L. G., O'CONNOR, C. M., DICHIRO, G. "ON THE RELATIONSHIP BETWEEN COMPUTED TOMOGRAPHY NUMBERS AND SPECIFIC GRAVITY", PHYSICAL AND MEDICAL BIOLOGY, VOL. 26(1), 1981, PP. 141-147.
- 21 BROWN, T. D., FERGUSON, A. D., "THE DEVELOPMENT OF A COMPUTATIONAL STRESS ANALYSIS OF THE FEMORAL HEAD", JOURNAL OF BONE AND JOINT SURGERY, JULY, 1978, PP. 619-622.
- 22 BROWN, T. D., DIGIOIA, A. M., "A CONTACT COUPLED FINITE ELEMENT ANALYSIS OF THE NATURAL ADULT HIP", JOURNAL OF BIOMECHANICS, VOL. 17(6), 1984, PP. 437-448.
- 23 BURSTEIN, A. H., FRANKEL, V. H., "THE VISCOELASTIC PROPERTIES OF SOME BIOLOGICAL MATERIALS", ANNALS OF THE NEW YORK ACADEMY OF SCIENCE, VOL. 146, 1968, PP. 158-165.
- 24 BURSTEIN, A. H., SHAFFER, B. W., FRANKEL, V. H., "ELASTIC ANALYSIS OF CONDYLAR STRUCTURES", ASME PUBLICATION, 70-WA/BHF-1, 1970.

- 25 BURSTEIN, A. H., CURREY, J. D., FRANKEL, V. H., REILLY, D. T., "THE ULTIMATE PROPERTIES OF BONE TISSUE: THE EFFECTS OF YIELDING", JOURNAL OF BIOMECHANICS, VOL. 5, 1972, PP. 35-44.
- 26 CANN, C. E., GENANT, H. K., "PRECISE MEASUREMENT OF VERTEBRAL MINERAL CONTENT USING COMPUTED TOMOGRAPHY", JOURNAL OF COMPUTER ASSISTED TOMOGRAPHY, VOL. 4(4), AUGUST, 1980, PP. 493-500.
- 27 CARTER, D. R., HAYES, W. C., "BONE COMPRESSIVE STRENGTH: THE INFLUENCE OF DENSITY AND STRAIN RATE", SCIENCE, VOL. 194, 1976, PP. 1174-1176.
- 28 CARTER, D. R., HAYES, W. C., "THE COMPRESSIVE BEHAVIOR OF BONE AS A TWO-PHASE POROUS STRUCTURE", JOURNAL OF BONE AND JOINT SURGERY, VOL. 59-A(7), OCTOBER, 1977, PP. 954-962.
- 29 CARTER, D. R., "ANISOTROPIC ANALYSIS OF STRAIN ROSETTE INFORMATION FROM CORTICAL BONE", JOURNAL OF BIOMECHANICS, VOL. 11, 1978, PP. 199-202.
- 30 CARTER, D. R., SCHWAB, G. H., SPENGLER, D. M., "THE EFFECT OF APPARENT DENSITY ON THE TENSILE AND COMPRESSIVE PROPERTIES OF CANCELLOUS BONE", 25TH ANNUAL ORS, FEBRUARY, 1979, PP. 87.
- 31 CARTER, D. R., "RESULTANT LOADS AND ELASTIC MODULUS CALIBRATION IN LONG BONE CROSS SECTIONS", JOURNAL OF BIOMECHANICS, VOL. 14(11), 1981, PP. 739-745.
- 32 CAVENDISH, J. C., "AUTOMATIC TRIANGULATION OF ARBITRARY PLANER DOMAINS FOR THE FINITE ELEMENT METHOD", INTERNATIONAL JOURNAL FOR NUMERICAL METHODS IN ENGINEERING, VOL. 8, 1974, PP. 679-696.
- 33 CEZAYIRLIOGLU, H., BAHNIUK, E., DAVY, D. T., "ANISOTROPIC YIELD BEHAVIOR OF BONE UNDER COMBINED AXIAL FORCE AND TORQUE", JOURNAL OF BIOMECHANICS, VOL. 18(1), 1985, PP. 61-69.
- 34 CHAND, R., HAUG, E., RIM, K., "STRESSES IN THE HUMAN KNEE JOINT", JOURNAL OF BIOMECHANICS, VOL. 9, 1976, PP. 417-422.
- 35 CHAO, E. Y., WONG, H. W., FRAIN, W. E., "STRESS ANALYSIS OF GEOMETRIC KNEE UNDER STATIC LOADING", ASME TECHNICAL PUBLICATION, 70-WA/BHF-6, 1977, PP. 1-20.
- 36 CHATTERJI, S., "ANISOTROPY OF YOUNG'S MODULUS OF BONE", NATURE, VOL. 288, NOVEMBER, 1980, PP. 196.

- 37 COOK, R. D., "CONCEPTS AND APPLICATIONS OF FINITE ELEMENT ANALYSIS", SECOND EDITION, JOHN WILEY & SONS, 1981.
- 38 CORMACK, A. M., "RECONSTRUCTION OF DENSITY FROM THEIR PROJECTION, WITH APPLICATION IN RADIOLOGICAL PHYSICS", PHYSICAL AND MEDICAL BIOLOGY, VOL. 18, 1963, PP. 195-207.
- 39 CORMACK, A. M., "COMPUTED TOMOGRAPHY: SOME HISTORY AND RECENT DEVELOPMENTS", PROCEEDINGS OF SYMPOSIA IN APPLIED MATHEMATICS, VOL. 27, 1982, PP. 35-42.
- 40 CORONDAN, G., HAWORTH, W. L., "A FRACTOGRAPHIC STUDY OF HUMAN LONG BONE", JOURNAL OF BIOMECHANICS, VOL. 19(3), 1986, PP. 207-218.
- 41 COWIN, S. C., "WOLFF'S LAW OF TRABECULAR ARCHITECTURE AT REMODELLING EQUILIBRIUM", JOURNAL OF BIOMECHANICAL ENGINEERING, VOL. 108, FEBRUARY, 1986, PP. 83-89.
- 42 CT/T CONTINUUM; EVALUATION CRITERIA, GENERAL ELECTRIC, MEDICAL SYSTEM DIVISION, MILWAUKEE, WISCONSIN, 1980.
- 43 CURREY, J. D., "THE MECHANICAL CONSEQUENCES OF VARIATION IN THE MINERAL CONTENT OF BONE", JOURNAL OF BIOMECHANICS, VOL. 2(1), 1969, PP.
- 44 CURREY, J. D., "THE MECHANICAL PROPERTIES OF BONE", CLINICAL ORTHOPEDICS AND RELATED RESEARCH, VOL. 73, 1970, PP. 210-231.
- 45 DODES, I. A., "NUMERICAL ANALYSIS FOR COMPUTER SCIENCE, NEW YORK, ELSAVIER NORTH HOLLAND, 1980.
- 46 DUCHEINE, P., HEYMANS, L., MARTENS, M., AERNOUDT, E., "THE MECHANICAL BEHAVIOR OF INTERCONDYLAR CANCELLOUS BONE OF THE FEMUR AT DIFFERENT LOADING RATES", JOURNAL OF BIOMECHANICS, VOL. 10, 1977, PP. 747-762.
- 47 DUERINCKX, A. J., MACOVSKI, A., "CLASSIFICATION OF ARTIFACTS IN X-RAY CT IMAGES DUE TO NONLINEAR SHADOWS", IEEE TRANSACTIONS ON NUCLEAR SCIENCE, VOL. NS-26(2), APRIL, 1979, PP. 2848-2852.
- 48 DUERINCKX, A. J., MAKOVSKI, A., "NONLINEAR POLYCHROMATIC AND NOISE ARTIFACTS IN X-RAY COMPUTED TOMOGRAPHY IMAGES", JOURNAL OF COMPUTER ASSISTED TOMOGRAPHY, VOL. 3, 1979B, PP. 519-526.
- 49 DUROCHEN, L. L., GASPER, A., "A VERSATILE TWO-DIMENSIONAL MESH GENERATOR WITH AUTOMATIC BANDWIDTH REDUCTION", COMPUTER AND STRUCTURES, VOL. 10, 1979, PP. 561-575.
- 50 ECLIPSE LINE COMPUTERS, DATA GENERAL CORPORATION, NO. 014-000626, WESTBORO, MASSACHUSETTS, AUGUST, 1979.

- 51 EHLER, E., CHRISTMAN, C., PFAU, H., "THE INFLUENCE OF INHOMOGENEITY ON STRENGTH OF BONES", ANATOMICAL ANZ., VOL. 142, 1977, PP. 512-518.
- 52 ELSASSER, U., REEVE, J., "BONE DENSITY MEASUREMENTS WITH COMPUTED TOMOGRAPHY", BRITISH MEDICAL BULLETINE, VOL. 36(3), 1980, PP. 293-296.
- 53 ENGIN, A. E., KORDE, M. S., "BIOMECHANICS OF NORMAL AND ABNORMAL KNEE JOINT", JOURNAL OF BIOMECHANICS, VOL. 7, 1974, PP. 325-334.
- 54 EVANS, F. G., LEBOW, M., "STRENGTH OF HUMAN COMPACT BONE UNDER REPETITIVE LOADING", JOURNAL OF APPLIED PHYSIOLOGY, VOL. 10, 1957, PP. 127-130.
- 55 EVANS, F. G., KING, A. I., "REGIONAL DIFFERENCES IN SOME PHYSICAL PROPERTIES OF HUMAN SPONGY BONE", BIOMECHANICAL STUDIES OF THE MUSCULOSKELETAL SYSTEMS, SPRINGFIELD, THOMAS BROOKS, 1961, PP. 49-67.
- 56 EVANS, F. G., "MECHANICAL PROPERTIES AND HISTOLOGICAL STRUCTURE OF HUMAN CORTICAL BONE", ASME TECHNICAL PUBLICATION, 70-WA/BHF-7, 1970.
- 57 EVANS, F. G., "MECHANICAL PROPERTIES OF BONE", SPRINGFIELD, IL., CHARLES C. THOMAS, 1973.
- 58 EVANS, F. G., VINCENTELLI, R., "RELATIONS OF THE COMPRESSIVE PROPERTIES OF HUMAN CORTICAL BONE TO HISTOLOGICAL STRUCTURE AND CALCIFICATION", JOURNAL OF BIOMECHANICS, VOL. 7, 1974, PP. 1-10.
- 59 FISCHER, L. P., "THE ROLE OF THE MUSCLES AND LIGAMENTS IN STABILIZATION OF THE KNEE JOINT", ANATOMIA CLINICA, VOL. 1, 1978, PP. 123-142.
- 60 FRANKEL, V. H., BURSTEIN, A. H., "LOAD CAPACITY OF TUBULAR BONE", BIOMECHANICS AND RELATED BIOENGINEERING TOPICS", ED: KENEDI, R. M., PERGAMENT PRESS, OXFORD, 1965, PP. 381-396.
- 61 FRASCA, P., JACYNA, G., HARPER, R., "STRAIN DEPENDANCE OF DYNAMIC YOUNG'S MODULUS FOR HUMAN SINGLE OSTEON", JOURNAL OF BIOMECHANICS, VOL. 14(10), 1981, PP. 691-696.
- 62 FREDERICK, C. D., WONG, Y. C., EDGE, F. W., "TWO-DIMENSIONAL AUTOMATIC MESH GENERATION FOR STRUCTURAL ANALYSIS", INTERNATIONAL JOURNAL FOR NUMERICAL METHODS IN ENGINEERING, VOL. 2, 1970, PP. 133-144.

- 63 FYHRIE, D. P., CARTER, D.R., "PREDICTION OF CANCELLOUS BONE APPARENT DENSITY AND ORIENTATION", ADVANCES IN BIOENGINEERING, ED: LANGRANA, N. A., THE AMERICAN SOCIETY OF MECHANICAL ENGINEERING, NEW YORK, 1985, PP. 30-31.
- 64 GALANTE, J., ROSTOKER, W., RAY, R. D., "PHYSICAL PROPERTIES OF TRABECULAR BONE", CALCIFIED TISSUE RESEARCH, VOL. 5, 1970, PP. 236-246.
- 65 GARG, A., WALKER, P. S., "COMPARISON OF INTERFACE STRESSES FOR CEMENTED AND UNCEMENTED TIBIAL COMPONENTS", TRANS 31ST ANNUAL ORS, JANUARY, 1985, PP. 124.
- 66 GENNANT, H. K., BOYD, D. "QUANTITATIVE BONE MINERAL ANALYSIS USING DUAL ENERGY COMPUTED TOMOGRAPHY", INVESTIGATIVE RADIOLOGY, VOL. 12, 1977, PP. 545-551.
- 67 GENNANT, H. K., BOYD, D., ROSENFELD, D., ABOLS, Y., CANN, C. E., "COMPUTED TOMOGRAPHY IN NON INVASIVE MEASUREMENTS OF BONE MASS AND THEIR CLINICAL APPLICATION, ED: COHN, S. H., CRC PRESS, BOCA RATON, FLORIDA, 1981.
- 68 GIBSON, L. J., "THE MECHANICAL BEHAVIOR OF CANCELLOUS BONE", JOURNAL OF BIOMECHANICS, VOL. 18(5), 1985, PP. 317-328.
- 69 GIES, A. A., CARTER, D. R., "EXPERIMENTAL DETERMINATION OF A WHOLE LONG BONE SECTIONAL PROPERTIES", JOURNAL OF BIO-MECHANICS, VOL. 15(4), 1982, PP. 297-303.
- 70 GOLDSTEIN, S. A., WILSON, D. L., SONSTEGARD, D. A., "AN EXPERIMENTAL DETERMINATION OF NUMERICAL VALUES FOR ELASTIC MODULUS AND ULTIMATE STRENGTH OF HUMAN TRABECULAR BONE AS A FUNCTION OF LOCATION", TRANSACTIONS 26TH ANNUAL ORS, VOL. 5, 1980, P. 58.
- 71 GOLDSTEIN, S. A., WILSON, D. L., SONSTEGARD, D. A., "THE MECHANICAL PROPERTIES OF HUMAN TIBIAL TRABECULAR BONE AS A FUNCTION OF METAPHYSEAL LOCATION", JOURNAL OF BIOMECHANICS, VOL. 16(12), 1983, PP. 965-969.
- 72 GONG, J. K., ARNOLD, J. S., COHN, S. H., "COMPOSITION OF TRABECULAR AND CORTICAL BONE", ANATOMICAL RECORD, VOL. 149, 1964, PP. 325-331.
- 73 GORDON, W. J., "BLENDING-FUNCTION METHODS OF BIVARIATE AND MULTIVARIATE INTERPOLATION AND APPROXIMATION", SIAM JOURNAL OF NUMERICAL ANALYSIS, VOL. 8(1), 1971, PP. 158-177.
- 74 HARRIGAN, T. P., OH, I., HARRIS, W. H., "THE ANISOTROPIC PROPERTIES OF TRABECULAR BONE", TRANS 26TH ANNUAL ORS, FEBRUARY, 1980, P. 60.

- 75 HARRIGAN, T. P., CARTER, D. R., MANN, R. W., HARRIS, W.H., "THE INFLUANCE OF APPARENT DENSITY AND TRABECULAR ORIENTATION ON THE ELASTIC MODULUS OF CANCELLOUS BONE", TRANS 27TH ANNUAL ORS, FEB, 1981, PP. 277.
- 76 HARRINGTON, I. J., "A BIOENGINEERING ANALYSIS OF FORCE ACTIONS AT THE KNEE IN NORMAL AND PATHOLOGICAL GAIT", BIO-MEDICAL ENGINEERING, VOL. 11, 1976, PP. 167-172
- 77 HARRIS, L. J., CHAO, R., BLOCH, R., WEINGARTEN, V., "A THREE-DIMENSIONAL FINITE ELEMENT ANALYSIS OF THE PROXIMAL THIRD OF THE FEMUR", TRANS 24TH ANNUAL ORS, 1978, P. 16.
- 78 HASSLER, C. R., RYBICKI, E. F., CUMMINGS, K. D., CLARK, L. C., "QUANTIFICATION OF BONE STRESSES DURING REMODELLING", JOURNAL OF BIOMECHANICS, VOL. 13, 1980, PP. 185-190.
- 79 HAYES, W. C., SWENSON, L. W. Jr., SCHURMAN, D. J., "AXISYMMETRIC FINITE ELEMENT ANALYSIS OF THE LATERAL TIBIAL PLATEAU", JOURNAL OF BIOMECHANICS, VOL. 11(1-2), 1978, PP. 21-33.
- 80 HAYES, W. C., SNYDER, B., "TOWARD A QUANTITATIVE FORMULATION OF WOLFF'S LAW IN TRABECULAR BONE", ASME APPLIED MECHANICS DIVISION, VOL.45, 1981, PP. 43-68.
- 81 HEIPLE, K. G., VERDIN, P. J., "TENSILE, COMPRESSIVE AND TORSIONAL TESTING OF CANCELLOUS BONE", TRANS 29TH ANNUAL ORS, MARCH, 1983, PP. 132
- 82 HEMINGSON, A., JUNG, B., YTTERBERGH, C., "DUAL ENERGY COMPUTED TOMOGRAPHY: SIMULATED MONOENERGETIC AND MATERIAL SELECTIVE IMAGING", JOURNAL OF COMPUTER ASSISTED TOMOGRAPHY, VOL. 10(3), MAY/JUNE, 1986, PP. 490-499.
- 83 HIGHT, T. K., NAGEL, D. A., PIZIALI, R. L., "A DETAILED STRUCTURAL ANALYSIS OF THE HUMAN TIBIA", ASME APPLIED MECHANICS DIVISION, VOL. 10, JUNE, 1975, PP. 97-99.
- 84 HORSMAN, A., SIMPSON, M., "THE MEASURMENT OF SEQUENTIAL CHANGES IN CORTICAL BONE GEOMETRY", BRITISH JOURNAL OF RADIOLOGY, VOL. 48, 1975, PP. 470-476.
- 85 HOUNSFIELD, G. N., "COMPUTERIZED TRANSVERSE AXIAL SCANNING (TOMOGRAPHY) PART 1. DESCRIPTION OF SYSTEM", BRITISH JOURNAL OF RADIOLOGY, VOL. 46, 1973, PP. 1016-1022.
- 86 HOUNSFIELD, G. N., "SOME PRACTICAL PROBLEMS IN COMPUTERIZED TOMOGRAPHY SCANNING", RECONSTRUCTIVE TOMOGRAPHY IN DIAGNOSTIC RADIOLOGY AND NUCLEAR MEDICINE, ED. TER-POGOSSIAN, M., BALTIMORE, UNIVERSITY PARK PRESS, 1977.

- 87 HUANG, H. K., WU, S. C., "THE EVALUATION OF MASS DENSITIES OF THE HUMAN BODY IN VIVO FROM CT SCANS", COMPUTERS IN BIOLOGY AND MEDICINE, VOL. 6, 1976, PP. 337-343.
- 88 HUANG, H. K., SUAREZ, F., TORIDIS, T. G., "UTILIZATION OF COMPUTERIZED TOMOGRAPHIC SCANS AS INPUT TO FINITE ELEMENT ANALYSIS", INTERNATIONAL CONFERENCE PROCEEDINGS: FINITE ELEMENTS IN BIOMECHANICS, VOL. 2., FEBRUARY, 1980, PP. 797-815.
- 89 HUANG, H. K., SUAREZ, F. R., "EVALUATION OF CROSS-SECTIONAL GEOMETRY AND MASS DENSITY DISTRIBUTIONS OF HUMANS AND LABORATORY ANIMALS USING COMPUTERIZED TOMOGRAPHY", JOURNAL OF BIOMECHANICS, VOL. 16(10), 1983, PP. 821-832.
- 90 HUISKES, R., JENSSEN, J. D., SLOOFF, T. J., "A DETAILED COMPARISON OF EXPERIMENTAL AND THEORETICAL STRESS ANALYSES OF A HUMAN FEMUR", ASME BIOENGINEERING CONFERENCE, APPLIED MECHANICS DIVISION, VOL. 45, 1981, PP. 211-234.
- 91 HUISKES, R., "ON THE MODELLING OF LONG BONES IN STRUCTURAL ANALYSES", JOURNAL OF BIOMECHANICS, VOL. 15(1), 1982, PP. 65-69.
- 92 HUISKES, R., CHAO, E. Y. S., "A SURVEY OF FINITE ELEMENT ANALYSIS IN ORTHOPEDIC BIOMECHANICS: THE FIRST DECADE", JOURNAL OF BIOMECHANICS, VOL. 16(6), 1983, PP. 385-409.
- 93 HVID, I., CHRISTENSEN, P., SONDERGAARD, J., "COMPRESSIVE STRENGTH OF TIBIAL CANCELLOUS BONE", ACTA ORTHOPEDIC SCANDINAVIA, VOL. 54(6), 1983, PP. 819-825.
- 94 HVID, I., JENSEN, J., "CANCELLOUS BONE STRENGTH AT THE PROXIMAL TIBIA", ENGINEERING IN MEDICIN, VOL. 13(1), JANUARY, 1984, PP. 21-25.
- 95 JENSEN, P. S., ORPHANOUDAKIS, S. C., RAUSCHKOLB, E. N., BARON, R., "ASSESSMENT OF BONE MASS IN THE RADIUS BY COMPUTED TOMOGRAPHY", RADIOLOGY, VOL. 134, 1980, PP. 285-292.
- 96 JOHNSON, F., WAUGH, W., "METHOD FOR ROUTINE CLINICAL ASSESMENT OF KNEE-JOINT FORCES", MEDICAL AND BIOLOGICAL ENGINEERING, VOL. 17, 1979, PP. 145-154.
- 97 JOHNSON, F., LEITL, S., WAUGH, W., "THE DISTRIBUTION OF LOAD ACROSS THE KNEE: A COMPARISON OF STATIC AND DYNAMIC MEASUREMENTS", THE JOURNAL OF BONE AND JOINT SURGERY, VOL. 62B(3), AUGUST, 1980, PP. 346-349.

- 98 JOSEPH, P. M., SPITAL, R. D., "A METHOD FOR CORRECTING BONE INDUCED ARTIFACTS IN COMPUTED TOMOGRAPHY SCANNERS", JOURNAL OF COMPUTER ASSISTED TOMOGRAPHY, VOL. 2, JANUARY, 1978, PP. 100-108.
- 99 JUNGERS, W. L., MINNS, R. S., "COMPUTED TOMOGRAPHY AND BIOMECHANICAL ANALYSIS OF FOSSIL LONG BONES", AMERICAN JOURNAL OF PHYSIOLOGY AND ANTHROPOLOGY, VOL. 50(2), 1977, PP. 285-290.
- 100 KAMEL, H. A., "AUXILIARY SOFTWARE FOR FINITE ELEMENTS ANALYSIS", INTERNATIONAL CONFERENCE PROCEEDINGS: FINITE ELEMENTS IN BIOMECHANICS, VOL. 1, FEBRUARY, 1980, PP. 83-104.
- 101 KATZ, J. L., "THE STRUCTURE AND BIOMECHANICS OF BONE", SYMPOSIUM OF THE SOCIETY FOR EXPERIMENTAL BIOLOGY, VOL. 34, 1980, PP. 137-168.
- 102 KATZ, J. L., "ANISOTROPY OF YOUNG'S MODULUS OF BONE", NATURE, VOL. 283, JANUARY, 1980, PP. 106-107.
- 103 KENNEDY, J. L., CARTER, D. R., "LONG BONE TORSION: EFFECTS OF HETEROGENEITY ANISOTROPY AND GEOMETRIC IRREGULARITY", JOURNAL OF BIOMECHANICAL ENGINEERING, VOL. 107, MAY, 1985, PP. 183-188.
- 104 KETTELKAMP, D. B., JOHNSON, R. J., SMIDT, G. L., "AN ELECTROGONIOMETRIC STUDY OF KNEE MOTION IN NORMAL GAIT", THE JOURNAL OF BONE AND JOINT SURGERY, VOL. 52A(4), JUNE, 1970, PP. 775-785.
- 105 KETTELKAMP, D. B., JACOBS, A. W., "TIBIOFEMORAL CONTACT AREA - DETERMINATION AND IMPLICATIONS", THE JOURNAL OF BONE AND JOINT SURGERY, VOL. 54A(2), MARCH, 1972, PP. 349-356.
- 106 KETTELKAMP, D. B., CHAO, E. Y., "A METHOD FOR QUANTITATIVE ANALYSIS OF MEDIAL AND LATERAL COMPRESSION FORCES AT THE KNEE DURING STANDING", CLINICAL ORTHOPEDICS AND RELATED RESEARCH, VOL. 83, MARCH-APRIL, 1972, PP. 202-213.
- 107 KIJEWski, P. K., BJARNGARD, B. E., "CORRECTION FOR BEAM HARDENING IN COMPUTED TOMOGRAPHY", MEDICAL PHYSICS, VOL. 5(3), 1978, PP. 209-214.
- 108 KING, A. I., "A REVIEW OF BIOMECHANICAL MODELS", JOURNAL OF BIOMECHANICAL ENGINEERING, VOL. 106, MAY, 1984, PP. 97-104.
- 109 KNETS, I. V., "MECHANICS OF BIOLOGICAL TISSUES", POLYMER MECHANICS, VOL. 13, 1978, PP. 434-440.
- 110 KOCH, J. C., "THE LAWS OF BONE ARCHITECTURE", AMERICAN JOURNAL OF ANATOMY, VOL. 21, 1917, PP. 177-289.

- 111 KOSSAKOWSKI, A., STALMASINSKI J., "EVALUATION OF THE MECHANICAL RESISTANCE OF THE COMPACT BONE FROM SHAFTS OF VARIOUS BOVINE BONES", FOLIA MORPHOLOGY, VOL. 40, 1981, PP. 329-335.
- 112 KOSTUIK, J. P., SCHMIDT, O., HARRIS, W. R., WOOLDRIDGE, C., "A STUDY OF WEIGHT TRANSMISSION THROUGH THE KNEE JOINT WITH APPLIED VARUS AND VALGUS LOADS", CLINICAL ORTHOPEDICS, VOL.108, 1975, PP. 95-98.
- 113 KULP, C. R., "AN EXPERIMENTAL AND FINITE ELEMENTS ANALYSIS OF THE ANISOTROPIC BEHAVIOR OF FOUR HUMAN LONG BONES", DOCTORAL DISSERTATION, UNIVERSITY OF KANSAS, SEPTEMBER, 1982.
- 114 KUROSAWA, H., WALKER, P. S., GARG, A., HUNTER, T., "GEOMETRY AND MOTION OF THE KNEE FOR IMPLANT AND ORTHOTIC DESIGN", JOURNAL OF BIOMECHANICS, VOL. 18(7), 1985, PP. 487-499.
- 115 LANG, S. B., "ULTRASONIC METHOD FOR MEASURING ELASTIC COEFFICIENTS OF BONE AND RESULTS ON FRESH AND DRIED BOVINE BONE", IEEE TRANSACTIONS ON BIOMEDICAL ENGINEERING, VOL. BME-17, 1970, PP. 101-105.
- 116 LANYON, N. E., HAMPSON, W. G. J., GOODSHIP, A. E., SHAH, J. S., "BONE DEFORMATION RECORDED IN VIVO FROM STRAIN GAUGES ATTACHED TO THE HUMAN TIBIAL SHAFT", ACTA ORTHOPEDIC SCANDINAVIA, VOL. 46, 1975, PP. 256-268.
- 117 LARSSON, S., BERGSTROM, M., DAHLQVIST, I., ISRAELSSON, A., LAGERGREN, C., "A METHOD FOR DETERMINING BONE MINERAL CONTENT USING FOURIER IMAGE RECONSTRUCTION AND DUAL SOURCE TECHNIQUE", JOURNAL OF COMPUTER ASSISTED TOMOGRAPHY, VOL. 2, JULY, 1978, PP. 347-351.
- 118 LAZENBY, R., "POROSITY GEOMETRY INTERACTION IN THE CONSERVATION OF BONE STRENGTH", JOURNAL OF BIOMECHANICS, VOL. 19(3), 1986, PP. 257-258.
- 119 LEWIS, J. L., "STRESS ANALYSIS OF SOME FEATURES OF KNEE PROSTHESIS BY FINITE ELEMENTS", TRANS 23RD ANNUAL ORS, VOL. 2, 1977, PP. 55.
- 120 LINDAHL, O., "MECHANICAL PROPERTIES OF DRIED DEFATTED SPONGY BONE", ACTA ORTHOPEDIC SCANDINAVIA, VOL. 47, 1976, PP. 11-19.
- 121 LIPSON, S. F., KATZ, J. L., "THE RELATIONSHIP BETWEEN ELASTIC PROPERTIES AND MICROSTRUCTURE OF BOVINE CORTICAL BONE", JOURNAL OF BIOMECHANICS, VOL. 17(4), 1984, PP. 231-240.

- 122 LITTLE, E. G., KNEAFSEY, A. G., LYNCH, P., "THE DESIGN OF A MODEL FOR A THREE DIMENSIONAL STRESS ANALYSIS OF THE CEMENT LAYER BENEATH THE MEDIAL PLATEAU OF A KNEE PROSTHESIS", JOURNAL OF BIOMECHANICS, VOL. 18(2), 1985, PP. 157-160.
- 123 LITTLE, E. G., WEVERS, H. W., SIN, D., COOKE, T. D. V., "THE THREE DIMENSIONAL FINITE ELEMENT ANALYSIS OF THE UPPER TIBIA", JOURNAL OF BIOMECHANICAL ENGINEERING, VOL. 108, MAY, 1986, PP. 111-119.
- 124 LOVEJOY, C. O., BURSTEIN, A. H., HEIPLE, K. G., "THE BIOMECHANICAL ANALYSIS OF BONE STRENGTH: A METHOD AND ITS APPLICATION TO PLATINEMIA", AMERICAN JOURNAL OF PHYSICAL ANTHROPOLOGY, VOL. 44, 1976, PP. 489-506.
- 125 LOVEJOY, C. O., BURSTEIN, A. H., "GEOMETRICAL PROPERTIES OF BONE SECTIONS DETERMINED BY LAMINOGRAPHY AND PHYSICAL SECTION", JOURNAL OF BIOMECHANICS, VOL. 10(9), 1977, PP. 527-528.
- 126 MACOVSKI, A., ALVAREZ, R. E., CHEN, J. L., STONESTROM, J. P., ZATZ, L. M., "ENERGY DEPENDENT RECONSTRUCTION IN X-RAY COMPUTERIZED TOMOGRAPHY", COMPUTERS IN BIOLOGY AND MEDICINE, VOL.6, 1976, PP. 325-336.
- 127 MAHANIAN, S., PIZIALI, R., "INCOMPRESSIBILITY IN BONE", JOURNAL OF BIOMECHANICS, VOL. 18(1), 1985, PP. 77-78.
- 128 MAROM, S. A., LINDEN, M. J., HUSSEIN, R., "A FINITE ELEMENT STRESS ANALYSIS OF A LONG BONE UTILIZING COMPUTED TOMOGRAPHY", ADVANCES IN BIOENGINEERING, ED: LANGRANA, N. A., THE AMERICAN SOCIETY OF MECHANICAL ENGINEERING, NEW YORK, NOVEMBER, 1985, PP. 162-163.
- 129 MARTENS, M., VAN AUDEKERCKE, R., DE MEESTER, P., "THE MECHANICAL CHARACTERISTICS OF THE LONG BONES OF THE LOWER EXTRIMITIES IN TORSIONAL LOADING", JOURNAL OF BIOMECHANICS, VOL. 13(8), 1980, PP. 667-676.
- 130 MARTIN, R. B., "THE EFFECTS OF GEOMETRIC FEEDBACK IN THE DEVELOPMENT OF OSTEOPOROSIS", JOURNAL OF BIOMECHANICS, VOL. 5, 1972, PP. 447-455.
- 131 MATHER, B. S., "CORRELATIONS BETWEEN STRENGTH AND OTHER PROPERTIES OF LONG BONES", THE JOURNAL OF TRAUMA, VOL. 7(5), 1967B, PP. 633-638.
- 132 MATHEW, L. S., "LOAD BEARING CHARACTERISTICS OF THE PATELLO FEMORAL JOINT", ACTA ORTHOPEDIC SCANDINAVIA, VOL. 48, 1977, PP. 511-516.

- 133 MAYOTT, C. W., LANGRANA, N., "AUTOMATED PROCEDURE TO DETERMINE THE MECHANICAL PROPERTIES OF LONG BONE", PROCEEDINGS OF BIOMEDICAL ENGINEERING SYMPOSIUM, JUNE, 1983, PP. 189-192.
- 134 MAYOTT, C. W., LANGRANA, N., ALEXANDER, H., CURTIS, G., "GEOMETRIC AND MASS PROPERTIES OF BONE AS MEASURED USING COMPUTER-AIDED TOMOGRAPHY", ASME ANNUAL MEETING, ADVANCES IN BIOENGINEERING, NOVEMBER, 1983, PP. 28-31.
- 135 MAYOTT, C. W., "THE USE OF COMPUTED TOMOGRAPHY AS A DIAGNOSTIC AND RESEARCH DEVICE", DOCTORAL DISSERTATION, RUTGERS UNIVERSITY, NEW JERSEY, OCTOBER, 1985.
- 136 MAZESS, R. B., ERRORS IN MEASURING TRABECULAR BONE BY COMPUTED TOMOGRAPHY DUE TO MARROW AND BONE COMPOSITION", CALCIFIED TISSUE INTERNATIONAL, VOL. 35, 1983, PP. 148-152.
- 137 McCULLOUGH, E. C., BAKER, H. L., HOUSER, O. W., "AN EVALUATION OF THE QUANTITATIVE AND RADIATION FEATURES OF A SCANNING X-RAY TRANSVERSE AXIAL TOMOGRAPH: THE EMI SCANNER", RADIOLOGY, VOL. 111, 1974, P. 709.
- 138 McCULLOUGH, E. C., "PHOTON ATTENUATION IN COMPUTED TOMOGRAPHY", MEDICAL PHYSICS, VOL. 2(6), 1975, PP. 307-320.
- 139 McCULLOUGH, E. C., "FACTORS AFFECTING THE USE OF QUANTITATIVE INFORMATION FROM A CT SCANNER", RADIOLOGY, VOL. 124, JULY, 1977, PP. 99-107.
- 140 McELHANEY, J., ALEM, N., ROBERTS, V., "A POROUS BLOCK MODEL FOR CANCELLOUS BONES", ASME TECHNICAL PUBLICATION, 70-WA/BHF-2, AUGUST, 1970, PP. 1-9.
- 141 MENSCH, J. S., AMSTUTZ, H. C., "KNEE MORPHOLOGY AS A GUIDE TO KNEE REPLACEMENT", CLINICAL ORTHOPEDICS AND RELATED RESEARCH, VOL. 112, OCTOBER, 1975, PP. 231-242.
- 142 MINNS, R. J., BREMBLE, G. R., CAMPBELL, J., "THE GEOMETRICAL PROPERTIES OF THE HUMAN TIBIA", JOURNAL OF BIOMECHANICS, VOL. 8, 1975, PP. 253-255.
- 143 MINNS, R. J., CAMPBELL, J., BREMBLE, G. R., "THE BENDING STIFFNESS OF THE HUMAN TIBIA", CALCIFIED TISSUE RESEARCH, VOL. 17(2), 1975, PP. 165-168.
- 144 MINNS, R. J., "FORCES AT THE KNEE JOINT : ANATOMICAL CONSIDERATIONS", JOURNAL OF BIOMECHANICS, VOL. 14(9), 1981, PP. 633-643.
- 145 MOEINZADEH, M. H., ENGIN, A. E., AKKAS, N., "TWO-DIMENSIONAL DYNAMIC MODELLING OF HUMAN KNEE JOINT", JOURNAL OF BIOMECHANICS, VOL. 16(4), 1973, PP. 253-264.

- 146 MORRISON, J. B., "BIOENGINEERING ANALYSIS OF FORCE ACTIONS TRANSMITTED BY THE KNEE JOINT", BIOMEDICAL ENGINEERING, VOL. 3, APRIL, 1968, PP. 164-170.
- 147 MORRISON, J. B., "THE MECHANICS OF THE KNEE JOINT IN RELATION TO NORMAL WALKING", JOURNAL OF BIOMECHANICS, VOL. 3, 1970, PP. 51-61.
- 148 MURASE, K., "A FINITE ELEMENT ANALYSIS OF TIBIAL COMPONENT DESIGN IN TOTAL KNEE ARTHROPLASTY", FUKUSHIMA JOURNAL OF MEDICAL SCIENCE, VOL. 27(3-4), 1981, PP. 117-132.
- 149 MURASE, K., CROWNSHIELD, R. D., PEDERSEN, D. R., CHANG, T. S., "AN ANALYSIS OF TIBIAL COMPONENT DESIGN IN TOTAL KNEE ARTHROPLASTY", JOURNAL OF BIOMECHANICS, VOL. 16(1), 1982, PP. 13-22.
- 150 NEIL, J. L., DEMOS, T. C., STONE, J. L., "TENSILE AND COMPRESSIVE PROPERTIES OF VERTEBRAL TRABECULAR BONE", TRANS 29TH ANNUAL ORS, VOL. 8, MARCH, 1983, P. 344.
- 151 NELSON, P. C., ROBERTSON, D. D., WALKER, J. W., "A COMPUTE-RIZED FEMORAL INTRAMEDULLARY IMPLANT DESIGN PACKAGE UTILIZING COMPUTED TOMOGRAPHY DATA", INSTITUTE OF ELECTRICIANS AND ELECTRONICAL ENGINEERS", AUGUST, 1985, PP. 200-201.
- 152 NISSEL, R., NEMETH, G., OHLSEN, H., "JOINT FORCES IN EXTENSION OF THE KNEE", ACTA ORTHOPEDIC SCANDINAVIA, VOL. 57, 1986, PP. 41-46.
- 153 OLDENDORF, W. H., "ISOLATED FLYING SPOT DETECTION OF RADIO-DENSITY DISCONTINUITIES IN THE INTERNAL STRUCTURAL PATTERN OF A COMPLEX OBJECT", INSTITUTE OF RADIOLOGICAL ENGINEERING, VOL. 8, 1961, PP 68.
- 154 ORPHANOUDAKIS, S. C., JENSEN, P. S., RAUSCHKOLB, E. N., "BONE MINERAL ANALYSIS USING SINGLE-ENERGY COMPUTED TOMO-GRAPHY", INVESTIGATIVE RADIOLOGY, VOL. 14, 1979, PP. 122-130.
- 155 OTIS, J. C., GOULD, J. D., "THE EFFECT OF EXTERNAL LOAD ON TORQUE PRODUCTION BY KNEE EXTENSORS", THE JOURNAL OF BONE AND JOINT SURGERY, VOL. 68-A(1), JANUARY, 1986, PP.65-70.
- 156 PALING, M. R., "THE COMPUTED TOMOGRAPHY OF NORMAL LONG BONE ANATOMY AND ITS SIMULATION OF DISEASE", COMPUTERIZED TOMOGRAPHY, VOL. 5(3), JULY-SEPTEMBER, 1981, PP. 201-213.
- 157 PAUL, J. P., "BIOENGINEERING STUDIES OF THE FORCES TRANSMITTED BY JOINTS", BIOMECHANICS AND RELATED BIOENGINEERING TOPICS, ED: KENEDI, R. M., PERMAGON PRESS, OXFORD, 1965, PP. 321-342.

- 158 PERREN, S. M., HUGGLER, A., RUSSENBERGER, M., "THE REACTION OF CORTICAL BONE TO COMPRESSION", ACTA ORTHOPEDIC SCANDINAVICA, VOL. 125, 1969, PP. 19-28.
- 159 PFAFROD, G. O., SAULGOZIS, YU. ZH., KNETS, I. V., "EXPERIMENTAL DETERMINATION OF THE SHEAR MODULUS OF COMPACT BONE TISSUE", POLYMER MECHANICS, VOL. 8(4), JULY, 1972, PP. 601-608.
- 160 PIZIALI, R. L., HIGHT, T. K., NAGEL, D. A., "AN EXTENDED STRUCTURAL ANALYSIS OF LONG BONES - APPLICATION TO THE HUMAN TIBIA", JOURNAL OF BIOMECHANICS, VOL. 9, 1976, PP. 695-701.
- 161 PIZIALI, R. L., "GEOMETRIC PROPERTIES OF HUMAN LONG BONES", JOURNAL OF BIOMECHANICS, VOL. 13(10), 1980, PP. 881-885.
- 162 PLOT 10 INTERACTIVE GRAPHIC LIBRARY, TEK USER'S MANUAL, NO. 070-4482-00, TEKTRONIX, BEAVERTON, OREGON, 1983.
- 163 PUGH, J. W., ROSE, R. M., RADIN, E. L., "ELASTIC AND VISCOELASTIC PROPERTIES OF TRABECULAR BONE: DEPENDENCE ON STRUCTURE", JOURNAL OF BIOMECHANICS, VOL. 6, 1973, PP. 475-485.
- 164 PUGH, J. W., ROSE, R. M., RADIN, E. L., "A STRUCTURAL MODEL FOR THE MECHANICAL BEHAVIOR OF TRABECULAR BONE", JOURNAL OF BIOMECHANICS, VOL. 6, 1973A, PP. 657-670.
- 165 RADON, J., "ON THE DETERMINATION OF FUNCTIONS FROM THEIR INTEGRAL ALONG CERTAIN MANIFOLDS", BERICHTE UBER DIE VERHANLUGENDER SACHISDEN, GESELLSCHAFT DER WIENSHAFTER ZU LEIPZIG, PHYSICH KLASSE 69, 1917, PP. 262-272.
- 166 REICH, N. E., SEIDELMANN, F. E., TUBBS, R. R., MACINTYRE, W. J., "DETERMINATION OF BONE MINERAL CONTENT USING CT SCANNING", AMERICAN JOURNAL OF ROENGENOLOGY, VOL. 127, 1976, PP. 593-594.
- 167 REILLY, D. T., BURSTEIN, A. H., FRANKEL, V. H., "THE ELASTIC MODULUS FOR BONE", JOURNAL OF BIOMECHANICS, VOL. 7, 1974, PP. 271-275.
- 168 REILLY, D. T., BURSTEIN, A. H., "THE MECHANICAL PROPERTIES OF CORTICAL BONE", JOURNAL OF BONE AND JOINT SURGERY, VOL. 56A, JULY, 1974A, PP. 1001-1022.
- 169 REILLY, D. T., BURSTEIN, A. H., "THE ELASTIC AND ULTIMATE PROPERTIES OF COMPACT BONE TISSUE", JOURNAL OF BIOMECHANICS, VOL. 8, 1975, PP. 393-405.

- 170 ROBERTSON, D. D., "QUANTITATIVE MEASUREMENT OF BONE USING COMPUTED TOMOGRAPHY WITH SECOND ORDER CORRECTION", DOCTORAL DISSERTATION, GEORGETOWN UNIVERSITY, WASHINGTON D.C., JULY, 1983.
- 171 ROCKOFF, S. D., SWEET, C., BLEUSTEIN, J., "THE RELATIVE CONTRIBUTION OF TRABECULAR AND CORTICAL BONE TO THE STRENGTH OF HUMAN LUMBAR VERTEBRAE", CALCIFIED TISSUE RES., VOL. 3, 1969, PP. 163-175.
- 172 ROHRLE, H., SCHOLTEN, R., SOLLBACH, W., "ANALYSIS OF STRESS DISTRIBUTION IN NATURAL AND ARTIFICIAL KNEE JOINTS ON THE FEMUR SIDE USING THE FINITE ELEMENT METHOD", INTERNATIONAL CONFERENCE PROCEEDINGS: FINITE ELEMENTS IN BIOMECHANICS, VOL. 2, FEBRUARY, 1980, PP. 781-794.
- 173 RUEGSEGGER, P., HANGARTNER, T., KELLER, H., U., "STANDARDIZATION OF COMPUTED TOMOGRAPHY IMAGES BY MEANS OF A MATERIAL-SELECTIVE BEAM HARDENING CORRECTION", JOURNAL OF COMPUTER ASSISTED TOMOGRAPHY, VOL. 2, APRIL, 1978, PP. 184-188.
- 174 RUEGSEGGER, P., ANLIKER, M., DAMBUCHER, M., "QUANTIFICATION OF TRABECULAR BONE WITH LOW DOSE COMPUTED TOMOGRAPHY", JOURNAL OF COMPUTER ASSISTED TOMOGRAPHY, VOL. 5, 1980, PP. 493-500.
- 175 RUFF, C. B., HAYES, W. C., "CROSS SECTIONAL GEOMETRY OF PECOS PUEBLO FEMORA AND TIBIAE - A BIOMECHANICAL INVESTIGATION", AMERICAN JOURNAL OF PHYSICAL ANTHROPOLOGY, VOL. 60(3), MARCH, 1983, PP. 383-400.
- 176 RUFF, C. B., "THE CONTRIBUTION OF CANCELLOUS BONE TO LONG BONE STRENGTH AND RIGIDITY", AMERICAN JOURNAL OF PHYSICAL ANTHROPOLOGY, VOL. 61, 1983A, PP. 141-143.
- 177 RYBICKI, E. F., "THE ROLE OF FINITE ELEMENT MODELS IN ORTHOPEDICS", INTERNATIONAL CONFERENCE PROCEEDINGS, FINITE ELEMENTS IN BIOMECHANICS, VOL. 1, FEBRUARY, 1980, PP. 21-25.
- 178 SAHA, S., GORMAN, P. H., "STRENGTH OF HUMAN CANCELLOUS BONE IN SHEAR AND ITS RELATIONSHIP TO BONE MINERAL CONTENT", TRANS 27TH ANNUAL ORS, 1981, P. 217.
- 179 SAP IV STRUCTURAL ANALYSIS PROGRAM USER GUIDE, COLLEGE OF ENGINEERING, UNIVERSITY OF CALIFORNIA, BERKELEY, CA., 1974.
- 180 SHEPP, L. A., "SCOPE OF PURE AND APPLIED TOMOGRAPHY", PROCEEDINGS OF SYMPOSIA IN APPLIED MATHEMATICS, VOL. 27,

- 181 SIMKIN, A., ROBIN, G., "THE MECHANICAL TESTING OF BONE IN BENDING", JOURNAL OF BIOMECHANICS, VOL. 6, 1973, PP. 31-39.
- 182 SINGH, I., "THE ARCHITECTURE OF CANCELLOUS BONE", JOURNAL OF ANATOMY, VOL. 127(2), 1978, PP. 305-310.
- 183 SMITH, K. T., "RECONSTRUCTION FORMULAS IN COMPUTED TOMOGRAPHY", PROCEEDINGS OF SYMPOSIA IN APPLIED MATHEMATICS, VOL. 27, 1982, PP. 7-24.
- 184 STEIN, I. D., GRANIK, G., "THE HUMAN TIBIA: A SIMPLIFIED METHOD OF RADIOGRAPHIC ANALYSIS OF ITS CROSS SECTION WITH ANTHROPOMETRIC CORRELATIONS", ANNALS OF BIOMEDICAL ENGINEERING, VOL. 7, 1979, PP. 103-116.
- 185 STEIN, I. D., GRANIK, G., "THE HUMAN TIBIA: STATIC TESTING IN BENDING BY AN IN VIVO METHOD", ANNALS IN BIOMEDICAL ENGINEERING, VOL. 10(6), 1982 PP. 281-294.
- 186 STONE, J. L., BEAUPRE, G. S., HAYES, W. C., "MULTIAXIAL STRENGTH CHARACTERISTICS OF TRABECULAR BONE", JOURNAL OF BIOMECHANICS, VOL. 16(9), 1983, PP. 743-752.
- 187 SWANSON, S. A. U., "BIOMECHANICAL CHARACTERISTICS OF BONE", ADVANCES IN BIOMEDICAL ENGINEERING, ED: KENEDI, R. M., NEW YORK ACADEMIC PRESS, NEW YORK, 1971, PP. 137-187.
- 188 TEKTRONIX COMPUTER DISPLAY TERMINAL 4105, TEK USER MANUAL, NO. 070-4526-00, TEKTRONIX, BEAVERTON, OREGON, 1983.
- 189 TOFTS, P. S., "DEFINITIONS OF EFFECTIVE ENERGY IN COMPUTED TOMOGRAPHY", PHYSICAL AND MEDICAL BIOLOGY, VOL. 26(2), 1981, PP. 313-317.
- 190 TOWNSEND, P. R., ROSE, R. M., RADIN, E. L., "BUCKLING STUDIES OF SINGLE HUMAN TRABECULAE", JOURNAL OF BIOMECHANICS, VOL. 8, 1975, PP. 199-201.
- 191 TSAI, S. W., WU, E. M., "A GENERAL THEORY OF STRENGTH FOR ANISOTROPIC MATERIALS", JOURNAL OF COMPOSITE MATERIALS, VOL. 5, 1971, PP. 58-80.
- 192 TURNIER, H., HOUDEK, P., TREFLER, M., "MEASUREMENTS OF THE PARTIAL VOLUME PHENOMENON", COMPUTERIZED TOMOGRAPHY, VOL. 3, 1979, PP. 213-219.
- 193 VALLIAPPAN, S., SVENSSON, N. L., WOOD, R. D., "THREE DIMENSIONAL STRESS ANALYSIS OF THE HUMAN FEMUR", COMPUTERS IN BIOLOGY AND MEDICINE, VOL. 7, 1977, PP. 253-264.

- 194 VAN BUSKIRK, W. C., ASHMAN, R. B., "THE ELASTIC MODULI OF BONE", ASME APPLIED MECHANICS DIVISION, VOL. 45, 1981, PP. 131-143.
- 195 VAN DER VARST, G. T., MOOREN, L. P. M., "COMMENTS ON THE PAPER 'INCOMPRESSIBILITY OF BONE' BY MAHANIAN AND PIZIALI", JOURNAL OF BIOMECHANICS, VOL. 19(2), 1986, PP. 175-177.
- 196 VAX/VMS PRIMER, VERSION 3, NO. AA-D030C-TE, DIGITAL EQUIPMENT CORPORATION, MAYNARD, MASSACHUSETTS, 1982.
- 197 VICHNIN, H. H., HAYES, W. C., BATTERMAN, S. C., "FINITE ELEMENT ANALYSIS OF MULTI-AXIAL STRENGTH EXPERIMENTS FOR COMPACT BONE", ASME APPLIED MECHANICS DIVISION, VOL. 23, 1977, PP. 147-150.
- 198 VICHNIN, H. H., BATTERMAN, S. C., "EFFECTS OF CORTICAL BONE ANISOTROPY ON PROSTHESIS STEM STRESSES", TRANSACTIONS 28TH ANNUAL ORS, FEBRUARY, 1982, PP. 277.
- 199 WALL, J. C., CHATTERJI, S., JEFFERY, J. W., "HUMAN FEMORAL CORTICAL BONE: A PRELIMINARY REPORT ON THE RELATIONSHIP BETWEEN STRENGTH AND DENSITY", MEDICAL AND BIOLOGICAL ENGINEERING, VOL. 10, 1972, P. 673-676.
- 200 WHITEHOUSE, W. J., "THE QUANTITATIVE MORPHOLOGY OF ANISOTROPIC TRABECULAR BONE", JOURNAL OF MICROSCOPY, V. 101(2), 1974, PP. 153-168.
- 201 WHITEHOUSE, W. J., DYSON, E. D., "SCANNING ELECTRON MICROSCOPE STUDIES OF TRABECULAR BONE IN THE PROXIMAL END OF THE HUMAN FEMOR", JOURNAL OF ANATOMY, VOL. 118, 1974, PP. 417-444.
- 202 WILLIAMS, G., BYDDER, G. M., KREEL, L., "THE VALIDITY AND USE OF COMPUTED TOMOGRAPHY ATTENUATION VALUES", BRITISH MEDICAL BULLETINE, VOL. 36(3), 1980, PP. 279-287.
- 203 WILLIAMS, J. L., LEWIS, J. L., "PROPERTIES AND AN ANISOTROPIC TIBIAL EPIPHYSIS MODEL OF CANCELLOUS BONE FROM THE PROXIMAL TIBIA", JOURNAL OF BIOMECHANICAL ENGINEERING, VOL. 104, FEBRUARY, 1982, PP. 50-56.
- 204 WILSON, D. L., SONSTEGARD, D. A., MATTHEWS, L. S., "AN EXPERIMENTAL DETERMINATION OF NUMERICAL VALUES FOR ELASTIC MODULUS AND ULTIMATE STRENGTH OF HUMAN TIBIAL TRABECULAR BONE AS A FUNCTION OF LOCATION", TRANSACTIONS 26TH ANNUAL ORS, FEBRUARY, 1980, PP. 58.
- 205 WISMANS, J., VELDPAUS, F., JANSSEN, J., "A THREE DIMENSIONAL MATHEMATICAL MODEL OF THE KNEE JOINT", JOURNAL OF BIOMECHANICS, VOL. 13, 1980, PP. 677-685.

- 206 WITT, R. M., CAMERON, J. R., "AN IMPROVED BONE STANDARD CONTAINING DIPOTASSIUM HYDROGEN PHOSPHATE SOLUTION FOR THE INTERCOMPARISON OF DIFFERENT TRANSMISSION BONE SCANNING SYSTEMS", PROGRESS REPORT AEC GRANT NO. AT(11-1)-1422, 1970.
- 207 WOODARD, H. Q., "THE ELEMENTARY COMPOSITION OF HUMAN CORTICAL BONE", HEALTH PHYSICS, VOL. 8, 1962, PP. 513-517.
- 208 WOOLSON, S. T., YOUNG, S. W., WHITE, D. N., DEV, P., WOOD, S. L., "THREE-DIMENSIONAL BONE IMAGING AND MODELLING FROM COMPUTER ASSISTED TOMOGRAPHY", TRANSACTIONS 30TH ANNUAL MEETING ORS, FEBRUARY, 1984, PP. 59.
- 209 WRIGHT, T. M., HAYES, W. C., "TENSILE TESTING OF BONE OVER A WIDE RANGE OF STRAIN RATES: EFFECTS OF STRAIN RATE MICROSTRUCTURE AND DENSITY", MEDICAL AND BIOLOGICAL ENGINEERING, VOL. 14, 1976, 671-680.
- 210 YAMADA, H., "STRENGTH OF BIOLOGICAL MATERIALS", ED: EVANS, F. G., THE WILLIAMS AND WILKINS COMPANY, BALTIMORE, 1970.
- 211 ZATZ, L. M., ALVAREZ, R. E., "AN INACCURACY IN COMPUTED TOMOGRAPHY: THE ENERGY DEPENDENCE OF CT VALUES, RADIOLOGY, VOL. 124, JULY, 1977, PP. 91-97.
- 212 ZATZ, L. M., "BASIC PRINCIPLES OF COMPUTED TOMOGRAPHY SCANNING", TECHNICAL ASPECTS OF COMPUTED TOMOGRAPHY, ED. NEWTON, T., POTTS, D., ST. LOUIS, C. V. MOSBY CO., 1981.
- 213 ZIENKIEWICZ, O. C., PHILLIPS, D. V., "AN AUTOMATIC MESH GENERATION SCHEME FOR PLANE AND CURVED SURFACES BY ISOPARAMETRIC COORDINATES", INTERNATIONAL JOURNAL FOR NUMERICAL METHODS IN ENGINEERING, VOL. 3, 1971, PP. 519-528.